ENERGY BASED EVALUATION OF RC FRAME STRUCTURES

A THESIS SUBMITTED TO
THE GRADUATE SCHOOL OF NATURAL AND APPLIED SCIENCES
OF
MIDDLE EAST TECHNICAL UNIVERSITY

BY

MAHYAR AZIZI

IN PARTIAL FULFILLMENT OF THE REQUIREMENTS
FOR
THE DEGREE OF MASTER OF SCIENCE
IN
CIVIL ENGINEERING

AUGUST 2019

Approval of the thesis:

ENERGY BASED EVALUATION OF RC FRAME STRUCTURES

submitted by **MAHYAR AZIZI** in partial fulfillment of the requirements for the degree of **Master of Science in Civil Engineering Department, Middle East Technical University** by,

Prof. Dr. Halil Kalıpçılar
Dean, Graduate School of **Natural and Applied Sciences** _____

Prof. Dr. Ahmet Türer
Head of Department, **Civil Engineering** _____

Prof. Dr. Murat Altuğ Erberik
Supervisor, **Civil Engineering, METU** _____

Examining Committee Members:

Prof. Dr. Haluk Sucuoğlu
Civil Engineer, METU _____

Prof. Dr. Murat Altuğ Erberik
Civil Engineering, METU _____

Prof. Dr. Murat Dicleli
Engineering Science, METU _____

Prof. Dr. Eray Baran
Civil Engineer, METU _____

Assist. Prof. Dr. Fırat Soner Alıcı
Civil Engineer, Başkent University _____

Date: 28.08.2019

I hereby declare that all information in this document has been obtained and presented in accordance with academic rules and ethical conduct. I also declare that, as required by these rules and conduct, I have fully cited and referenced all material and results that are not original to this work.

Name, Surname: Mahyar Azizi

Signature:

ABSTRACT

ENERGY BASED EVALUATION OF RC FRAME STRUCTURES

Azizi, Mahyar
Master of Science, Civil Engineering
Supervisor: Prof. Dr. Murat Altuğ Erberik

August 2019, 90 pages

Nowadays, earthquake and structural engineers perceive that conventional seismic design method, which is based on force and strength, is not an adequate way of designing structures under ground motions. The reason is that the conventional seismic design method does not pay enough attention to inelastic displacements, plastic behavior of structures and duration of seismic motion. At the present time, there are new and popular alternatives to the force-based approach like displacement-based method, in which the aforementioned issues are mostly handled. The energy-based method is another convenient tool to study the performance of structures under seismic action and probably the best way to include the duration of ground motion within the analysis. In the energy-based approach, the energy input to the structure should be dissipated through inelastic action and damping. The inelastic energy dissipation mechanism is called as hysteretic energy. It is an important challenge to obtain the story-wise and component-wise distribution of the total hysteretic energy within the building in order to develop the energy-based design and analysis tools. Such studies have been conducted for steel frames in previous studies; however the distribution of hysteretic energy among the reinforced concrete (RC) beams and columns has not been studied extensively. Accordingly, this study is focused on the story-wise and component-wise distribution of hysteretic energy in RC moment-resisting frames. For this purpose, RC frames with a different number of stories and

bays are designed according to the 2018 Turkish Seismic Design Code. Then the designed frames are modeled with lumped plasticity model that introduces the inelasticity at the ends of the beam and column members. The developed models are subjected to a set of strong ground motion records and the distributions of hysteretic energy for each frame and analysis are obtained. The results indicate that it is possible to set up some rules for the hysteretic energy distribution in RC frames that can be used in energy-based design and analysis procedures.

Keywords: Energy-based Design, Hysteretic Energy, RC Frame, Story-wise Distribution, Inelastic behavior, Member-wise Distribution

ÖZ

BETONARME ÇERÇEVELİ YAPILARIN ENERJİ ESASLI DEĞERLENDİRMESİ

Azizi, Mahyar
Yüksek Lisans, İnşaat Mühendisliği
Tez Danışmanı: Prof. Dr. Murat Altuğ Erberik

Ağustos 2019, 90 sayfa

Günümüzde deprem ve yapı mühendisleri, kuvvete dayalı klasik deprem tasarım metodunun yapıların sismik etkiler altındaki tasarımı için yeterli olmadığını düşünmektedirler. Bunun en başlıca nedeni; geleneksel tasarım yönteminin elastik ötesi yerdeğiştirme, yapıların plastik bölgedeki davranışı ve yer hareketi süresi gibi parametrelere önem vermemesidir. Şu anda, kuvvete dayalı yaklaşımın yeni ve gözde bir alternatifi olarak yerdeğiştirmeye bağlı tasarım yaklaşımı yukarıda bahsi geçen hususları dikkate aldığı için ön plana çıkmaktadır. Bunlara ek olarak, deprem analizlerinde yer hareketi süresini doğrudan hesaba katan enerjiye dayalı yöntemin de yapıların deprem performanslarının belirlenmesi için uygun bir araç olduğu düşünülmektedir. Enerjiye dayalı yöntemde, yapıya yer hareketi yoluyla giren enerjinin elastik ötesi davranış ve sönüm mekanizmalarıyla tüketilmesi gerekmektedir. Bahsi geçen bu iki enerji tüketim mekanizmalarından ilkine histeretik enerji (veya elastik ötesi davranışta tüketilen enerji) adı verilmektedir. Enerjiye dayalı tasarım ve analiz yöntemlerinin geliştirilebilmesi için bu enerjinin yapı içinde katlara ve elemanlara göre dağılımının elde edilmesi önemli bir aşamadır. Bu tür çalışmalar yakın zamanda çelik çerçeveli yapılar için gerçekleştirilmiş olsa da betonarme yapılarda kolonlar ve kirişler tarafından tüketilen elastik ötesi enerjinin dağılımı ile

ilgili olarak yapılmış çalışma sayısı azdır. Bu bağlamda; söz konusu çalışma elastik ötesi enerjinin betonarme çerçeveli yapılarda katlara ve elemanlara göre hangi oranlarda tüketildiğini araştırmaktadır. Bu amaçla, 2018 Türkiye Bina Deprem Yönetmeliği esas alınarak farklı kat ve açıklık sayılarına sahip olan betonarme çerçeveli yapı sistemleri tasarlanmıştır. Bir sonraki aşamada, tasarımı yapılmış olan çerçevelerin sayısal modelleri elastik ötesi davranışın elemanın uç noktalarında dikkate alındığı yığılı plastik davranış yaklaşımı kullanılarak geliştirilmiştir. Daha sonra bir deprem yer hareketi veri seti sayesinde söz konusu modellerin dinamik analizleri gerçekleştirilmiş ve enerji tüketim dağılımları çıkarılmıştır. Sonuçlar irdelendiğinde, elastik ötesi enerji tüketiminin yapı içindeki dağılımı ile ilgili olarak bazı kuralların tanımlanabileceği ve bu kuralların enerjiye dayalı tasarım ve analiz yöntemlerinin geliştirilmesi amacıyla doğrudan kullanılabileceği ortaya çıkmıştır.

Anahtar Kelimeler: Enerjiye Dayalı Tasarım, Histeretik Enerji, Betonarme çerçeve, Katlararası Dağılım, Elastik ötesi Davranış

To my dear family and my love

ACKNOWLEDGEMENTS

It would have been impossible to achieve the goal of this study without the endless encouragement and support of many people who I shared the best and worst moments of this long but beautiful journey.

First and foremost, I would like to extend my sincere thanks to my supervisor, Prof. Dr. Murat Altuğ Erberik. I attribute the level of my Master's degree to him, which offered his continuous advice and encouragement throughout this thesis.

Moreover, I would like to pay my deepest gratitude to Prof. Dr. Eray BARAN for his precious friendship and guidenece.

I take this opportunity to offer my sincerest gratitude with all of my heart to my beloved parents, Reza Azizi, Mahnaz Habibpanah, and my brother Yavar Azizi. They raised me, supported me, taught me, and loved me.

I would like to show my greatest appreciation to my best friend, love of my life, Shima Ebrahimi. Her passion and continuous support have been great sources of motivation and encouragement at every stage of my life.

Last but not least I want to thank my dear friends Taher Ghalandary, Sahra Shakouri, Anil Arli, Serdar Atesal, Emren Alemdag, and Ali Gharibdoust, for their priceless friendship and their academic and non-academic supports.

TABLE OF CONTENTS

LIST OF TABLES

TABLES

LIST OF FIGURES

FIGURES

CHAPTER 1

INTRODUCTION

1.1. General

In the conventional seismic design methodology, structures and its components are designed to provide enough strength to withstand the maximum applied earthquake force, which is defined as the base shear force. Linear elastic structural systems under strong seismic actions demand to be designed with large lateral forces in medium fundamental period range, while the probability of such a strong earthquake is very seldom during the lifespan of the structure. So, in order to have an economic design, inelastic behavior of the structure under strong ground motion is inevitable (Sucuoglu and Akkar, 2014). For this purpose in the traditional method, Inelastic Design Response Spectra (IDRS), is employed with the introduction of displacement ductility factor. However, previous studies showed that the applied maximum earthquake force could not be a good representative of strength demand, and ductility factor is not an adequate parameter for seismic damage potential of structures. For these reasons, the performance-based design is a new trend in seismic and structural engineering. In the performance-based design, target demand of structure and performance of seismic action are measurable. Within the performance-based approach, energy-based design is an effective way to include the cumulative inelastic deformation of structure and duration of ground motion. For the first time, Housner (1956) proposed the energy-based philosophy, which is based on the fact that the input energy of earthquake should be less than dissipation capacity of the structure. Input energy of the earthquake is dissipated through damping and hysteretic action, which is representative of the damage potential of the structures. Although numerous studies have been conducted on energy-based design procedures, a practical design method has not been developed for real-life structures yet. The main aim of this study is to contribute to the

development of a practical energy-based design or assessment method. For this reason, six reinforced concrete (RC) moment-resisting frames with different number of stories and bays are designed according to TS500 (Requirements for Design and Construction of RC structures) and TBSC 2018 (Turkish Building Seismic Code). 20 ground motions are selected to carry out nonlinear time history (NLTH) analysis of the frame models. SAP2000 (2017) structural analysis and design software is used for all linear and nonlinear analysis of this work. After NLTH analysis, the energy response of the structures are calculated and evaluated. Estimation of the hysteretic energy from input energy and distribution of hysteretic energy through stories and structural members are spotlighted in this work.

1.2. Literature Survey

For the first time in 1956, George W. Housner proposed a limit-design method based on input energy of strong ground motion that applies to the structures. He claimed that controlled and ductile deformations cause energy dissipations and decrease stresses during ground motions. So, for economic design, ultimate capacity rather than elastic limits of structures, should be considered. He suggested a formula for maximum input energy in a typical structure with small damping (0.03~0.05) and period longer than 0.4s.

$$E = \frac{1}{2} M S_{V,n}^2 \tag{1.1}$$

In this equation, E is the maximum energy in the structure, M is the total mass of the structure and $S_{V,n}$ is the maximum relative velocity.

Housner claimed that in case of elastic behavior, the input energy of ground motion is dissipated by damping and the rest is stored in structure by the kinetic energy of mass and with strain energy of members. When ground motion is strong and causes permanent deformations in structure, total input energy of ground motion is equal to the sum motion of strain energy, kinetic energy, dissipated damping energy and dissipated energy of permanent deformations.

Gulkan and Sozen (1971) tested eleven scaled RC frames under dynamic and static forces. They tried to develop a realistic analytical model for the response of the RC structures under earthquake motion. They claimed that the work done or the energy supplied by structure is dependent both on the nature of ground motion and response of the structure to it. They showed that a large amount of earthquake energy could be dissipated through hysteretic in RC frames with enough ductility by proper detailing of longitudinal and transverse reinforcement in columns and joints.

McKevitt et al. (1980) carried out energy-based analysis on several single degree of freedom (SDOF) and multi degree of freedom (MDOF) systems with different ground motion records, different viscous damping values, and several force-deformation relationships. They gathered a wide range of data set for input energy and hysteretic energy. They developed spectra for SDOF systems that predict total input energy for related periods and yield strength ratios. The authors also proposed spectra for SDOF systems that shows the ratio of hysteretic energy to input energy of structures with different yield strength ratios, different viscous damping values, and several force-deformation relationships. They claimed that the proportion of hysteretic energy to input energy is independent of ground motion. They stated that it is also possible to predict the ratio of hysteretic energy to input energy of a MDOF structure from a SDOF structure with the same period, damping value and yield strength ratio.

In 1984, Zahrah and Hall focused on the amount of dissipated energy by hysteretic and damping actions under different ground motions in SDOF systems. The main focus of the study was on the number of yield excursions and reversals during ground motion time histories and the factors that affect them. Eight earthquake records were used over different displacement ductility ratios and frequencies for the SDOF systems to study energy time histories. The results show that as ground motion duration increase, number of yield excursions also increase. Besides ground motion duration, the displacement ductility and damping have a significant effect on the number of yield excursion. They claimed that the force-displacement relation is not an important factor in the number of yield excursions.

Akiyama (1985) proposed an energy-based design method based on an equivalent-velocity spectrum. He computed input energy of a five-story steel building under the 1940 EI Centro record and compared it with a one-story building having the same mass, yield strength and fundamental period. He showed that it is possible to calculate the total input energy of a five-story building with the equivalent one-story building having the same mass, yield strength, and fundamental period. He believed that the input energy per mass of MDOF structure could be predicted using the input energy per mass of equivalent SDOF structure. He proposed an equivalent-velocity spectrum (V_E) to calculate total input energy per unit mass (E_i/m) where T_G represents the predominant period of ground motion.

$$\frac{E_i}{m} = \frac{1}{2}(V_E)^2 \tag{1.2}$$

$$V_E = 2.5\, T_n \qquad \text{for} \quad T_n \leq T_G \tag{1.3}$$

$$V_E = 2.5\, T_G \qquad \text{for} \quad T_n \geq T_G \tag{1.4}$$

Uang and Bertero published a report in 1990 about energy concept in earthquake resistant design. Their main purpose of the study was to assess the difference in physical meanings between absolute and relative energy methods. They also aimed to test the reliability of predicting input energy of MDOF system from SDOF system. In the report, they developed input energy equivalent velocity spectra for different ductility ratios and ground motion records. The result showed that there is no difference between the two energy methods for intermediate structural periods (0.3s – 5.0s). However, there is a significant difference for short and long structural periods. The main difference for short and long structural periods is in terms of peak ground velocity, which plays an important role. They suggested using absolute energy method for short periods and relative energy method for long periods. They used the experiment data of six-story steel building to test the accuracy of predicting input energy of MDOF system from input energy spectra of the SDOF system. The study results showed that there is an excellent match between experiment data and input energy spectra proposed by Akiyama. Finally, they carried out several experiments on

steel beams, reinforced concrete shear walls and composite beams to study the energy dissipation capacity of structural members under cyclic loads. They concluded that it is hard and complex to predict energy dissipation capacity of structural members because it is not unique and depends mainly on loading path and deformation.

Fajfar et al. (1990) attempted to find the best formulation to express the damage capacity of ground motion for medium-period range structures (0.5 s – 5.0 s). They believed that only peak ground acceleration is not an adequate parameter to define the intensity of ground motion. They also claimed that the maximum input energy of structure and relative displacements during an earthquake are two significant parameters for expressing structural damage. 40 ground motion records were used in the study to investigate inelastic displacement and input energy spectra. They proposed formulation with parameters of peak ground velocity and ground motion duration as an adequate instrument for measuring ground motion damage capacity of medium-period structures.

Another study by Fajfar et al. (1992) was taken to investigate energy demand and supply of SDOF systems. These systems were selected with different damping ratios, strength, period, ductility factors and hysteretic behaviors under six ground motion groups. The survey of results showed that the maximum input energy emerges to the structures with natural periods close to the predominant period of the earthquake. The study modified the formula for estimation of maximum input energy that was proposed by Kuwamura and Galambos (1989). They claimed that the ratio of hysteretic to input energy is the most stable parameter because it is dependent on the damping ratio and not much dependent on structural and ground motion parameters.

Zhu et al. (1993) wanted to extend the energy-based design concept to MDOF systems, and they focused on RC ductile moment-resisting frames (DMRF). The study also examined the validity of using equivalent SDOF systems to predict input energy on DMRF buildings during seismic action. 45 strong ground motion records were selected and divided into three groups according to the ratio of peak ground

acceleration to velocity (A/V). DMRFs with three different number of stories (4,10 and 18) were selected and designed to observe energy input and its components. They claimed that the values of input energy and hysteretic energy are adequate parameters to define the performance of DMRF buildings. However, these parameters are not adequate to describe the distribution path of inelastic deformation through stories and members. They claimed that it is possible to estimate input energy of low and medium-rise DMRF buildings using an equivalent SDOF system. However, the prediction method did not work for 18 story frame which means that the higher modal contributions are significant and cause underestimation of input energy.

Energy response of steel moment-resisting frames was studied by Shen and Akbas (1999) to extend energy design concept from SDOF systems to MDOF system and develop a rational energy design process for steel moment-resisting frames. Energy response of 3, 6 and 10 story steel moment-resisting frames with different bay lengths under six ground motion records were obtained by NLTH analysis. The results show that dissipation of energy in the form of damping is dominant in weak earthquakes, and as the ground motion gets stronger, the percentage of damping decreases whereas hysteretic energy increases. They stated that the distribution of damping and hysteretic energy is independent of ground motion parameters, and it is much dependent on structure. The distribution pattern of energy response shows that the distribution of hysteretic energy dissipation is more uniform for taller structures because of higher modal effects. They stated that there is a limitation in using equivalent SDOF systems to predict the response of real buildings, and more research is needed to develop an energy design concept.

Akbas et al. (2001) proposed an energy design method for steel moment-resisting frames that considers energy input earthquake according to structure and ground motion properties. Distribution pattern of energy throughout the structure and energy dissipation capacity of members are taken into account in the method. The method contains formulas and graphs to calculate input energy and damping energy of structures under seismic action. Then hysteretic energy was calculated by subtraction

of input energy from damping energy. According to this study, the distribution path of hysteretic energy is independent of ground motion, and it is possible to calculate the hysteretic energy portion of each story and members. Finally, 3, 6, and 10 story steel frames were designed with the proposed method, and the results were compared with the ones achieved by the conventional force-based design method. They concluded that the proposed energy design method resulted in better distribution of plastic hinges and strong column-weak beam mechanism.

A large number of ground motions were used on SDOF systems to obtain hysteretic and input energy spectra by Manfredi (2001). He tried to propose a new energy-based design method and extend the energy spectra of SDOF systems to multi-story buildings. He stated that the relation between hysteretic and input energy mostly depends on ductility demand and not dependent on ground motion characteristics. The proposed method for computing input and hysteretic energy is consistent with the ductility demand. In the design process, a seismic index based on ground motion parameters was proposed to estimate the required cyclic work for the dissipation of all hysteretic energy. He claimed that it is a useful way to take the duration effect of ground motion.

Khashaee et al. (2003) conducted extensive research about energy time histories of SDOF systems using 20 ground motion records and they summarized results. The results showed that despite some previous studies, input energy does not only depend on earthquake properties but also depends on structural property like ductility, damping, and hysteretic type. They stated that maximum strength and energy demand do not occur at similar times. So, strength demand should also be considered while developing an energy-based design concept. The results indicated that damping ratios less than 5 percent do not have a significant effect on the input energy, but a serious influence on the damage potential. So input energy should not be considered as a structural damage index. The report examined existing methods for evaluating input energy of structure, distribution of input energy components, specially hysteretic energy distribution, and the structural and ground motion parameters that affects them.

They claimed that the distribution of energy and shear force through the stories are independent of duration and frequency content of ground motion. According to their results it was interesting to observe that maximum shear force occurs in the first story, while maximum ductility and energy demand do not necessarily appear in the first story. Authors concluded that ductility has a major influence on the story-wise distribution of energy.

Chou and Uang (2003) presented a method based on static pushover analysis to predict energy demand at each story of MDOF systems during seismic action. They emphasized the contribution of the second mode on input energy and its distribution among stories. They tried to predict the total input energy of MDOF system from the equivalent SDOF system using first and second modes. Ductility factor of each mode is determined for establishing constant-ductility energy spectra and calculating input energy.Then static pushover analysis is used for both modes to predict energy distribution pattern among stories. They claimed that the proposed method is accurate for low-rise and mid-rise frames.

In the following years, more researches were carried out to propose energy-based design methods and develop seismic energy concepts for MDOF systems by Estes and Anderson (2004), Mollaioli et al. (2004) ,Surahman (2007) and Li et al. (2007).

The relationship between relative and absolute input energy in seismic energy concept was studied again by Kalkan and Kunnath in 2008. They examined the difference of absolute and relative input energy on both SDOF and MDOF systems under a wide range of ground motion parameters considering near-fault and far-fault effects. They claimed that the results of absolute and relative input energy are very close for far-fault records. However, for near-fault records with large acceleration pulse, there is a significant difference between two definitions. While some researchers believe absolute input energy is more meaningful in seismic energy concept, they stated that relative input energy is more meaningful for near-fault motions.

In order to find a suitable energy-based parameter for seismic damage assessment of MDOF systems, Amiri et al. (2008) analyzed energy time histories of 40 RC frames under four ground motion records. They believed that total input energy is highly dependent on ground motion duration. So, input energy is not an adequate parameter to distinguish damage potential of low duration-high amplitude and long duration-low amplitude ground motions. For this purpose, besides total input energy, maximum momentary input energy is studied. The results show that, in low duration-high amplitude ground motions like Naghan and Kobe, energy transforms to the structure in short duration and in these cases, maximum momentary input energy is a more meaningful parameter for potential damage estimation.

Leelataviwat et al. (2009) presented an energy-based method to determine the target displacement of MDOF structures. The proposed method uses nonlinear pushover analysis and calculates the area under the force-displacement curve to achieve energy capacity curve of the structure. Then the energy demand curve is calculated with input energy formula and ductility factor. Finally, target displacement of structure is obtained with the intersection of energy capacity curve and energy demand curve. They compared the results of the proposed method with the result of NLTH analysis and well-known methods presented in FEMA and ATC40 to determine target displacement of 3 story steel frame. They stated that calculated displacement demand by proposed energy method is reliable compared to other methods.

Guan and Du (2013) stated that only few studies have focused on the distribution of hysteretic energy in energy-based design. Prediction of hysteretic energy from input energy and the distribution of hysteretic energy among stories and elements are the main focus of the study. They aimed to develop the energy-based design concept for MDOF structures. A 6 story RC frame was selected to carry out NLTH analysis under El Centro and Northridge ground motion records with different scale factors. They stated that the ratio of hysteretic to input energy is not very sensitive to ground motion characteristics like peak ground acceleration (PGA). However, the distribution of hysteretic energy is effected by ground motion and PGA. The result shows that as

PGA increase, the accumulation of hysteretic energy moves from the second story to the first story, and most of the energy is dissipated at lower stories.

A popular procedure was proposed by FEMA-356 (2000) to obtain the target displacement of structures using pushover analysis. However, the effect of cyclic loading was not considered in the suggested method. To overcome this issue, an energy-based approach is suggested by Massumi and Monavari (2013) to determine the target displacement of RC moment-resisting frames. In the proposed method, structures were analyzed using cyclic loading, and energy at each cycle of loading was calculated. Then, pushover analysis was applied to obtain the force-displacement curve until the collapse of the structure. Finally, the target displacement was determined, equalizing the sum of the energy of all cycles with the energy of pushover analysis. The obtained results were rational and close to target displacements that were proposed by FEMA-356.

Okur and Erberik (2014) worked on the adaptation of energy-based design procedures for Turkish RC buildings. The first part of the study focused on the estimation of input energy. In the second part, they tried to estimate the hysteretic energy for SDOF and MDOF systems. Story-wise distribution of the hysteretic energy was also taken into account in their work. They studied the hysteretic to input energy (E_h/E_i) for many SDOF systems under different structural properties and several ground motions. The results showed that the E_h/E_i ratio is stable within the fundamental period range of (0s~0.3s) and for periods longer than 0.3s, the E_h/E_i ratio decreases as the fundamental period increases. It was reported that a mean value of 0.7 for the E_h/E_i ratio can be assumed for inelastic systems. In their study, the story-wise hysteretic energy distribution of several RC frames with different numbers of stories and bays under a single ground motion was plotted. The results showed that the dissipation energy contribution of lower stories are more for low-rise buildings. However, the results showed that hysteretic energy demand in upper stories does not increase significantly as the number of stories increase.

A simple and practical energy-based design methodology was proposed by Merter and Ucar (2014) for RC frames. In the methodology, energy demand was calculated by interstory drift ratio according to ATC-13 (1985) and equivalent lateral seismic force of stories according to TEC (2007). The method was limited to regular and mid-rise RC frames. The same researchers published another energy-based study in 2017. In this latter study, contribution of the dissipated hysteretic energy at column and beam hinges in RC frames was the main focus of the study. They concluded that as expected, a significant amount of energy is dissipated by beam hinges.

Distribution of hysteretic energy in MDOF systems was also taken into account by Tu and Zhao (2018). They evaluated the story-wise distribution of hysteretic energy in MDOF systems. In this study, a formulation was proposed for the estimation of the ratio of hysteretic energy of each story to total hysteretic energy. The validity of the proposed formula was verified using NLTH analysis and comparing the results. The authors also claimed that in structures with the number of stories more than three, maximum hysteretic energy occurs at two-thirds height from the base.

Alici and Sucuoglu (2018) focused on input energy of energy-based concept, and they aimed to develop a method for prediction of input energy of near-fault motions for elastic and inelastic systems. For this reason, 157 near-fault ground motions were selected to study the near-fault effects on earthquake input energy. A model was proposed for estimation of the input energy of the near-fault ground motions by using nonlinear regression analysis. In their study, the effect of damping ratio and lateral strength ratio on near-fault input energy spectra were also considered. They stated that the effect of damping is negligible on the input energy spectra for elastic and inelastic systems. In the study input energy of structural systems with 5% damping ratio and different reduction factors (R=1, 2, 4, 6) were examined. The results showed that while reduction factor has some effect on input energy of near-fault motions for short-period systems, near-fault input energy from near-fault records is independent of the reduction factor for intermediate and long period structures.

1.3. Objective and Scope

Input energy applied to a structure depends on both structural properties and ground motion characteristic and estimation of the input energy is one of the most challenging parts of energy-based design philosophy. Surveying the previous literature about energy-based concept show that mostly, prediction of the input energy is the main focus. Hysteretic energy, which is the representative of inelastic deformation capacity of the structures, is another challenging part of the energy-based design concept, and in order to develop a practical energy-based design or assessment method, it is vital to estimate the hysteretic energy demand of structures and determine the distribution pattern of the hysteretic energy through the structure. However, estimation of hysteretic energy and its distribution in RC structures have been highlighted by a few studies (Guan and Du, 2013; Okur and Erberik, 2014; Tu and Zhao, 2018). There are also studies that focused on hysteretic energy in a detailed manner. However steel frames were used in these works (Uang and Bertero, 1990; Akbas et al., 2001; Leelataviwat et al., 2009; Akbas et al., 2016).

This study aims to carry out an energy-based evaluation on RC moment-resisting frames, with estimation of hysteretic energy and its story-wise and member-wise distribution. For this reason, RC moment-resisting frames with different numbers of stories and bays are selected, and their energy response under 20 ground motions are evaluated.

The outline of the thesis is described as below:

- Chapter 2 is allocated to describe the theory of energy-based design concept. It is shown how the energy balance equation is derived from the equation of motion for SDOF systems. Also, relative and absolute energy equations and

their differences are discussed. The last section of the chapter explains how is to extend the energy equation from SDOF systems to MDOF systems.

- In Chapter 3, selected RC moment-resisting frames and their geometric and material properties are described. Summary of the design process and selected standards for applied loads and design are reported. In the next part of the chapter, finite element model of the frames are created using the SAP2000 software. Finally, the structural analysis results of the frames and design summary of all structural sections are presented.
- Chapter 4 is dedicated to NLTH analysis of the case study frames. There is a brief summary of the lumped plasticity modeling and existing hysteresis models of reinforced concrete sections. The elastic models of frames are converted to nonlinear models to carry out time history analysis. For this purpose, 20 ground motions with different characteristics are selected.
- Chapter 5 presents the NLTH analysis results of Chapter 4 to calculate the time history of input energy and its components. The energy results are presented and discussed in three main parts. First, the input energy is presented in a parametric manner to discuss the effect of structural properties and ground motion characteristics on input energy. Then the ratios of hysteretic energy to input energy for all analysis cases are calculated. The results are presented in figures and tables to have a better understanding of this energy parameter. The last section of the chapter, which is the main focus of this work, is dedicated to the story-wise and member-wise distribution of hysteretic energy. The percentage of dissipated hysteretic energy by each structural joint is calculated and presented in the figures for the six RC frames under 20 ground motions.
- Chapter 6 presents a brief summary and conclusion drawn from the given results. Limitations of this study and recommendations for future studies are also discussed.

CHAPTER 2

ENERGY-BASED SEISMIC RESPONSE

2.1. Introduction

An energy-based design philosophy was proposed by Housner for the first time in 1956. The energy method is based on the premise that the energy demand of the structure during seismic action can be estimated and the energy supply of the structure can be provided. In order to have a satisfactory design, the structural energy supply should be larger than structural energy demand.

The energy-based method makes it is possible to take into account the cumulative damage of structure under the effect of ground motion duration, which is impossible with the conventional design method. Housner presented a formula for input energy of SDOF systems. In the following years, many studies have been done to develop the energy-based design concept from SDOF systems to MDOF systems (McKevitt et al., 1980; Akiyama, 1985; Zhu et al., 1993; Shen and Akbas, 1999; Manfredi, 2001; Chou and Uang, 2003; Amiri et al., 2008).

In the energy-based approach, the input energy, which is representative of the intensity of the seismic action, is transmitted to the structure by kinetic energy, damping energy, elastic strain energy, and hysteretic energy. Kinetic energy represents the work done by inertia forces, and elastic strain energy is the stored energy in the form of elastic deformation. Damping energy reflects the dissipated energy by damping material. Hysteretic energy represents the dissipated input energy through cumulative plastic deformation, and it shows damage potential of the structure (Khashaee et al., 2003).

The energy equation is developed by integration of the equation of motion. In this chapter, the equation of motion would be reminded, and the derivation of the energy balance equation from the equation of motion for SDOF systems is presented.

Absolute and relative energy equations that were proposed by Uang and Bertero are mentioned, and their different physical meanings are discussed. In the last section, the extension of the energy equation from SDOF systems to MDOF systems is described.

2.1.1. Equation of Motion

Figure 2.1 shows an idealized SDOF system under base excitation where the inverted pendulum moves with the ground. Ground displacement during an earthquake is represented by u_g and u is the relative displacement of the mass with respect to the ground. The total (or absolute) displacement of the mass, u_t is equal to

$$u_t = u_g + u \tag{2.1}$$

Velocity and acceleration terms can be written by taking the first and the second derivative of Equation 2.1 with respect to time, respectively.

$$\dot{u}_t = \dot{u}_g + \dot{u} \tag{2.2}$$

$$\ddot{u}_t = \ddot{u}_g + \ddot{u} \tag{2.3}$$

In the following figures and equations *m*, *c*, *k* and f_s represent mass, viscous damping coefficient, stiffness and restoring force of SDOF system, respectively.

In the linear system f_s is equal to ku and force is proportional to displacement. In the nonlinear system, f_s is a nonlinear function of displacement, and it represents the hysteretic behavior of the system under dynamic loading.

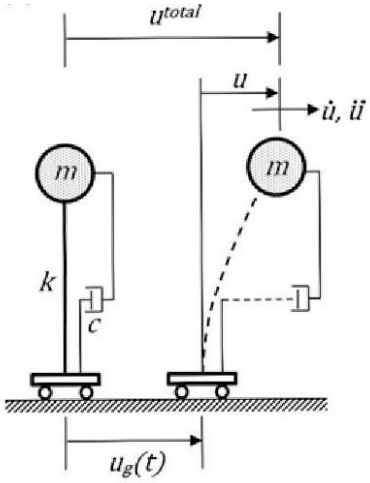

Figure 2.1. SDOF system under base excitation (Sucuoglu and Akkar, 2014)

Equation of motion of an inelastic (SDOF) system subjected to horizontal earthquake component can be written as

$$m\ddot{u}_t + c\dot{u} + f_s = 0 \tag{2.4}$$

Using Equation 2.3, Equation 2.4 can be shown as

$$m\ddot{u} + c\dot{u} + f_s = -m\ddot{u}_g \tag{2.5}$$

2.2. Energy Equation for SDOF Systems

In 1990, Uang and Bertero proposed two equations of energy, which are absolute and relative energy equations. Derivation of these two equations are reported as below.

2.2.1. Absolute Energy Equation

It is obtained by taking the integral of Equation 2.4 with respect to the relative displacement (u) for the whole time history record.

$$\int m\ddot{u}_t du + \int c\dot{u} du + \int f_s du = 0 \tag{2.6}$$

Using Equation 2.1 and replacing u by $u_t - u_g$ in the first term of Equation 2.6

$$\int m\ddot{u}_t du = \int m\ddot{u}_t d(u_t - u_g) =$$

$$\int m\frac{\dot{u}_t}{dt}du_t - \int m\ddot{u}_t du_g = \frac{m(\dot{u}_t)^2}{2} - \int m\ddot{u}_t du_g \quad (2.7)$$

Substituting Equation 2.7 into Equation 2.6

$$\frac{m(\dot{u}_t)^2}{2} + \int c\dot{u}du + \int f_s du = \int m\ddot{u}_t du_g \quad (2.8)$$

The first term of Equation 2.8 represents 'absolute' kinetic energy(E_k') as

$$E_k' = \frac{m(\dot{u}_t)^2}{2} \quad (2.9)$$

The second term of Equation 2.8 represents damping energy(E_D) as

$$E_D = \int c\dot{u}du = \int c\dot{u}^2 dt \quad (2.10)$$

The third term of Equation 2.8 is absorbed energy (E_a) that is composed of recoverable elastic strain energy(E_s), and irrecoverable hysteretic energy(E_h) as

$$E_a = \int f_s du = E_s + E_h \quad (2.11)$$

Elastic strain energy E_s is given by

$$E_s = \frac{(f_s)^2}{2k} \quad (2.12)$$

The right-hand side of Equation 2.8 is called absolute input energy (E_i') since it is in terms of absolute or total acceleration($\ddot{u}_t$).

$$E_i' = \int m\ddot{u}_t du_g \tag{2.13}$$

So Equation 2.8 can be written as

$$E_i' = E_k' + E_D + E_a = E_k' + E_D + E_s + E_h \tag{2.14}$$

Equation 2.14 is called as the absolute energy equation.

2.2.2. Relative Energy Equation

It is obtained by taking the integral of Equation 2.5 with respect to the relative displacement (u) for the whole time history record.

$$\int m\ddot{u}du + \int c\dot{u}du + \int f_s\, du = -\int m\ddot{u}_g du \tag{2.15}$$

The first term of the equation can be written as

$$\int m\ddot{u}du = \int m\frac{d\dot{u}}{dt}du = \int md\dot{u}(\dot{u}) = \frac{m(\dot{u})^2}{2} \tag{2.16}$$

Substituting Equation 2.16 into Equation 2.15, one can get

$$\frac{m(\dot{u})^2}{2} + \int c\dot{u}du + \int f_s\, du = -\int m\ddot{u}_g du \tag{2.17}$$

The first term of Equation 2.17 is in terms of relative velocity, and it is called 'relative' kinetic energy (E_k) as

$$E_k = \frac{m(\dot{u})^2}{2} \tag{2.18}$$

Second and third terms of Equation 2.17 are the same as the terms in absolute energy equation, and they represent damping energy (E_D) and absorbed energy (E_a) respectively. The right-hand side of Equation 2.17 is called relative input energy (E_i) and it is in terms of relative acceleration ($\ddot{u}$)

$$E_i = -\int m\ddot{u}_g du \tag{2.19}$$

The relative energy equation may be expressed as

$$E_i = E_k + E_D + E_a = E_k + E_D + E_s + E_h \tag{2.20}$$

In Equations 2.14 and 2.20, kinetic energy E_k and elastic strain energy E_s are the instant response of the structure and they vanish at the end of strong ground motion. Damping energy E_D and hysteretic energy E_h are the irrecoverable and cumulative responses of the structure. Considering the inelastic behavior of the structure, E_k and E_s are very small compared to E_D and E_h during seismic action. It is possible to state that almost all the input energy of the earthquake is dissipated by damping energy E_D and hysteretic energyE_h at the end of the earthquake (Shen and Akbas, 1999).

$$E_i \cong E_D + E_h \tag{2.21}$$

Equation 2.21 can also be written for absolute energy equation by replacing relative input energy with absolute input energy.

2.2.3. Discussion About the Two Energy Approaches

Although both approaches are achieved by derivation of the equation of motion, there is a slight difference between the physical meanings of these methods. As it is given

in Equation 2.13, absolute input energy E_i^t is the integral of $m\ddot{u}_t$ which is the inertia force exerted to the structure. Equation 2.4 shows that this force is equal to the total damping force plus restoring force applied to the foundation of the structure. Hence, absolute input energy E_i^t reflects the work done by base shear at the foundation. An idealized model of an SDOF system for absolute energy equation is shown in Figure 2.2 a.

Relative input energy E_i is in terms of $m\ddot{u}_g$ as it is mentioned in Equation 2.19. This is analogous to the equivalent static lateral force in a fixed-based system that the effect of rigid-body translation of structure is neglected (Uang and Bertero, 1990). The idealized model of an SDOF system used for relative energy equation is shown in Figure 2.2 b.

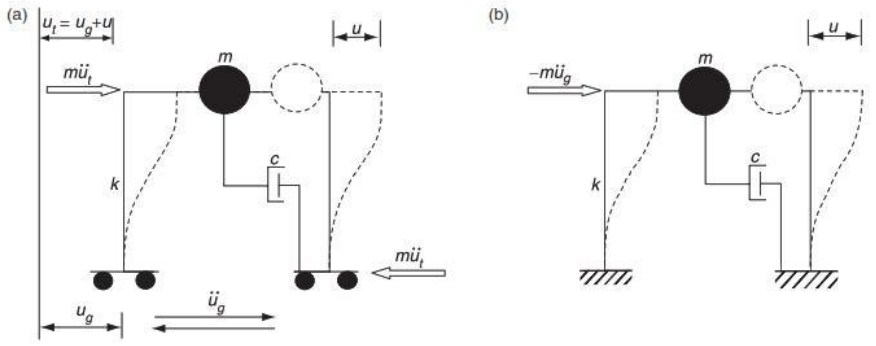

Figure 2.2. Idealized models of SDOF system for (a) absolute and (b) relative energy equation. (Kalkan and Kunnath, 2008)

Some studies have discussed the differences between the two methods and compared them. Uang and Bertero (1990) stated that there is no difference between relative and absolute input energy for the structures having fundamental periods within the ranges of 0.3s-5s. Chopra (1995) and Bruneau and Wang (1996) found the relative energy equation more meaningful since all the internal forces are computed using relative displacements and velocities. Similarly, Kalkan and Kunnath (2008) stated that the results of the relative input energy are more rational for near-fault ground motion records.

Regarding the above discussions, relative energy approach is selected in this study because the equation has been verified by many studies for intermediate fundamental period ranges. Also, it is more practical to use relative velocity and acceleration data regarding the output parameters of the finite element structural analysis program. Hence relative energy equation parameters are used in all calculations and results in this study.

2.3. Energy Equation for MDOF Systems

It is possible to extend equations of motion and energy from SDOF systems to MDOF systems. The idealized MDOF system is shown in Figure 2.3.

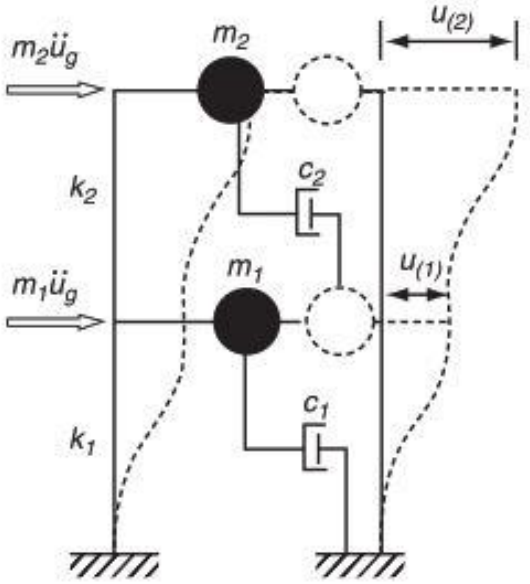

Figure 2.3. Idealized models of MDOF system for energy equation. (Kalkan and Kunnath, 2008).

The equation of energy for a building with n degrees of freedom is described as below (Kalkan and Kunnath, 2008).

$$\frac{1}{2}\dot{U}^T M\dot{U} + \int \dot{U}C dU + \int F_s\, dU = -\int Mr\ddot{u}_g dU = -\int Mr\ddot{u}_g \dot{U} dt \qquad (2.22)$$

where M is the diagonal mass matrix, C represents the damping matrix, U is the relative displacement vector, $\dot{U}$ is the relative velocity vector, F_s is the n-dimensional non-linear stiffness force matrix and r is the n-dimensional influence vector. Kinetic energy for a MDOF system is

$$E_k = \frac{1}{2}\dot{U}^T M\dot{U} \tag{2.23}$$

Damping energy for a MDOF system is

$$E_D = \int \dot{U} C dU \tag{2.24}$$

Absorbed energy for a MDOF system is

$$E_a = \int F_s \, dU = E_s + E_h \tag{2.25}$$

And finally, input energy for a MDOF system is

$$E_i = -\int Mr\ddot{u}_g \dot{U} dt \tag{2.26}$$

Overall, the complete energy equation for a MDOF system can be written as

$$E_i = E_k + E_D + E_s + E_h \tag{2.27}$$

CHAPTER 3

DESIGN OF THE CASE STUDY FRAMES

3.1. Introduction

In this study 3, 5, 7, and 9 story RC moment resisting frame building models with different number of bays are selected in order to study hysteretic energy performance of the MRF structures, using NLTH analysis. All span lengths of frames are taken as 6 meters from column centerlines, and all story heights are considered as 3 meters. Figure 3.1 shows the plan view of the floor for the 3 bay generic building model. Figure 3.2 shows elevation view of 3, 5, 7 and 9 story frame building models:

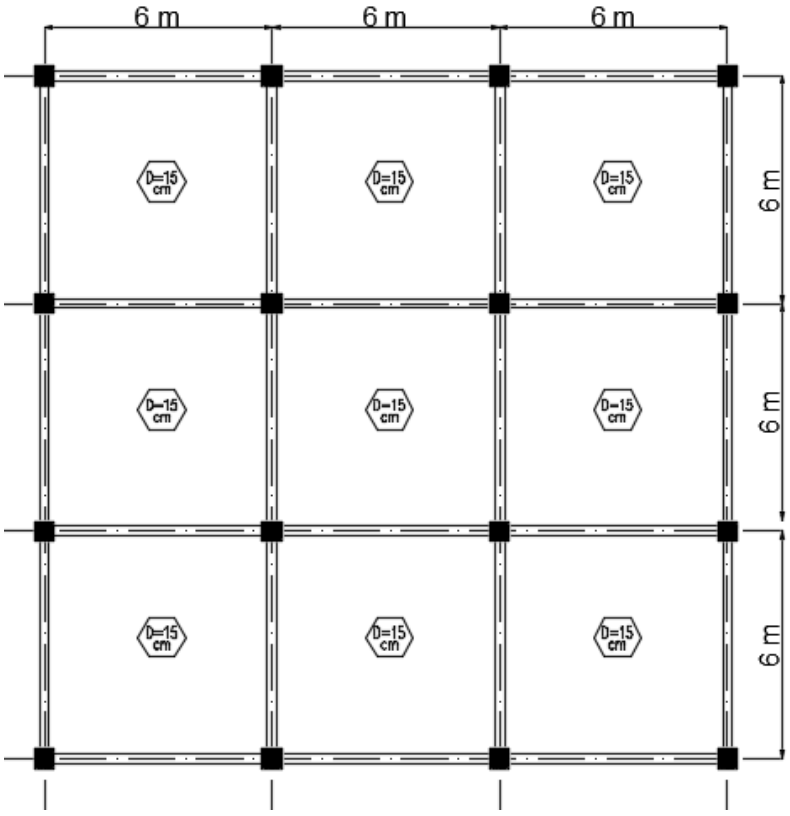

Figure 3.1. Floor plan view of the 3 bay building model

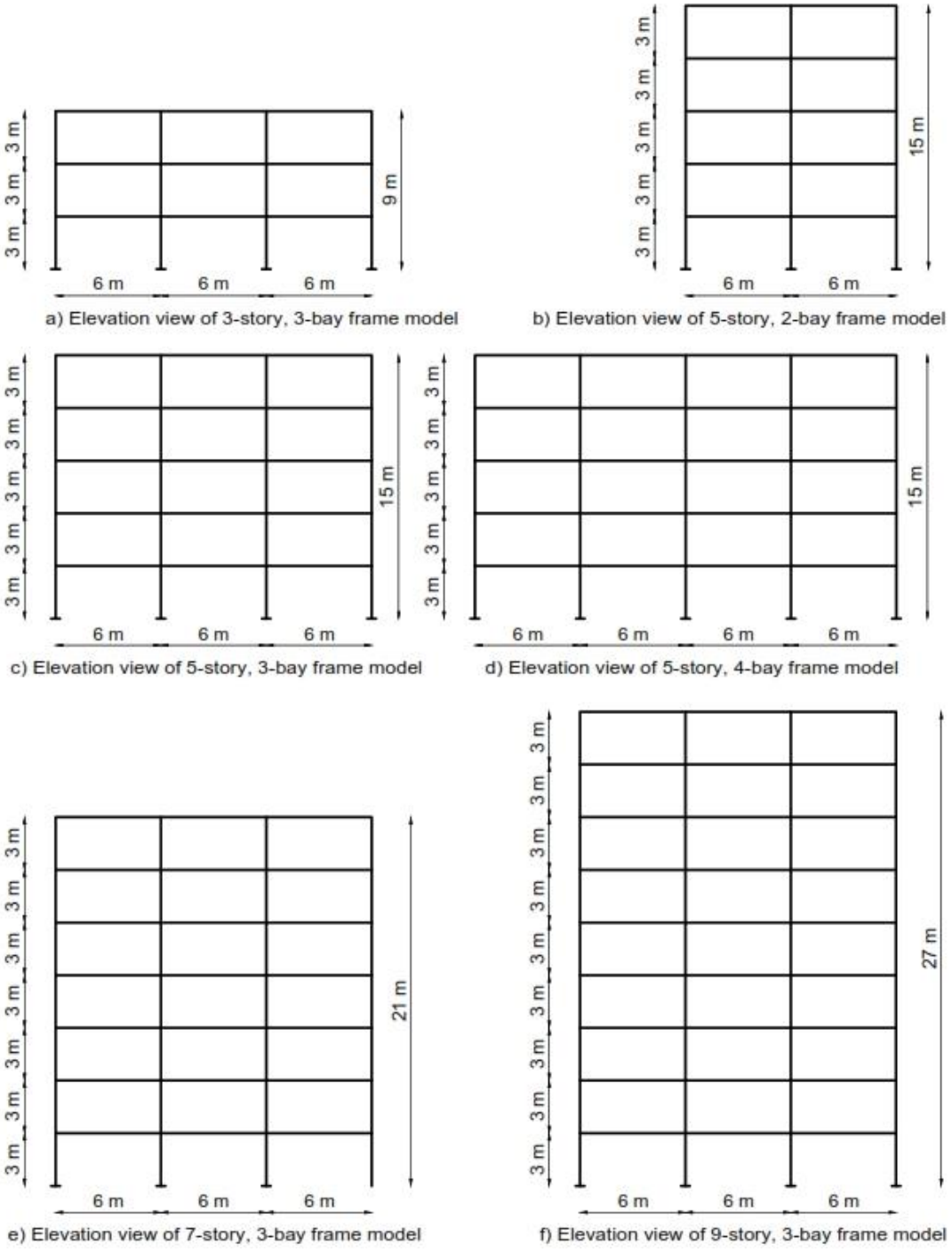

Figure 3.2. Elevation view of frame models

3.2. Material Properties

In the design and analysis process, C25 for concrete and S420 for reinforcement is used. Material properties are shown in Table 3.1.

Table 3.1. *Material properties*

Concrete Characteristic Compressive Strength	$f_{ck} = 25\ MPa$
Concrete Characteristic Tension Strength	$f_{ctk} = 1.75\ MPa$
Elastic Modulus of Concrete	$E_c = 30{,}000\ MPa$
Shear Modulus of Concrete	$G_c = 12{,}000\ MPa$
Yield Strength of Reinforcement Steel	$F_{yk} = 420\ MPa$
Elastic Modulus of Reinforcement Steel	$E_s = 200{,}000\ MPa$

3.3. Design of RC Frames

The selected RC moment resisting frames are designed and detailed to satisfy requirements according to TS500 (Requirements for Design and Construction of Reinforced Concrete Structures) and TBSC 2018 (Turkish Building Seismic Code). The conventional force-based design method is adequate for low and mid-rise ordinary RC frames. Modal response spectrum analysis with elastic section properties and 5% damping ratio is used for the RC frames under seismic action.

3.3.1. Gravity Loading

Applied gravity dead (G) and live load (Q) loads are selected, as stated in TS498 (Design Loads for Buildings). According to TS498 (1997), live load for residential buildings is selected as 2 kN/m^2 that is applied to the slabs uniformly. Flooring dead load is considered as 2 kN/m^2. Also, 3 kN/m wall weight load is applied to the beams directly. The live load reduction factors according to TS498 for residential buildings, are applied while designing frames.

3.3.2. Seismic Loading

The location of the selected frame models is assumed to be in Izmit city, in Kocaeli province of Turkey. Peak ground acceleration (PGA) of the selected site is 0.404g with a return period of 475 years (DD-2). According to TBDY (2018) Table 16.1, local soil class is assumed as ZD soil type which is composed of stiff clay and medium compact sand. Importance factor (I) and building usage class (BKS) are selected as 1 and 3, respectively, as stated in TBDY (2018) Table 3.1 for residential buildings. In order to investigate hysteretic behavior and energy dissipation of frames under earthquake, frames are designed as high ductile (A11) with structure system behavior factor (R) of 8 and over strength factor (D) of 3 according to Table 4.1 of the of TBDY. Horizontal elastic design spectrum is defined according to Chapter 2 of TBDY (2018). Elastic design spectrum for 5% damped response is shown in Figure 3.3.

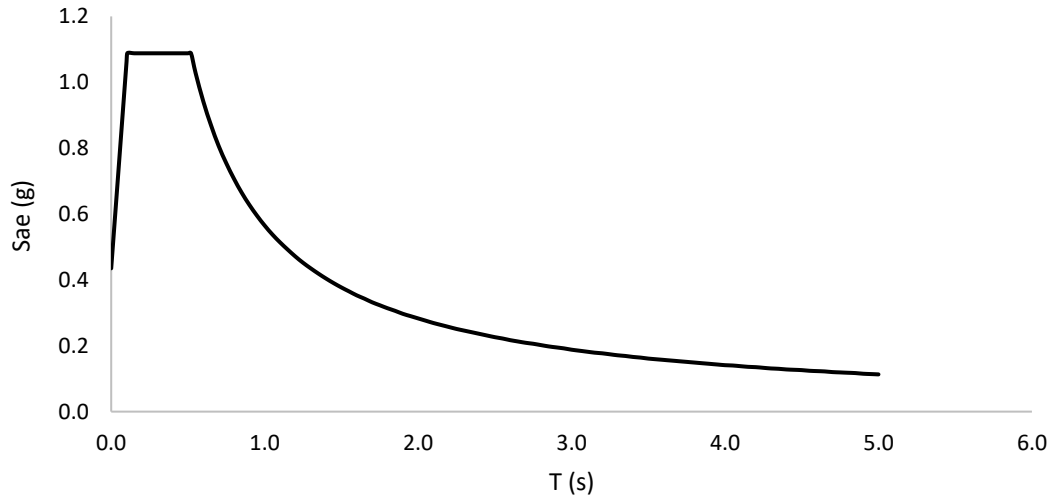

Figure 3.3. 5% damped response spectrum

3.3.3. Design Combinations

Design combinations are considered as reported in TS500 (2000) for gravity loads and TBDY (2018) for the combination of gravity loads and seismic action. Design combinations are displayed in Table 3.2, in which G is the dead load, Q represents the

live load, Ex is the earthquake load in x direction and Ey represents the earthquake load in y direction.

Table 3.2. *Design combinations*

1.4G+1.6G
G+Q+Ex+0.3Ey
G+Q+Ex-0.3Ey
G+Q-Ex+0.3Ey
G+Q-Ex-0.3Ey
0.9G+Ex+0.3Ey
0.9G+Ex-0.3Ey
0.9G+Ex+0.3Ey
0.9G+Ex-0.3Ey

3.3.4. Modeling of the Frames

All linear and nonlinear analysis in this study is carried out by SAP2000 structural analysis and design program. SAP2000 is a user friendly finite element software, which is used by many structural engineers. Also, in recent years, the program has been enhanced to include nonlinear analysis and performance-based design options.

Frame elements are used in order to model all columns and beams in moment resisting frames and shell elements are used for modeling slabs. Dynamic analysis is carried out with 5% viscous damping ratio.

According to TBSC (2018) Section 4.5, three-dimensional structural models have to be used for elastic analysis. Also, it is essential to have a three-dimensional model to consider 30 percent of the earthquake in orthogonal direction in design combination. So all buildings are analyzed as three-dimensional models with elastic section properties. TBSC (2018) Section 4.5 claims that cracked section rigidity should be used in force based design and effective section rigidity factors are suggested in Table 4.2 of the code. According to the table, flexure rigidity factor in moment resisting frame is 0.35 for beam elements and 0.70 for column elements, and flexure rigidity

factor for slab shell elements is 0.25. Figure 3.3 shows three dimensional finite element model of the 5-story 3-bay frame.

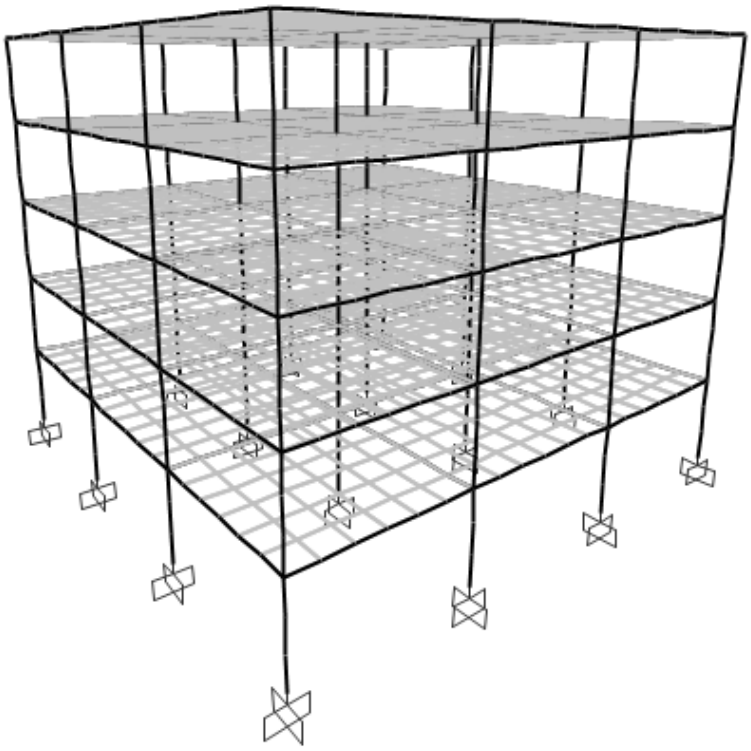

Figure 3.4. 3D finite element model of 5-story, 3-bay frame

3.4. Design Details and Member Sizes

First, all section dimensions are decided by primary design hand calculations. Then the structures are modeled as discussed before and designed under gravity and seismic loads according to TS500 and TBSC 2018.

Slab thickness is taken as 15 cm for all buildings. 15 cm thickness satisfies all strength and deflection requirements.

All beams are considered as T-beam section, since it is assumed that RC beams and slabs are cast monolithically like typical residential buildings. Beam dimensions for selected frames are decided as 25 cm x 45 cm with 100 cm effective flange width.

Although the dimension of beams does not change, the amount of reinforcement differs according to strength demand. While equivalent flange width contributes to the compression area and increases positive moment capacity, it also increases negative moment capacity because of the existing rebar in the upper section of the slab.

Column sections are square, and the section dimensions and reinforcements differ from story to story for all frames. Since the structures are chosen as high ductile moment resisting frames with R=8, strong column-weak beam check is also verified. According to the Turkish seismic code, in the beam-column joints, sum of the ultimate moment capacity of the columns shall be at least 20 % greater than the sum of ultimate moment capacity of the beams.

Table 3.3 shows some structural parameters of buildings like base shear, fundamental nature period, weight, and spectral acceleration. Table 3.4 and 3.5 represent the final sections and reinforcement details for all beams and columns in 3, 5, 7, and 9 story buildings. The presented transverse reinforcements for columns in Table 3.5 are valid for both perpendicular directions of the sections. Longitudinal reinforcement details of beams and columns are given in Figures 3.4 and Figure 3.5, respectively.

Table 3.3. *Structural analysis results of the frames*

Building Type	Base shear of an interior frame (KN)	Mass of an interior frame (ton)	First period (s)	Second period (s)	Elastic design spectral acceleration (g)
3-Story, 3-Bay	202	285.2	0.87	0.27	0.64
5-Story, 2 Bay	170	325.7	1.16	0.34	0.49
5-Story, 3-Bay	242	482.2	1.15	0.36	0.49
5-Story, 4-Bay	320	640.8	1.16	0.36	0.49
7-Story, 3-Bay	267	680.1	1.49	0.48	0.38
9-Story, 3-Bay	314	882.2	1.83	0.61	0.31

Table 3.4. *Member section design summary (longitudinal reinforcement).*

Building Type	Floor Number	Column size (cm)	Column Rebar	T-Beam Size (cm)	Beam Rebar	
					Top	Bottom
3-Story 3-Bay	1	35 x 35	8ϕ25	25 x 45	3ϕ18+6ϕ10	4ϕ16
	2	35 x 35	8ϕ25	25 x 45	3ϕ16+6ϕ10	3ϕ16
	3	35x 35	8ϕ20	25 x 45	3ϕ16+6ϕ10	3ϕ16
5-Story 2-Bays	1	50x50	12ϕ20	25 x 45	3ϕ18+6ϕ10	4ϕ16
	2	50x50	12ϕ20	25 x 45	3ϕ18+6ϕ10	4ϕ16
	3	50x50	12ϕ20	25 x 45	3ϕ18+6ϕ10	4ϕ16
	4	40 x 40	8ϕ25	25 x 45	3ϕ16+6ϕ10	3ϕ16
	5	40 x 40	8ϕ25	25 x 45	3ϕ16+6ϕ10	3ϕ16
5-Story 3-Bays	1	50x50	12ϕ20	25 x 45	3ϕ18+6ϕ10	4ϕ16
	2	50x50	12ϕ20	25 x 45	3ϕ18+6ϕ10	4ϕ16
	3	50x50	12ϕ20	25 x 45	3ϕ18+6ϕ10	4ϕ16
	4	40 x 40	8ϕ25	25 x 45	3ϕ16+6ϕ10	3ϕ16
	5	40 x 40	8ϕ25	25 x 45	3ϕ16+6ϕ10	3ϕ16
5-Story 4-Bays	1	50x50	12ϕ20	25 x 45	3ϕ18+6ϕ10	4ϕ16
	2	50x50	12ϕ20	25 x 45	3ϕ18+6ϕ10	4ϕ16
	3	50x50	12ϕ20	25 x 45	3ϕ18+6ϕ10	4ϕ16
	4	40 x 40	8ϕ25	25 x 45	3ϕ16+6ϕ10	3ϕ16
	5	40 x 40	8ϕ25	25 x 45	3ϕ16+6ϕ10	3ϕ16
7-Story 3-Bays	1	60x60	16ϕ20	25 x 45	4ϕ18+6ϕ10	4ϕ16
	2	60x60	16ϕ20	25 x 45	4ϕ18+6ϕ10	4ϕ16
	3	50x50	12ϕ20	25 x 45	4ϕ18+6ϕ10	4ϕ16
	4	50x50	12ϕ20	25 x 45	4ϕ18+6ϕ10	4ϕ16
	5	50x50	12ϕ20	25 x 45	4ϕ18+6ϕ10	4ϕ16
	6	40 x 40	8ϕ20	25 x 45	3ϕ16+6ϕ10	3ϕ16
	7	40 x 40	8ϕ20	25 x 45	3ϕ16+6ϕ10	3ϕ16
9-Story 3-Bays	1	70 x 70	20ϕ20	25 x 45	4ϕ18+6ϕ10	4ϕ16
	2	70 x 70	20ϕ20	25 x 45	4ϕ18+6ϕ10	4ϕ16
	3	60 x 60	16ϕ20	25 x 45	4ϕ18+6ϕ10	4ϕ16
	4	60 x 60	16ϕ20	25 x 45	4ϕ18+6ϕ10	4ϕ16
	5	50 x 50	12ϕ20	25 x 45	4ϕ18+6ϕ10	4ϕ16
	6	50 x 50	12ϕ20	25 x 45	3ϕ18+6ϕ10	4ϕ16
	7	50 x 50	12ϕ20	25 x 45	3ϕ18+6ϕ10	4ϕ16
	8	40 x 40	8ϕ20	25 x 45	3ϕ16+6ϕ10	3ϕ16
	9	40 x 40	8ϕ20	25 x 45	3ϕ16+6ϕ10	3ϕ16

Table 3.5. *Member section design summary (Transverse reinforcement).*

	Member Section (cm)	Number of Legged	Transverse Reinforcement	Spacing in Confinement Zone (cm)	Spacing in Central Zone (cm)
Column	35 x 35	2	φ10	10	20
	40 x 40	2	φ10	10	20
	50 x 50	3	φ10	10	20
	60 x 60	4	φ12	10	20
	70 x 70	5	φ12	10	20
Beam	25 x 45	2	φ10	10	17

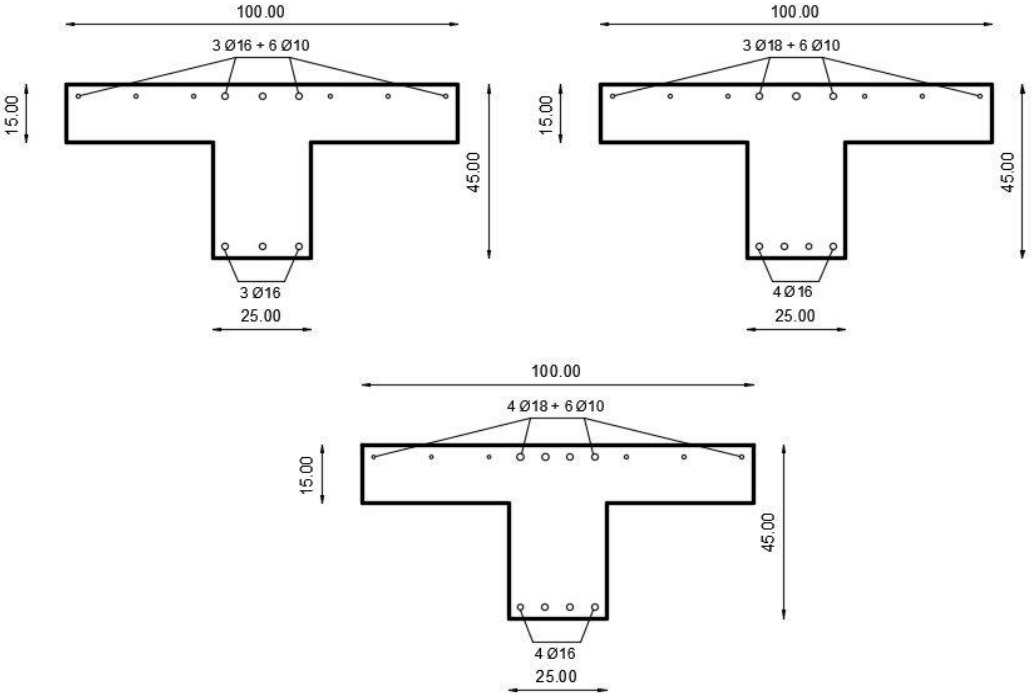

Figure 3.5. Interior beam reinforcement details

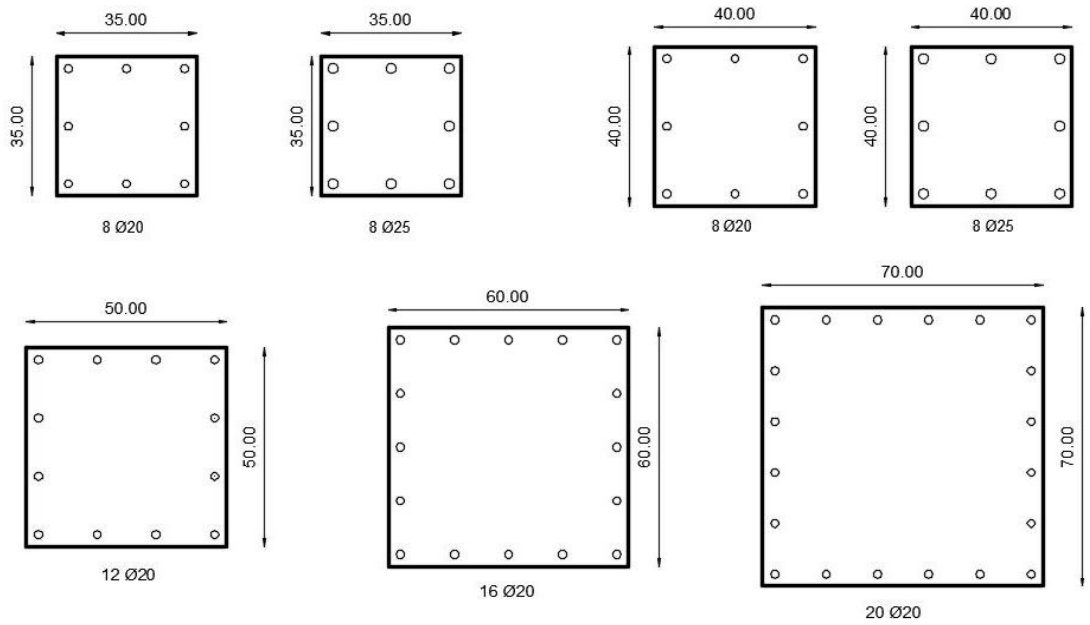

Figure 3.6. Column reinforcement details

CHAPTER 4

NONLINEAR MODELING AND ANALYSIS OF THE CASE STUDY FRAMES

4.1. Introduction

In order to investigate the energy-based seismic response of RC frame models under seismic action, nonlinear time history (NLTH) analysis is essential since it is possible to monitor the force-deformation relationship of all elements in each time step of ground motion record with NTHA. In this chapter, some general information about different types of nonlinear models is given first. Then, more details about the selected nonlinear model are presented. Finally, selected ground motions and nonlinear models of the case study frames are given.

4.2. Types of Nonlinear Models

Global models, discrete finite element models and micro finite element models are three main ways of modeling nonlinear structures. Global models are the simplest way of modeling nonlinearity of structures. In this method, the nonlinear behavior of the structure is represented by the selected degrees of freedom. The method is not always reliable, and it is not possible to study nonlinear behavior member by member. It is possible to increase the reliability of this method by selecting more degrees of freedom**.**

Micro finite element models are the most complex and advanced nonlinear models. In these models, the members are divided into many finite elements for which features like creep, relaxation, thermal effects, bond, and cracked geometric discontinuities are considered.

Discrete finite element models are more advanced and need more computational power comparing to global models. However, these models are simpler compared to the micro finite element models. Consequently, discrete finite element models propose the best choice between integrity and simplicity among nonlinear models. There are two types of discrete finite element models: distributed nonlinearity and lumped nonlinearity. In these models, the structural model is established by the assembly of interconnected elements with either distributed or lumped nonlinearities.

In lumped plasticity models, the nonlinearity of the element is concentrated at specific locations of the element, while the rest of the element is modeled with elastic properties. In this study, lumped plasticity model is used. It has sufficient accuracy with appropriate computational time, and it is possible to apply it with the SAP2000 software.

In distributed nonlinearity models, the plastic behavior of element can occur in any element section using numerical models, and it is one of the most accurate and reliable models. However, it is more complex and needs much computational time, especially in the case of NLTH analysis.

4.2.1. Lumped Plasticity Model

In this modeling approach, nonlinear properties and moment-curvature relationship of the section are applied to the specific region of the element that is expected to go under plastic deformation. This plastic zone is called the plastic hinge. Usually, nonlinear properties of the plastic hinge are lumped at one or two nodes which are assumed to be constant within plastic hinge length (Lp), while plastic hinge and the rest of element has elastic section properties. Figure 4.1 shows the actual curvature plot and idealized curvature plot by lumped plasticity model for a single cantilever column under horizontal force. As it is shown, the actual curvature behavior is similar to lumped assumption with constant plastic curvature within plastic hinge length.

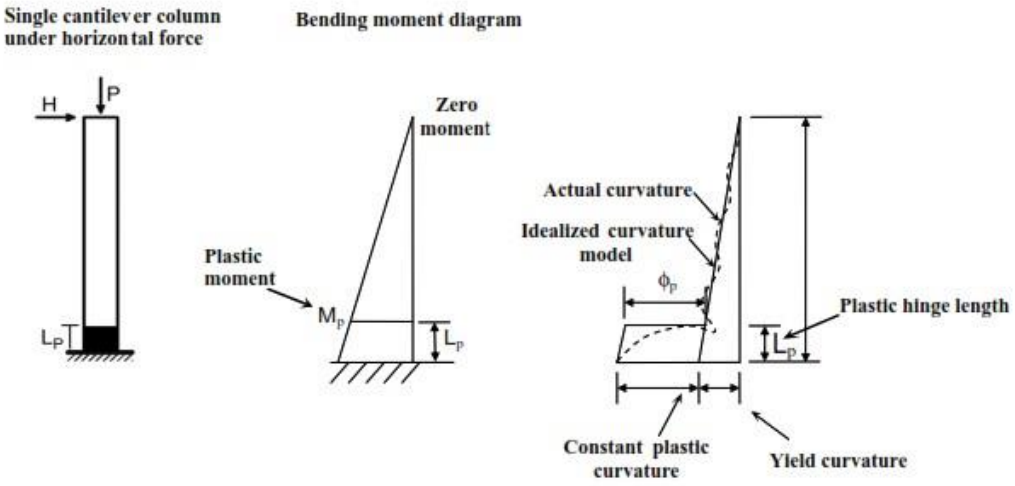

Figure 4.1. Comparison of actual and idealized curvature diagram (Aviram et al., 2008)

In moment-resisting frames maximum moment occurs at the ends of the columns and beams under seismic action. So, it would be rational to assume the concentration of plastic behavior of moment resisting frames in the end zones of the beams and columns elements.

4.3. Plastic Hinge

Plastic hinges play a vital role in lumped plasticity models. Many factors should be considered while selecting the length and type of plastic hinge. There are many studies about the use of plastic hinges that are beyond the scope of this study. In this section, selected type and length of the plastic hinge are described shortly.

4.3.1. Plastic Hinge Length (Lp)

Plastic hinge length (Lp) has an integral role in the nonlinear models, and it affects deformation capacity of members. Plastic rotation of the plastic hinge could be calculated by multiplying plastic curvature with plastic hinge length (Lp). Plastic

hinge length (Lp) in reinforced concrete members depends on many factors like axial force, section dimension, and section material properties. Numerous equations and methods have been proposed to predict the plastic hinge length. TBSC (2018) suggests that plastic hinge length should be equal to the half of the section depth (h/2) in the considered direction. This is a straightforward and practical assumption for the prediction of plastic hinge and it is used in this study for the sake of simplicity.

4.3.2. Plastic Hinge Types

Many plastic hinge models have been proposed by studies and implemented in structural analysis software. These plastic hinges are usually selected according to material type, structural model, and analysis method. There are simple hinge models like M (flexural nonlinear model in one direction) and P-M (axial and flexural nonlinear model in one direction) hinges for nonlinear static analysis and two-dimensional models. In the case of three-dimensional models, more complex hinge models like P-M-M (axial and flexural nonlinear model in two direction) should be considered. For NLTH analysis, the selected hinge could be capable of showing hysteresis behavior since hysteresis models make it possible to simulate the loading-unloading cycles and energy dissipation characteristics under time history of ground motions. As a result, in this study, a specific hysteretic model is assigned to the plastic hinge. In the following sections, different types of hysteresis models for reinforced concrete are briefly described. Also, details of the selected hysteresis model are given.

4.4. RC Hysteresis Models

Behavior of RC members and structures under cyclic loading is very complex, and a considerable number of studies and experiments has been done to find an analytical model to define realistic hysteretic behavior of RC members. Bilinear model is a simple elastic-perfectly plastic hysteresis model that was used in many studies and

developed by Veletsos and Newmark (1960). Stiffness degradation was not included in the model therefore it is not suitable for RC members or structures.

In 1966, a hysteresis model for RC members was proposed by Clough, in which degradation of stiffness and strain-hardening was included. In 1970, a more sophisticated hysteresis model was developed by Takeda et al. The model is more realistic, and complex compared to the Clough model. The flexural cracking, strain hardening, yielding, and stiffness degradation are all included in the model. Takeda model was developed and modified by many studies like Otani and Sozen (1972) and Powell (1975) to make it more realistic. Most of the proposed hysteresis models for RC members like Takeda and Clough can describe only hysteretic flexural behavior of RC, while shear capacity and pinching effect during hysteresis action is not considered. In the following years, a hysteresis model by Ozcebe and Saatcioglu (1989) was developed to describe combined shear and flexural behavior of RC members.

Pivot hysteresis model is also another common hysteresis model type for RC members. The model has been proposed by Dowell et al. (1998). It is a modified version of the Takeda model in which new parameters have been added to simulate the unloading degradation during hysteresis cycles.

An energy-based hysteresis model was proposed by Sucuoglu and Erberik (2003) to predict the seismic behavior of structures that show deterioration in strength and energy dissipation capacity. This is a memory dependent model and considers the previous cycles to calculate the deterioration within the member. It is more complex than the previous models and requires some additional parameters which can be determined by conducting low-cycle fatigue tests under constant amplitude loading.

Considering all the above mentioned hysteresis models, Takeda model is used in this study for modeling hysteresis behavior of hinges. In the next section, Takeda model is explained in more details.

4.5. Takeda Hysteresis Model

Takeda hysteresis model was developed based on the experimental result of RC beams and columns under reversal loads. As discussed in the previous section, shear damage and bond deterioration are not considered in the rules of the model. The model represents the hysteresis behavior of RC members with low to medium range of axial force so that the flexural failure mode is dominant. In this study, it is also assumed that the column and beam members have adequate shear strength with dominant ductile flexural behavior under seismic action. Takeda model has been used in many studies and it has been proven that it shows a reasonable response for flexural behavior of RC under cyclic loading.

16 rules are used in the hysteresis model to determine the stiffness of the member at each load and unloading step. Takeda model uses a trilinear moment-curvature curve (backbone) that consists of moment and curvature/rotation values for tensile cracking (C), yielding of longitudinal reinforcement (Y) and ultimate capacity (U) of the section. These values have to be defined for both positive and negative bending directions with the addition of origin point O (0, 0). Figure 4.2 shows the moment-curvature/rotation backbone for Takeda hysteresis model. Moment-curvature analysis is discussed in detail in Section 4.6**.**

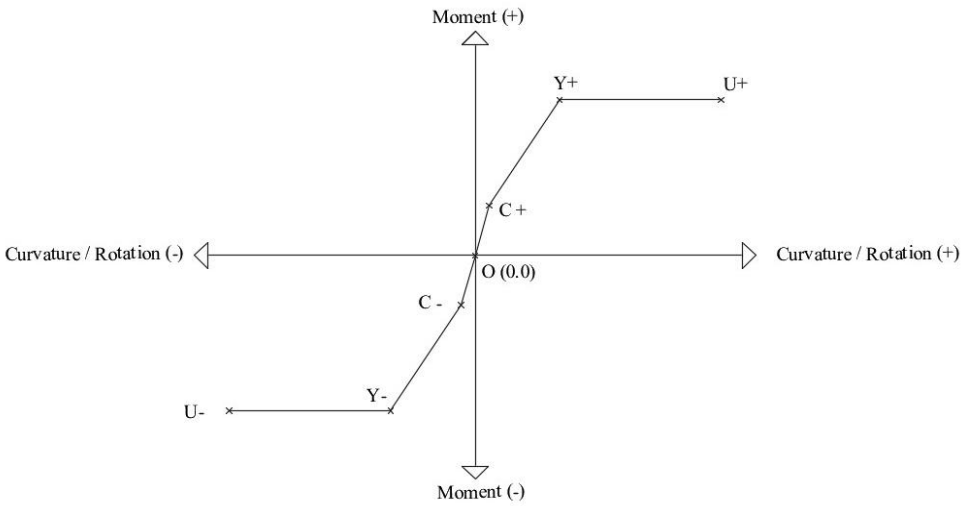

Figure 4.2. Backbone curve for Takeda hysteresis model

The rules of Takeda model are not stated in this report. Figure 4.3 only shows different rules of hysteresis model in different loading and unloading steps schematically.

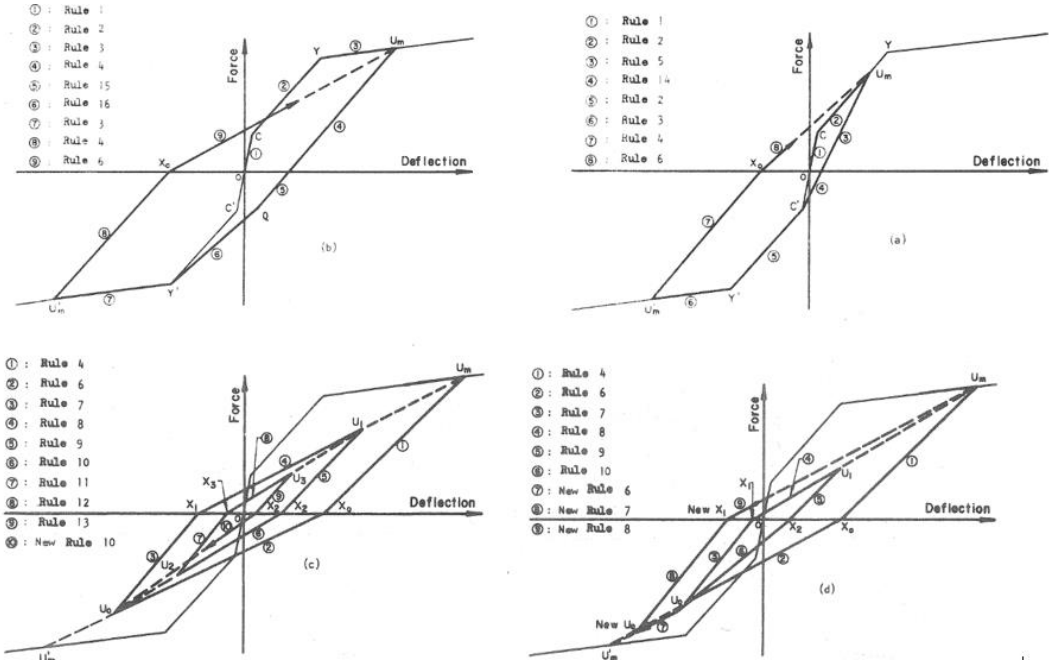

Figure 4.3. Takeda hysteresis rules (Otani and Sake, 1974)

Takeda hysteresis model is already implemented in SAP2000 software. In the following section, the employment of the Takeda model in SAP2000 is discussed.

4.5.1. Applying Takeda Hysteresis Model in SAP2000

It is possible to have a plastic hinge in SAP2000 software that describes hysteresis behavior of RC members by using nonlinear links. Link elements are used to connect two joints with a set of structural properties. There are many types of linear and nonlinear links in the software that should be selected according to the purpose. For defining hysteretic behavior, multi-linear plastic links are provided. Various types of hysteresis models are available like bilinear, pivot, and Takeda. Multi-linear plastic link is an uncoupled element with 2 nodes and each node with 6 degrees of freedom.

It is possible to select linear or nonlinear behavior for each degree of freedom. Then nonlinear properties like moment-rotation relations and hysteresis type can be defined to the nonlinear degrees of freedom. Figure 4.4 shows internal forces and moment for the nonlinear link element as described in SAP2000 manual.

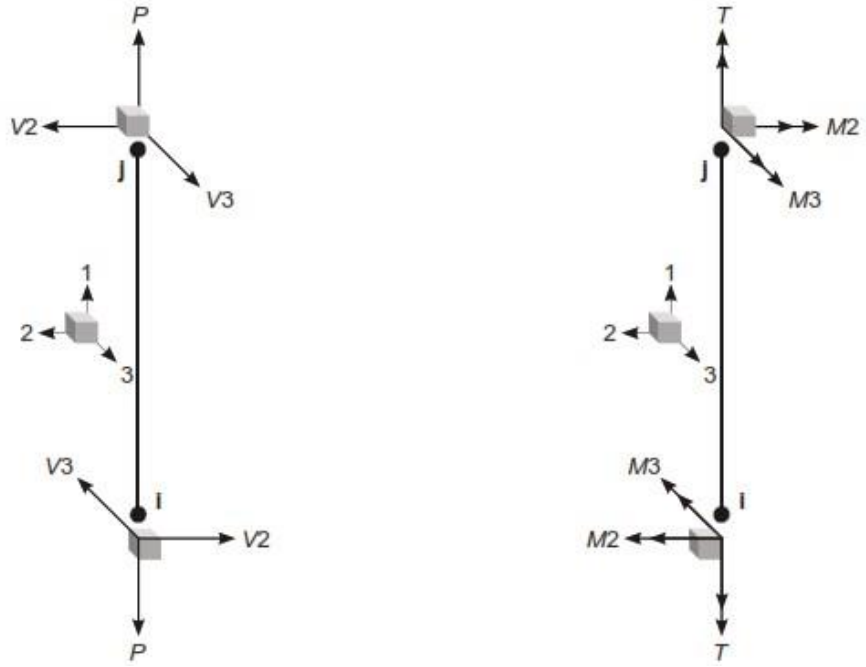

Figure 4.4. Internal forces and moments of link in SAP2000 (CSI Analysis Reference Manual, 2017)

Linear effective stiffness and damping should be defined for each degree of freedom. During nonlinear analysis, predefined nonlinear and hysteresis properties are used for each nonlinear degree of freedom and linear effective stiffness and damping are used for the remaining degrees of freedom. Linear effective stiffness is used for all degrees of freedom during linear analysis, regardless of whether nonlinear behavior is defined to any degree of freedom or not. Linear effective damping ratio of ζ=5% is applied to all degrees of freedom of nonlinear link elements. Applied linear effective damping ratio of nonlinear links are used only in a linear analysis. Damping of the structures in NLTH analysis is discussed in detail in Section 4.7. Table 4.1 shows effective stiffness for nonlinear link element.

Table 4.1. *Effective stiffness of nonlinear link element*

K_1- Axial (U1)	K_2, K_3- Translation (U2,U3)	K_4 - Torsion (R1)	K_5, K_6- Flexture (R2,R3)
EA/L	$12EI/L^3$	GJ/L	EI/L

In this study, nonlinear behavior is selected for only flexural bending directions (M2-R2, M3-R3) and the structural behavior of the plastic hinge in axial, transverse and torsional directions are equal to the elastic region of the member between hinges. Nonlinear properties like moment-rotation relationship are constant throughout nonlinear plastic hinge length (Lp).

4.6. Moment-Curvature (M-ϕ) Analysis

Moment-curvature (M-ϕ) analysis is essential as discussed in Section 4.5 to define plastic hinge and Takeda hysteresis model. For this reason, moment-curvature analysis of each hinge section is performed by using Section Designer option of the SAP2000 software. Then moment-curvature relationship is converted to the moment-rotation relationship by multiplying curvature values by plastic hinge length (Lp) since the hysteresis plastic hinge input in SAP2000 needs moment-rotation relationship instead of moment-curvature. Section material properties are used according to Table 3.1. Uniaxial stress-strain behavior of confined concrete proposed by Mander et al. (1988) is used in the moment-curvature analysis

An idealized moment-curvature model based on strain hardening of steel that is described in Caltrans (1995) is used. In the idealized model, elastic part of curve passes through the point that the first tensile rebar yields and the limit of elastic behavior is the point that concrete compressive strain has reached to 0.003. Then idealize moment-curvature model is obtained by balancing the area between actual

and idealized moment-curvature curve beyond the elastic portion. The moment-curvature analysis of column sections is carried out under permanent dead load. Table 4.2 and 4.3 show the moment-curvature analysis result for column and beam sections respectively. Also, example of defined Takeda backbone curve for a 50x50 column and a beam is illustrated in Figure 4.5 and Figure 4.6.

Table 4.2. *Moment-Curvature analysis results for column Takeda models*

Column Size (cm)	Column Rebar	Axial Force (kN)	Crack Point (C)		Yield Point (Y)		Ultimate Point (U)	
			Moment (kN.m)	Curvature	Moment (kN.m)	Curvature	Moment (kN.m)	Curvature
35 x 35	8Φ25	770	40.21	0.0013	254.20	0.0144	298.00	0.0400
35 x 35	8Φ25	510	29.59	0.0009	229.00	0.0130	280.00	0.0357
35 x 35	8Φ20	250	18.97	0.0007	148.00	0.0115	185.00	0.0858
40 X 40	8Φ25	560	44.79	0.0009	281.50	0.0108	352.00	0.0572
40 X 40	8Φ20	560	42.13	0.0009	212.00	0.0095	259.00	0.0300
40 X 40	8Φ20	250	27.20	0.0005	178.00	0.0090	220.00	0.0454
50 x 50	12Φ20	1780	184.78	0.0016	527.00	0.0093	614.00	0.0300
50 x 50	12Φ20	1420	154.78	0.0013	481.00	0.0085	576.00	0.0358
50 x 50	12Φ20	1060	124.78	0.0015	429.45	0.0080	528.20	0.0338
50 x 50	12Φ20	771	100.70	0.0022	220.80	0.0050	367.00	0.0275
60 x 60	16Φ20	1840	296.40	0.0013	770.20	0.0066	939.00	0.0320
60 x 60	16Φ20	1600	267.60	0.0012	728.20	0.0066	900.00	0.0350
70 x 70	20Φ20	2535	553.88	0.0015	1187.00	0.0057	1496.00	0.0700
70 x 70	20Φ20	2120	486.12	0.0013	1105.00	0.0055	1390.00	0.0410

Table 4.3. *Moment-Curvature analysis results for beam Takeda models*

T-Beam Size (cm)	Beam Tension Side	Beam Rebar	Crack Point (C)		Yield Point (Y)		Ultimate Point (U)	
			Moment (kN.m)	Curvature	Moment (kN.m)	Curvature	Moment (kN.m)	Curvature
25 X45	Top (T-shape)	3Φ16 + 6Φ10	39.38	0.0015	169.30	0.0070	180.70	0.0410
	Bottom (Rectangle)	3Φ16	19.69	0.0009	100.62	0.0058	106.50	0.0670
25 X45	Top (T-shape)	3Φ18 + 6Φ10	39.38	0.0015	194.60	0.0072	207.20	0.0368
	Bottom (Rectangle)	4Φ16	19.69	0.0009	135.75	0.0058	140.60	0.0585
25 X45	Top (T-shape)	4Φ18 + 6Φ10	39.38	0.0015	230.70	0.0080	248.00	0.0331
	Bottom (Rectangle)	4Φ16	19.69	0.0009	135.75	0.0058	140.60	0.0585

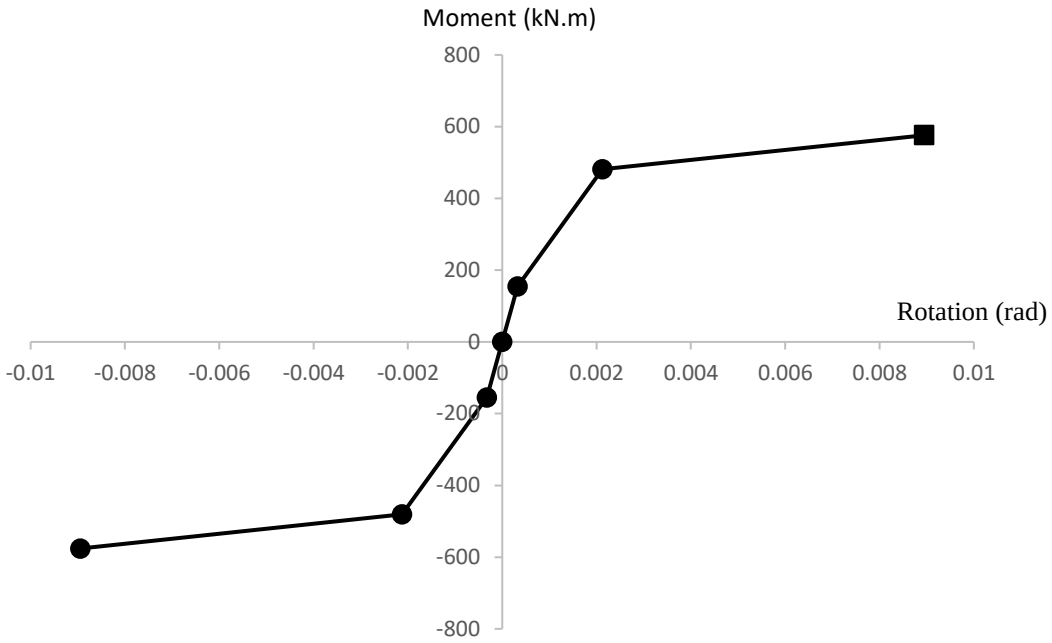

Figure 4.5. Defined backbone curve for Takeda model of 50x50 column under 1420 kN load.

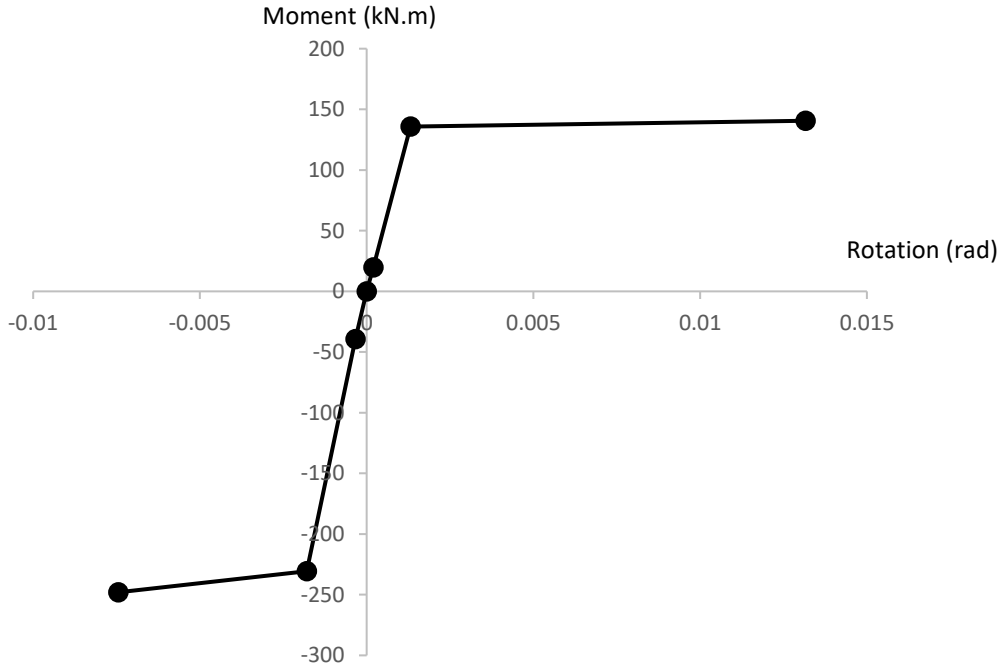

Figure 4.6. Defined backbone curve for Takeda model of 25x45 beam with 4ϕ16, 4ϕ18+6ϕ110 rebar.

4.7. Damping Model

In nonlinear time history analysis by direct integration, damping is calculated by using a full damping matrix. The damping matrix is obtained by proportional or Rayleigh damping. Rayleigh damping matrix is a linear combination of the mass and stiffness matrices. Proportional damping coefficients of mass (C_m) and stiffness (C_k) are calculated by using the first two natural frequencies of the structure and damping ratio, which is equal to ζ=5%. Figure 4.5 shows Rayleigh damping model used for direct-integration time history analysis.

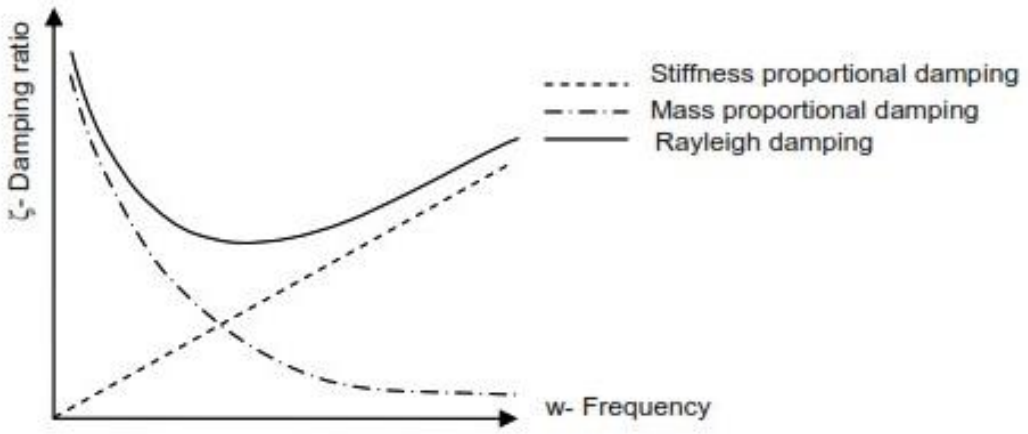

Figure 4.7. Rayleigh damping model using in NLTH analysis (CSI Analysis Reference Manual, 2017).

4.8. Ground Motions

In this study, 20 ground motions are selected for nonlinear time history analysis and energy calculations. These 20 ground motions are categorized into 2 groups as local and global ground motion records. Local ground motions are composed of 10 records from past earthquakes in Turkey, and global ground motions are composed of 10 records that were recorded in different locations around the world. In the selection of earthquakes, the main criterion is to have ground motion variability in terms of duration, intensity and frequency content.

All ground motions are scaled for each case study RC frames according to the target design spectrum shown in Section 3.3.2**.** For this purpose, 5 percent-damped response spectrum was obtained for each ground motion record.

The main characteristics of the selected ground motion records are presented in Table 4.4. In the second column of Table 4.4, a label is used for each ground motion record for the sake of simplicity. Local set of ground motions are labeled between L1 to L10 whereas global ground motions set are labeled between G1 to G10. Figure 4.8 and 4.9 show local and global unscaled ground motion records**.** Scaling factors of ground motion records for all 3, 5, 7, and 9 story frames are illustrated in Table 4.5.

Since fundamental periods of all 5 story frames with different bay numbers are the same, the scale factors for 5 story frame are valid for all 5-story frames with 2, 3 and 4 bays.

Table 4.4. *Characteristics of the selected ground motion records*

No	Label	Event	Country	Date	Location	M_W	PGA (g)	PGV (cm/s)	V/A (s)
1	L1	Horasan	Turkey	1983	Horasan Meteorology Station	6.7	0.126	36.92	0.30
2	L2	Erzincan	Turkey	1992	Erzincan	7.3	0.469	92.05	0.20
3	L3	Dinar	Turkey	1995	Dinar Meteorology Station	6.1	0.319	40.61	0.13
4	L4	Marmara	Turkey	1999	Yarımca	7.8	0.322	79.60	0.25
5	L5	Marmara	Turkey	1999	Yarımca	7.8	0.230	84.70	0.37
6	L6	Marmara	Turkey	1999	Düzce	7.8	0.337	60.59	0.18
7	L7	Düzce	Turkey	1999	Düzce	7.3	0.410	65.76	0.16
8	L8	Düzce	Turkey	1999	Düzce	7.3	0.513	86.05	0.17
9	L9	Bingöl	Turkey	2003	Bingöl	6.4	0.509	34.48	0.07
10	L10	Ceyhan	Turkey	1998	Ceyhan	6.2	0.226	29.82	0.13
11	G1	Imperial Valley	USA	1979	El Centro Array #5, James Road	6.5	0.367	95.89	0.27
12	G2	Montenegro	Yugoslavia	1979	Ulcinj, Hotel Olimpic	7	0.241	47.08	0.20
13	G3	Loma Prieta	USA	1989	Hollister, South St. & Pine Dr.	7	0.369	62.78	0.17
14	G4	Manjil	Iran	1990	Abhar	7.3	0.209	55.44	0.27
15	G5	Cape Mendocino	USA	1992	Petrolia, General Store	7	0.662	89.45	0.14
16	G6	Northridge	USA	1994	Slymar, Converter Station	6.7	0.373	118.89	0.33
17	G7	Northridge	USA	1994	Jensen Filter Plant	6.7	0.424	106.22	0.26
18	G8	Kobe	Japan	1995	JMA	6.9	0.833	90.70	0.11
19	G9	Chi Chi	Taiwan	1999	TCU074, Nantou Nanguang School	7.6	0.595	74.64	0.13
20	G10	Tabas	Iran	1978	Tabas	7.3	0.241	47.08	0.20

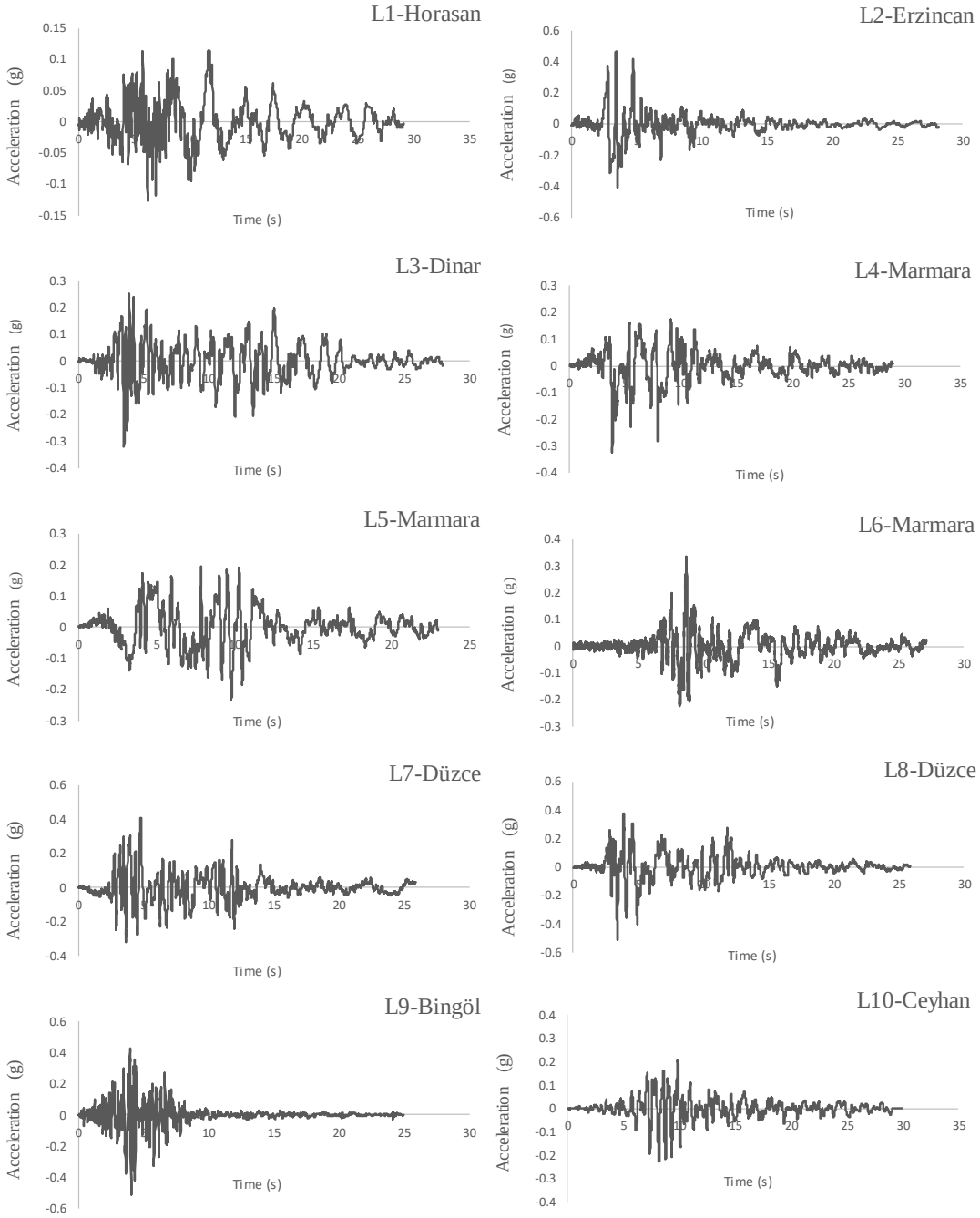

Figure 4.8. Local ground motions

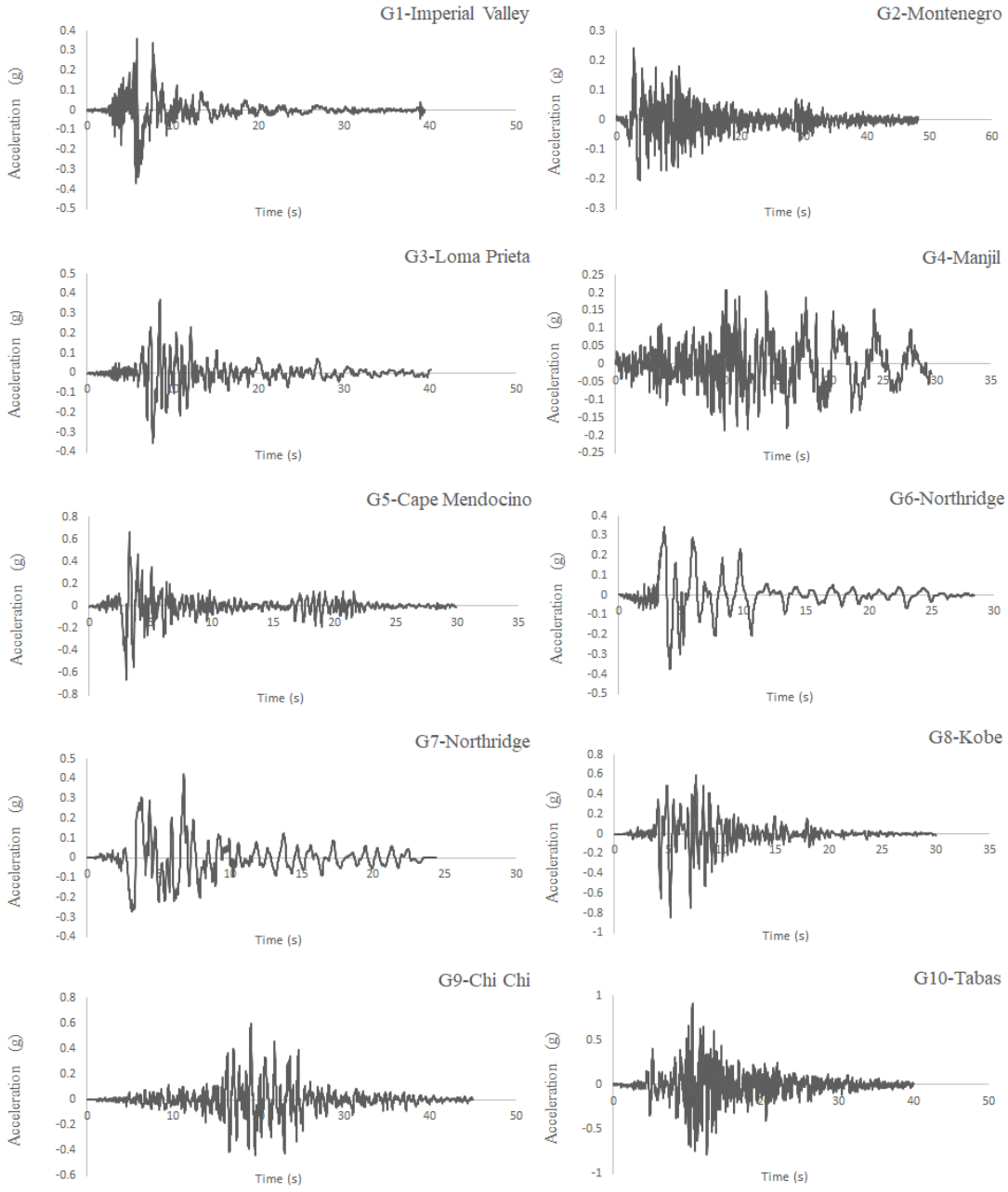

Figure 4.9. Global ground motions

Table 4.5. *Scale factors of ground motions*

Frame stories	3		5		7		9	
Spectral acceleration from design spectrum (g)	0.64		0.49		0.38		0.31	
Ground motion record	Specrtal acceleration (g)	Scale factor	Specrtal acceleration (g)	Scale factor	Specrtal acceleration (g)	Scale factor	Specrtal acceleration (g)	Scale factor
L1	0.136	4.72	0.212	2.30	0.192	1.98	0.156	1.97
L2	0.775	0.83	0.619	0.79	0.377	1.01	0.423	0.73
L3	0.479	1.34	0.593	0.82	0.440	0.86	0.418	0.74
L4	0.489	1.31	0.466	1.05	0.561	0.68	0.265	1.16
L5	0.526	1.22	0.370	1.32	0.245	1.55	0.234	1.31
L6	0.454	1.41	0.306	1.59	0.245	1.55	0.224	1.37
L7	0.785	0.82	0.348	1.40	0.285	1.33	0.245	1.26
L8	1.121	0.57	0.543	0.90	0.559	0.68	0.398	0.77
L9	0.336	1.90	0.147	3.32	0.165	2.30	0.157	1.96
L10	0.408	1.57	0.310	1.57	0.099	3.84	0.093	3.32
G1	0.632	1.01	0.516	0.94	0.306	1.24	0.326	0.94
G2	0.367	1.74	0.536	0.91	0.530	0.72	0.382	0.81
G3	0.958	0.67	0.765	0.64	0.499	0.76	0.489	0.63
G4	0.285	2.24	0.245	1.99	0.224	1.69	0.169	1.82
G5	1.203	0.53	0.738	0.66	0.486	0.78	0.387	0.80
G6	1.060	0.60	1.070	0.46	0.724	0.53	0.535	0.58
G7	0.846	0.76	0.823	0.59	0.647	0.59	0.499	0.62
G8	1.876	0.34	1.026	0.47	0.805	0.47	0.499	0.62
G9	1.397	0.46	0.837	0.58	0.968	0.39	0.530	0.58
G10	1.529	0.42	0.694	0.70	0.596	0.64	0.559	0.55

4.9. Nonlinear Models of Case Study Frames

As mentioned before, 6 RC moment resisting frames with different stories and bays are selected and designed in Chapter 3. In the design part, all structural elements are modeled based on elastic behavior.

In order to carry out NLTH analysis, all elastic models are converted to nonlinear models with lumped plasticity using hysteresis nonlinear links as discussed in previous sections. These nonlinear link elements have uncoupled behavior in both orthogonal direction for linear and nonlinear range. According to Aviram et al. (2008), it was strongly recommended that in case of using uncoupled nonlinear links in NLTH analysis, 2D models should be used. Also, NLTH analysis needs much computational effort with more computational time. So, it would be an enormous computational effort to carry out NLTH analysis of 6 frames under 20 ground motions by using 3D nonlinear models. Hence 2D models are used in NLTH analysis in this study. Interior frames of the buildings are selected to be modeled in 2D. Figure 4.8 shows the selected frame for the 3-bay building model. It is important to state that after converting 3D elastic models to 2D nonlinear models, fundamental periods of 3D and 2D models are almost the same. Also other structural outputs like, base shear force and weight of an interior frame of 3D models are the same as 2D models.

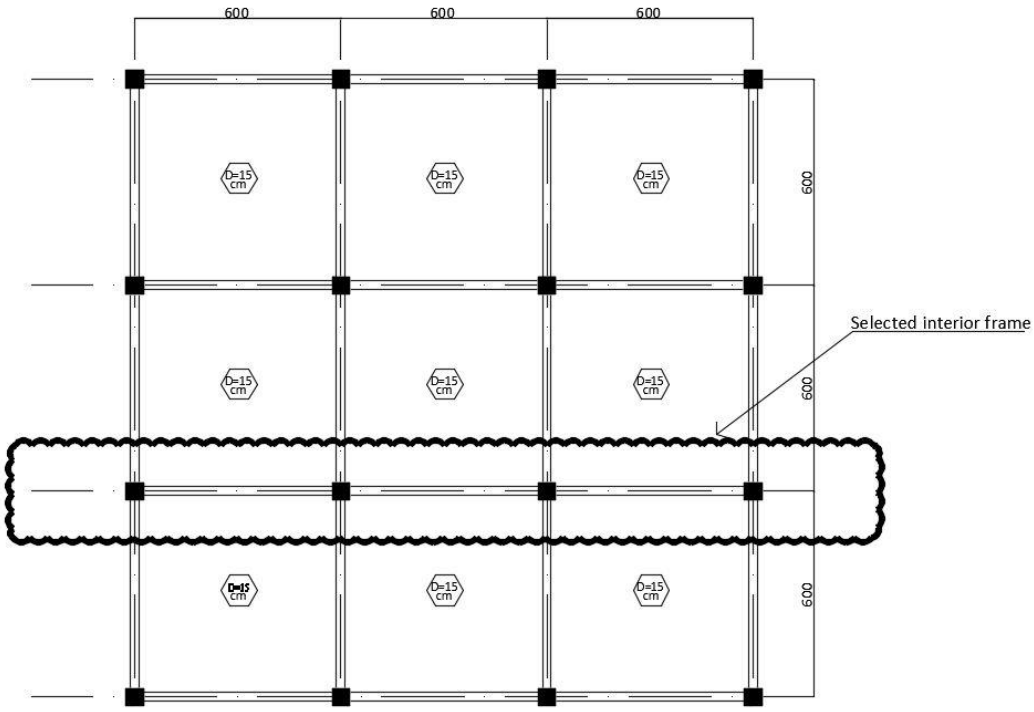

Figure 4.10. Selected interior frame of 3-bay building for 2D nonlinear model

4.9.1. Applied Loads for 2D Nonlinear Models

All loads from neighbour slabs and beams that is carried by the interior frame are calculated and applied to the selected frames. Transformed loads from neighbour slabs and beams are calculated as presented in Table 4.4. The mentioned live loads are without live load reduction factors and the live load reduction factors are also applied to the nonlinear models. Figures 4.9-4.12 show the applied dead and live loads on 2D nonlinear model for 5-story, 3-bay frame.

Self-weight of the selected frame's beams and columns are included by the structure analysis software itself, and it is not included in the following calculations.

Table 4.6. Transformed loads from neighbor beams and columns to the selected interior frame

Transformed loads from neighbor slabs connected to the interior frame's beams	
Distributed slab self-weight on the beams (kN/m) =	11.25
Distributed floor finishing load on the beams (kN/m) =	6
Distributed wall weight on the beams (kN/m) =	3
Distributed total dead load on the beams (kN/m)=	20.25
Distributed live load on the beams (kN/m)	6
Transformed loads from neighbor beams connected to the interior frame's columns	
Beam self-weight on columns (kN) =	16.9
Wall self-weight on columns (kN) =	18
Slab load on interior columns (kN) =	103.5
Slab load on exterior columns (kN) =	51.8
Total dead load on exterior columns (kN) =	138.4
Total dead load on interior columns (kN) =	86.7
Live load on interior columns (kN) =	36
Live load on exterior columns (kN) =	18

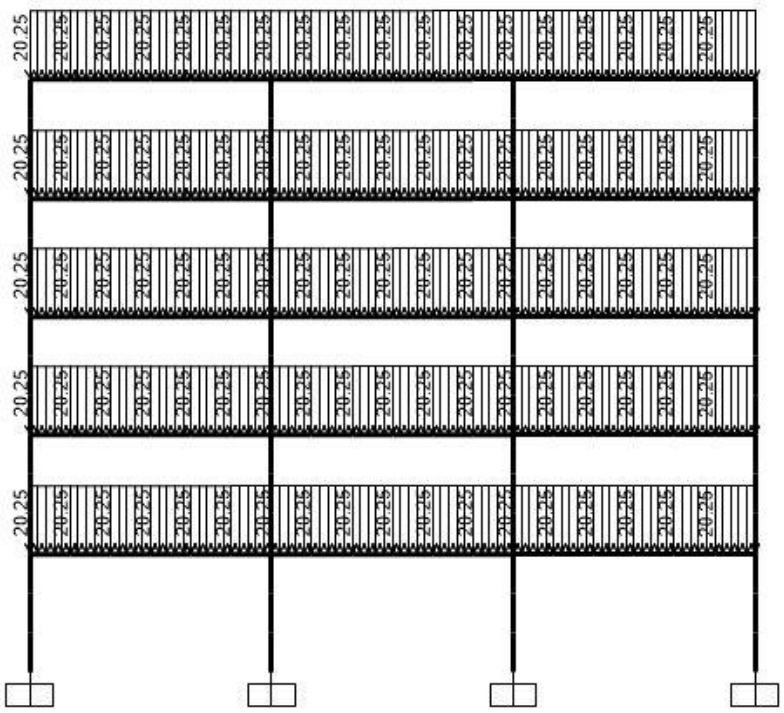

Figure 4.11. Applied distributed dead load for 5-story,3bays 2D model

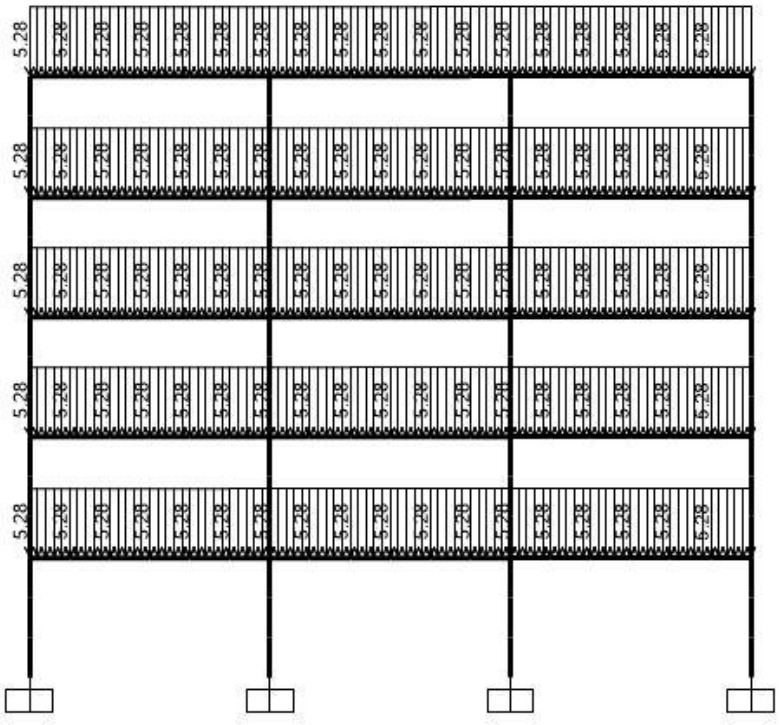

Figure 4.12. Applied distributed live load for 5-story,3bays 2D model

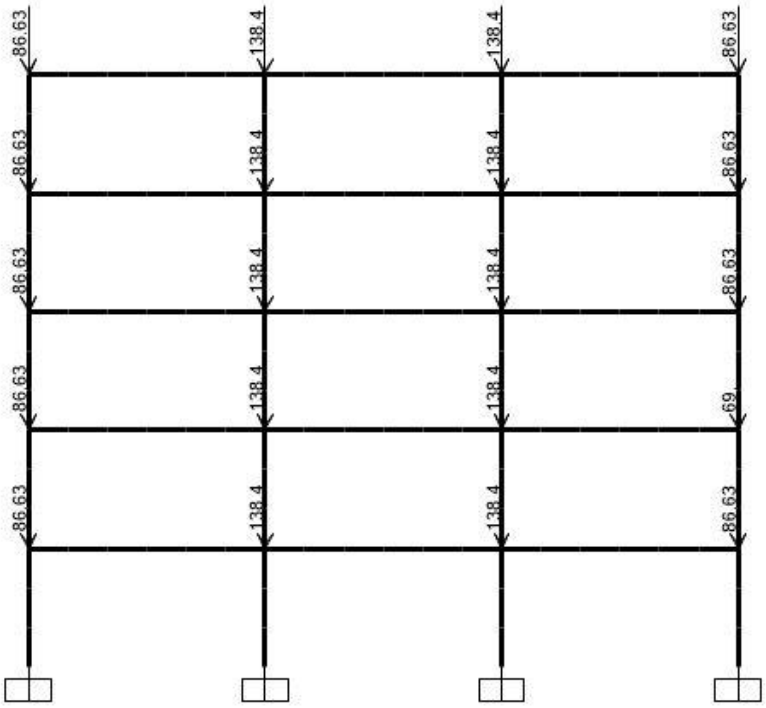

Figure 4.13. Applied point dead load for 5-story,3bays 2D model

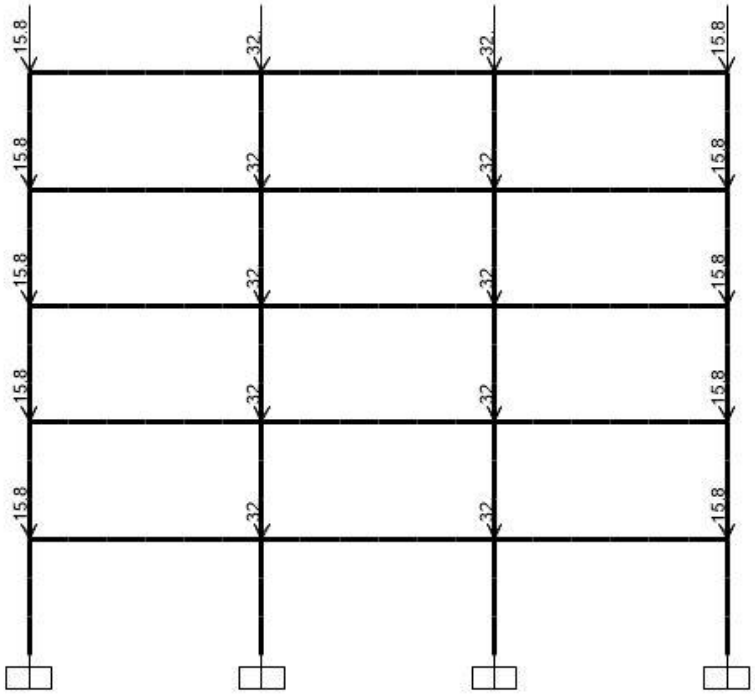

Figure 4.14. Applied point live load for 5-story,3bays 2D model

CHAPTER 5

ENERGY CALCULATIONS AND RESULTS

5.1. Introduction

This chapter focuses on the energy-based response of the selected frame structures subjected to the given set of ground motion records. For this purpose, three primary steps are considered, which are: estimation of input energy, calculating the ratio of hysteretic energy to input energy (E_h/E_i) and evaluation of the distribution of hysteretic energy among stories and structural members. Estimation of the input energy is spotlighted by many studies while determination of the hysteretic energy of RC buildings has been taken into account in fewer previous work. Estimation of hysteretic energy and its distribution through stories and elements are the main focus of this study, and it is discussed in more detail in this chapter.

In the first section of this chapter, the NLTH analysis and energy calculations are verified by a case study. Using the analysis results, input energy of each time history analysis and its components, which are kinetic energy, elastic strain energy, damping energy, and hysteretic energy are calculated according to equations given in Chapter 2.

In the following sections, the input energy and the ratio of hysteretic to input energy are shown for all analysis cases. The results are compared with each other to understand the effect of ground motion and structural properties on input energy and hysteretic energy.

The last part of this chapter is devoted to the story-wise and component-wise distribution of hysteretic energy. Hysteretic energy demand of each story over the height of the frames are plotted and total dissipated hysteretic energy by column and

beam hinges are calculated. The results are evaluated to propose a trend for the distribution of hysteretic energy demand in frame buildings.

5.2. Verification of the Energy Calculations in a Case Study

As it is described in previous chapters, 6 RC moment-resisting frames were designed, and NLTH analyse were carried out for each frame structure by using 20 ground motion records. Next task is to obtain energy parameters from the NLTH analyses. With 6 frames and 20 ground motions, there are 120 analysis cases which requires a considerable time and effort to get analysis results and calculate the hysteretic energy of all plastic hinges. So, before starting the energy calculations, it is decided to verify the NLTH analysis and energy calculations by using a benchmark case study.

Zhu (1989) aimed to investigate the effect of ground motion characteristics on inelastic behavior of RC frames under seismic action. He also studied seismic performance of RC frames using the energy-based method. Finally, he proposed a simplified analysis process to estimate inelastic deformation of RC frames. For this purpose, he carried out NLTH analysis of 4 story, 10 story, and 18 story RC moment-resisting frames under 40 ground motions. In the study, member sizes, reinforcement details, material property, applied loads, analysis process, static and dynamic analysis results, and energy components of the structures were reported. For comparing the results, 10 story frame under the 1985 Nahanni (Canada) ground motion record is selected from that study. Story height and span length of the 10 story frame is 3.5m and 8m, respectively. Although it is not possible to model and analyze the same case as was done in that study exactly, it is expected to achieve close results. Figure 5.1a shows the elevation view of the 10 story frame and its member sizes from the report. Figure 5.1b shows the finite element model used to compare the analysis results.

Figure 5.2 illustrates the 1985 Nahanni ground motion record used to verify the analysis and energy calculations. The ground motion data is scaled to the peak velocity of 0.4 m/s. Figure 5.3 shows the time history of energy components given by that study

for 10 story frame under Nahanni record. After modeling and analyzing the same case, time history of the energy components is plotted in Figure 5.4.

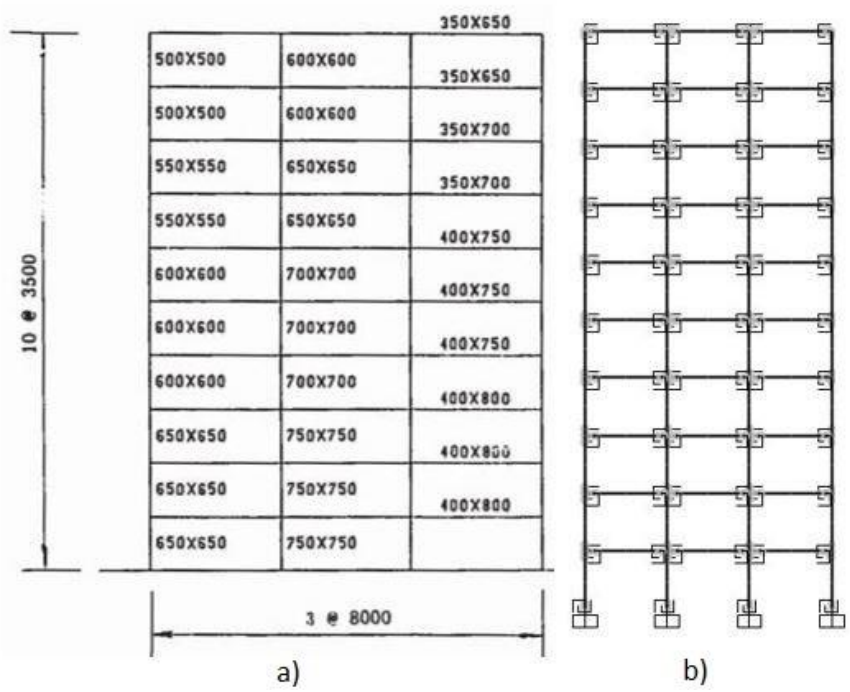

Figure 5.1. a) 10 story frame used by Zhu (1989). b) Finite element model of 10 story frame for verification.

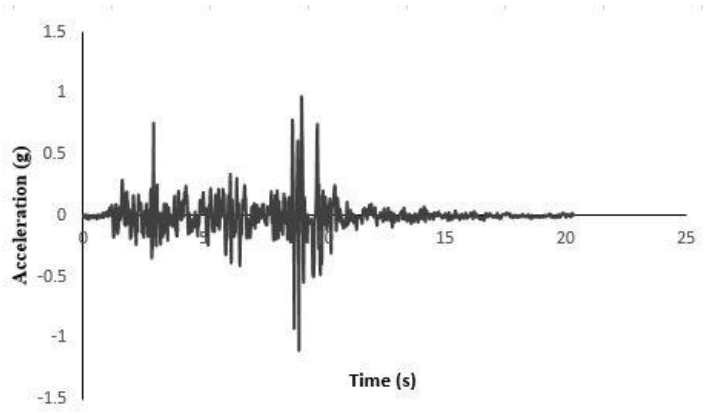

Figure 5.2. 1980 Nahanni (Canada) ground motion record

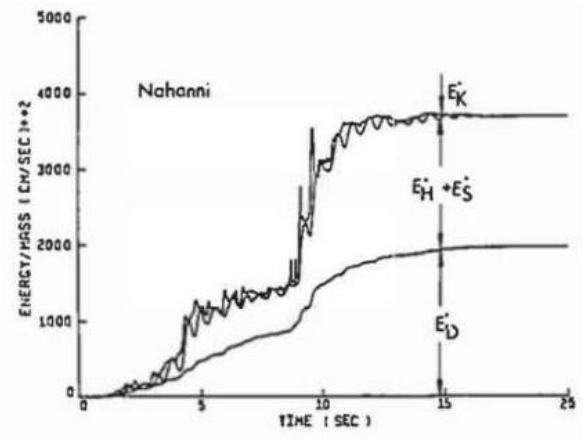

Figure 5.3. Time history of energy components for 10 story frame under Nahanni record by Zhu (1989)

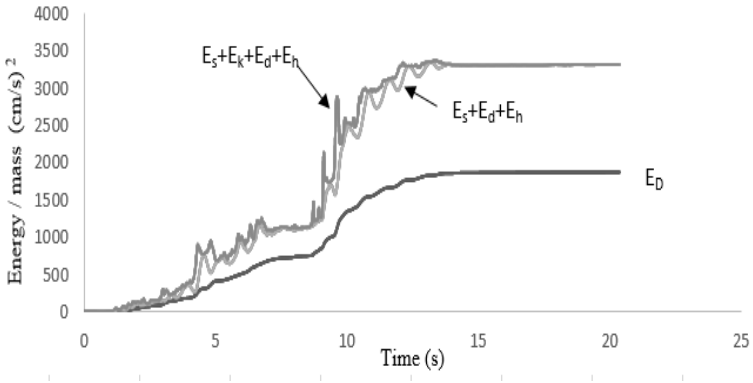

Figure 5.4. Time history of energy components for 10 story frame under Nahanni record for verification

Comparison of the energy responses from Figures 5.3 and 5.4 show that the calculated energy component values in the energy time history plots are very similar to the ones reported by Zhu. This verification gives the confidence to start NLTH analysis and energy calculations.

5.3. Time History of the Energy Parameters

As mentioned earlier, input energy is dissipated within the structure through recoverable elastic strain energy, kinetic energy, damping energy and irrecoverable plastic hysteretic energy. In this section, the time history of input energy and its

components are plotted for selected cases. Since there are 120 analysis cases, it would take pages to show all energy time histories. So, one ground motion is selected for each of the 3, 5, 7 and 9-story, 3-bay frame models. In order to have diverse behavior of the energy time history, selected ground motions are not the same. Figures 5.5 to 5.8 show the plotted energy time histories.

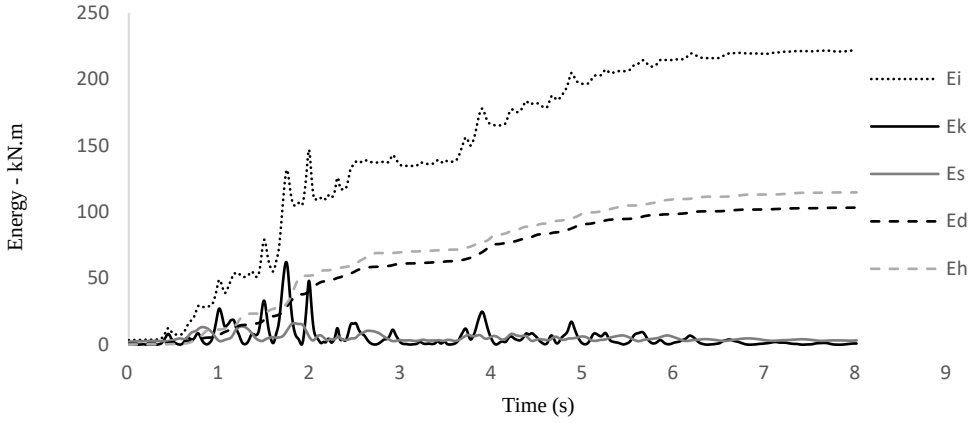

Figure 5.5. Energy time history of L9 Ground motion for 3-Story, 3-Bay frame

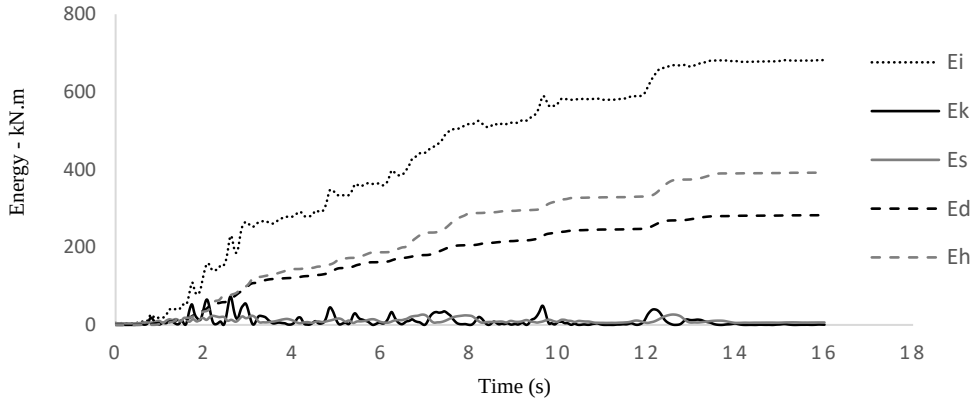

Figure 5.6. Energy time history of L7 Ground motion for 5-Story, 3-Bay frame

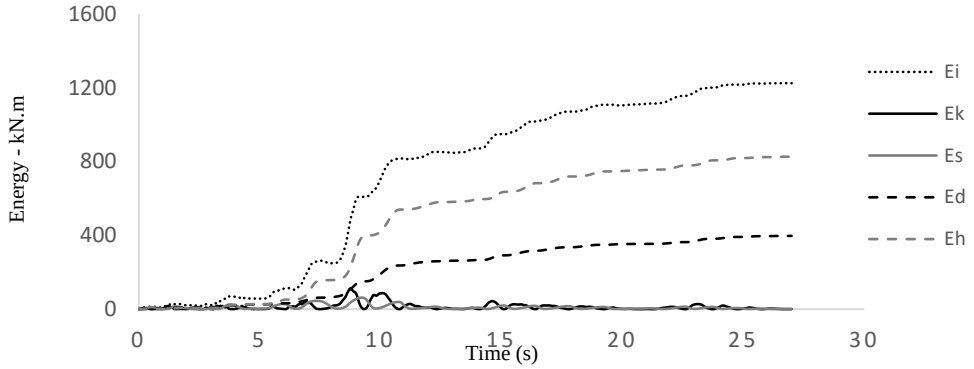

Figure 5.7. Energy time history of L1 Ground motion for 7-Story, 3-Bay frame

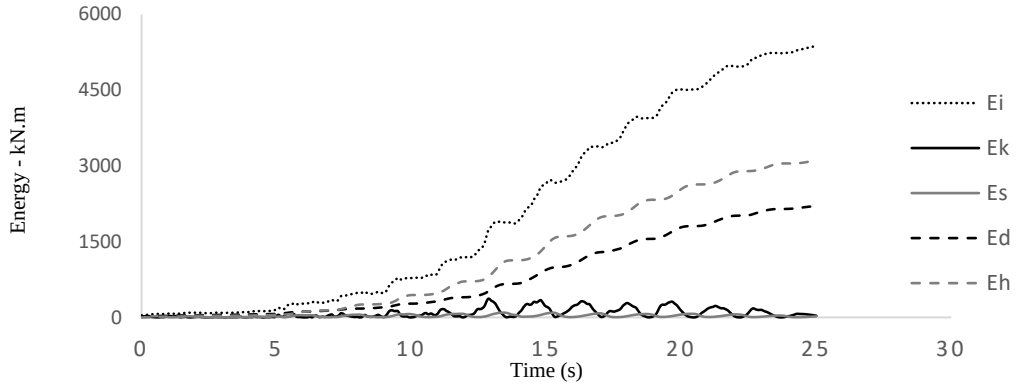

Figure 5.8. Energy time history of G4 Ground motion for 9-Story, 3-Bay frame

The plotted energy time histories show that the contributions of elastic strain energy and kinetic energy are nearly negligible compared to damping energy and hysteretic energy. Elastic strain energy and kinetic energy vanish at the end of ground motion and input energy is dissipated by damping energy and hysteretic energy, as expected and described in Equation 2.21. Also, the energy time history plots prove that damping energy and hysteretic energy are irrecoverable and cumulative over the ground motion.

Margin between E_h and E_d plots differs in the energy time histories, which means that the percentage of damping energy and hysteretic energy with respect to the input energy is not the same for all analysis cases. Hence it is a function of both ground

motion and structural parameters. In the following sections, energy responses of frame models are assessed for all ground motions and the differences in the energy responses are discussed.

5.4. Input Energy Results

Estimating the input energy of the earthquake is the first step in all the energy-based methods. Housner (1956) and Akiyama (1985) proposed alternative approaches to predict the input energy for SDOF systems. Many studies have been carried out to extend the prediction of input energy from SDOF systems to MDOF systems (Shen and Akbas 1999, Manfredi 2001, Amiri et al. 2008). Okur and Erberik (2014) proposed a design energy input spectra for residential reinforced concrete buildings. A reliable model is developed by Alici and Sucuoglu (2018) to predict input energy spectra considering near-fault ground motion effect, damping, and lateral strength.

Although the focus of this work is on the hysteretic energy, this section is dedicated to input energy since the estimation of input energy is vital for developing energy-based design method. Structures go into inelastic behavior range and exhibit degradation in stiffness and strength under strong ground motion. In such systems, it is known that the characteristics of ground motion have a major effect on the input energy of the earthquake. The number of high amplitude cycles and the presence of a long acceleration pulse are the two significant characteristics of ground motions that cause a high amount of input energy and are critical for deteriorating structures (Sucuoglu and Erberik, 2004). In this study, input energy of each frame case is calculated for twenty ground motion records. The results are illustrated and compared to each other and the effect of ground motion characteristics on input energy is discussed. To recall, input energy for MDOF systems is presented in Equation 2.26.

Figures 5.9-5.14 show the input energy of all ground motions for each frame type and compare them with each other. Table 5.1 shows input energy per unit mass (E_i/m) of each ground motion for all frame models.

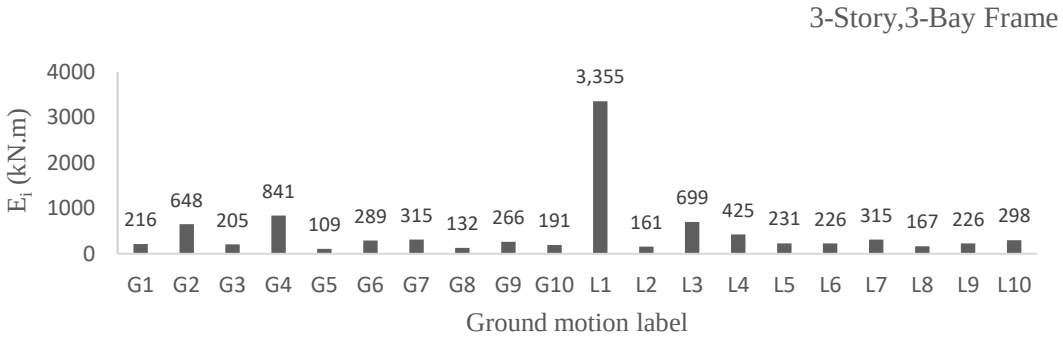

Figure 5.9. Input energy of 3-story, 3-bay frame under all ground motions

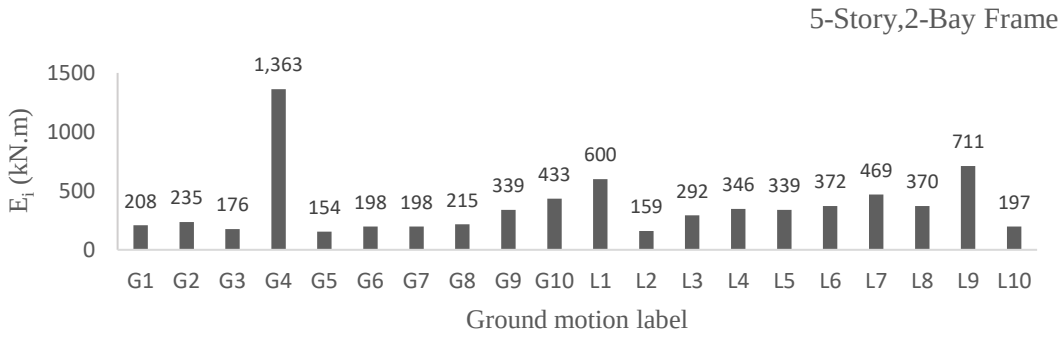

Figure 5.10. Input energy of 5-story, 2-bay frame under all ground motions

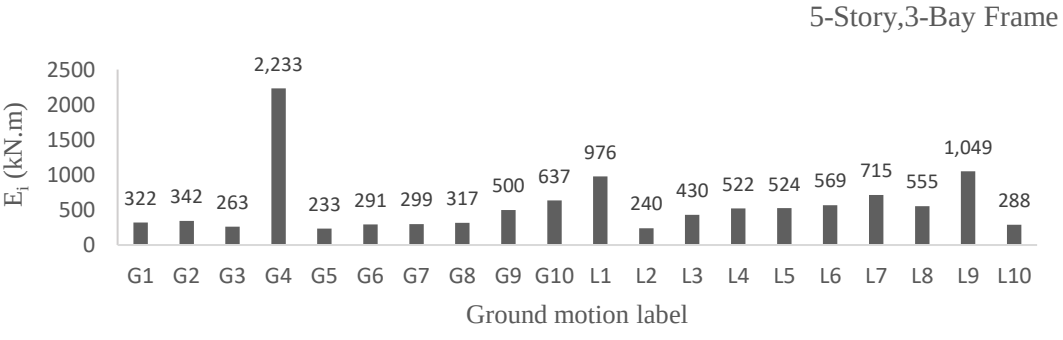

Figure 5.11. Input energy of 5-story, 3-bay frame under all ground motions

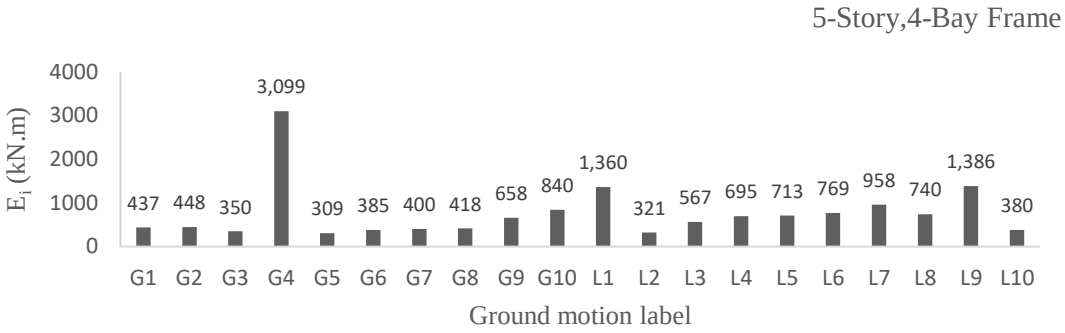

Figure 5.12. Input energy of 5-story, 4-bay frame under all ground motions

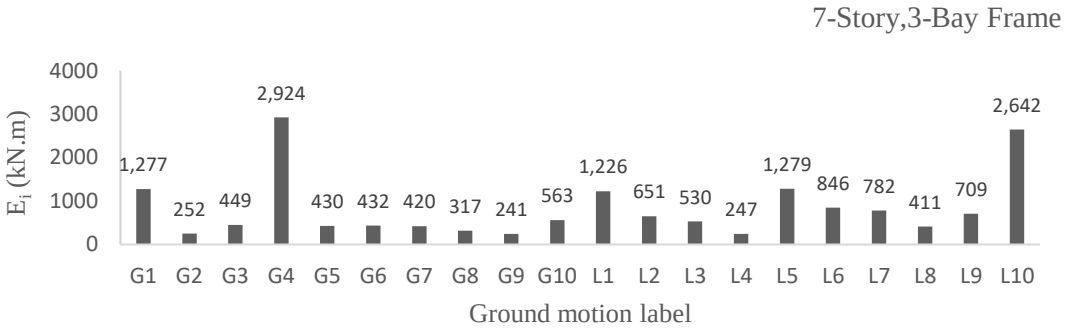

Figure 5.13. Input energy of 7-story, 3-bay frame under all ground motions

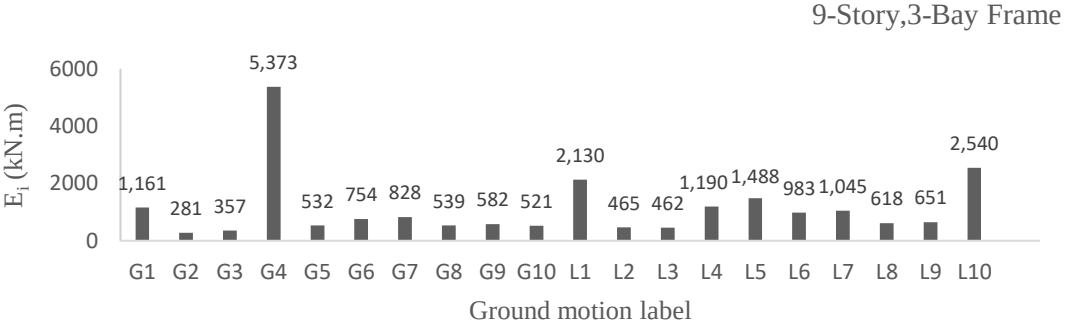

Figure 5.14. Input energy of 9-story, 3-bay frame under all ground motions

Table 5.1. *E_i/m of 20 ground motions for all frame cases*

E_i/m $(cm/s)^2$						
Ground motion	3-Story 3-Bay	5-Story 2-Bay	5-Story 3-Bay	5-Story 4-Bay	7-Story 3-Bay	9-Story 3-Bay
G1	771.0	650.4	680.6	694.6	1914.3	1341.7
G2	2315.6	736.2	723.4	713.2	378.3	325.0
G3	731.2	549.7	556.3	557.5	673.6	412.3
G4	3004.1	4265.9	4719.9	4930.0	4382.7	6208.9
G5	388.3	481.5	492.1	492.3	643.9	614.9
G6	1032.7	619.8	615.9	612.0	647.8	871.7
G7	1126.1	619.1	631.5	637.0	630.1	957.1
G8	473.2	674.0	670.4	664.9	475.3	622.3
G9	951.9	1062.4	1056.6	1046.7	360.9	672.8
G10	681.4	1356.6	1346.3	1336.2	843.7	602.1
L1	11990.1	1879.1	2063.7	2163.5	1837.0	2461.8
L2	576.3	498.0	507.3	511.3	975.1	536.9
L3	2499.2	913.3	908.1	902.8	795.1	533.8
L4	1517.4	1082.6	1104.6	1105.2	369.5	1374.9
L5	824.6	1060.4	1107.4	1135.0	1916.8	1719.9
L6	808.0	1163.1	1202.6	1223.3	1267.9	1136.0
L7	1126.1	1468.8	1510.8	1524.0	1172.2	1207.8
L8	597.2	1158.6	1173.9	1177.6	615.7	714.1
L9	808.2	2226.5	2218.3	2205.1	1062.5	751.9
L10	1065.1	617.6	609.6	604.6	3960.0	2935.5

Comparing the input energies of all ground motions for all moment-resisting frames, the following observations can be stated:

- Figures 5.9-5.14 show that although all ground motions are scaled to the equivalent spectral acceleration, the energies of different ground motion records have totally different values. Input energy also seems to be period-dependent. This means that input energy is dependent on both ground motion characteristics and structural properties.
- G4 (Manjil 1990) record gives the highest amount of input energy for 5-story,7-story and 9-story frame models. For the 3-story frame model, G4 record yields the second-highest input energy value after L1 record. PGA and PGV values of the G4 record is 0.21 g and 47.1 cm/s, respectively, which are not high compared to L2, L7, L8 and G8 records (Table 4.2). However Figure 4.7 shows that G4 record has a long duration with many high amplitude acceleration cycles. It is possible to conclude that PGA and PGV are not adequate ground motion parameters for the representation of earthquake damage potential and other ground motion characteristics like duration and number of high amplitude acceleration cycles should be taken into account.
- Table 5.1 shows that input energy is almost constant among 5 story frames and it shows that each ground motion record gives similar values of input energies for 5-Story 2-Bay. 5-Story 3-Bay and 5-Story 4-Bay frames. This is expected because all 5 story frames with different bay numbers have similar fundamental periods and damping ratios. So, the fundamental period is an important parameter, and a ground motion record applies nearly the same input energy to different structures with similar fundamental periods and damping ratios although geometrical properties (like number of bays) may differ.
- Evaluating the input energy results shows that the formulation that predicts input energy should depend on both structural properties and ground motion characteristics. For example, while L10 record yields high values of input energy for 7-story and 9-story frame models, it yields very low values of input

energy for the 5-story frame model and moderate value of input energy for the 3-story frame model.

In the following section, contribution of damping energy and hysteretic energy for the dissipation of earthquake input energy is evaluated.

5.5. The Ratio of Hysteretic to Input Energy:

In order to propose a practical energy-based design or evaluation methodology, hysteretic energy, which is the representative of the damage potential of the structure, should be predictable. Fajfar et al. (1990) stated that it is possible to predict hysteretic energy demand using the ratio of hysteretic to input energy. They claimed that this ratio is a stable parameter, and it mostly depends on the damping ratio. Some studies focused on a predictable relationship between input energy and its dissipation components, which are damping energy and hysteretic energy for SDOF systems (Khashaee 2003, Sawada et al. 2005, Ucar and Merter 2018). Akbas et al. (2016) proposed E_h/E_i ratio spectrum for inelastic SDOF and MDOF systems for steel moment-resisting frames.

In this section E_h/E_i and E_d/E_i ratios of all frame models under 20 ground motion records are calculated as presented in Table 5.2. Mean values and coefficient of variation percentages (COV%) of the ratios also illustrated in the last two rows of the table. In order to observe the effect of ground motion characteristics and structural properties on hysteretic energy, the percentage of E_h/E_i ratio for all ground motions are plotted for each frame model in Figure 5.15. As it is clearly seen in Table 5.2, E_h/E_i and E_d/E_i ratios add up to unity. This is provided in the table to verify that these two mechanisms of energy dissipation should be equal to the energy imparted to the structure at the end of the ground motion record. In addition, the ratio values of the 5 story frame models with different bay numbers are the same. So in the plotted figures, the 5 story frame with 3 bay number represents all 5 story frames.

Table 5.2. *E_d/E_i and E_h/E_d ratios of all ground motion records for all frame models*

Ground motion labels	3-Story, 3-Bay		5-Story, 2-Bay		5-Story, 3-Bay		5-Story, 4-Bay		7-Story, 3-Bay		9-Story, 3-Bay	
	Eh/Ei	Ed/Ei	Eh/Ei	Ed/Ei	Eh/Ei	Ed/Ei	Eh/Ei	Ed/Ei	Eh/Ei	Ed/Ei	Eh/Ei	Ed/Ei
G1	0.68	0.31	0.67	0.31	0.67	0.31	0.66	0.31	0.63	0.37	0.62	0.38
G2	0.63	0.37	0.61	0.37	0.61	0.37	0.61	0.37	0.56	0.44	0.53	0.46
G3	0.62	0.36	0.58	0.40	0.58	0.40	0.58	0.40	0.56	0.43	0.54	0.46
G4	0.69	0.31	0.67	0.32	0.67	0.33	0.67	0.33	0.65	0.35	0.58	0.41
G5	0.57	0.40	0.59	0.38	0.59	0.38	0.59	0.38	0.56	0.44	0.53	0.46
G6	0.66	0.33	0.61	0.37	0.61	0.37	0.61	0.37	0.60	0.40	0.60	0.40
G7	0.65	0.34	0.63	0.35	0.63	0.35	0.63	0.35	0.63	0.37	0.60	0.40
G8	0.58	0.39	0.55	0.44	0.54	0.44	0.54	0.44	0.51	0.49	0.47	0.53
G9	0.58	0.41	0.56	0.43	0.56	0.43	0.56	0.43	0.48	0.51	0.51	0.49
G10	0.54	0.45	0.59	0.40	0.58	0.41	0.58	0.41	0.55	0.45	0.51	0.49
L1	0.57	0.42	0.70	0.30	0.69	0.30	0.69	0.30	0.67	0.32	0.62	0.38
L2	0.63	0.35	0.61	0.37	0.61	0.36	0.61	0.36	0.60	0.40	0.58	0.42
L3	0.63	0.37	0.57	0.41	0.57	0.41	0.57	0.41	0.55	0.44	0.53	0.47
L4	0.66	0.33	0.64	0.35	0.64	0.34	0.65	0.34	0.57	0.43	0.62	0.38
L5	0.62	0.36	0.63	0.35	0.64	0.35	0.64	0.35	0.66	0.33	0.66	0.34
L6	0.62	0.37	0.63	0.35	0.63	0.35	0.63	0.35	0.63	0.36	0.61	0.38
L7	0.65	0.34	0.57	0.42	0.58	0.41	0.58	0.41	0.58	0.41	0.58	0.41
L8	0.59	0.39	0.61	0.38	0.61	0.38	0.61	0.38	0.58	0.42	0.59	0.41
L9	0.52	0.47	0.52	0.47	0.52	0.47	0.52	0.47	0.52	0.48	0.50	0.50
L10	0.56	0.42	0.49	0.49	0.49	0.49	0.49	0.49	0.54	0.46	0.53	0.47
Mean	0.61	0.37	0.60	0.38	0.60	0.38	0.60	0.38	0.58	0.41	0.57	0.43
Cov %	7.48	11.65	8.26	12.84	8.16	12.60	8.07	12.50	8.59	12.33	8.76	11.68

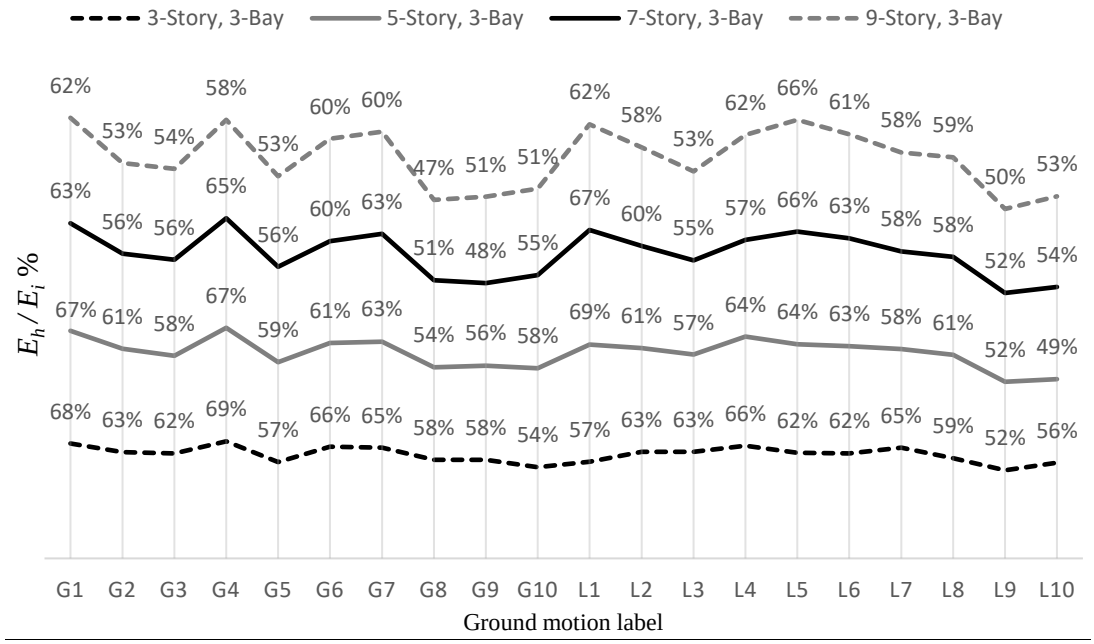

Figure 5.15. Comparison of the E_h/E_i ratio shown as percentage for each frame model for all ground motion records

Evaluating the results in Table 5.2 and Figure 5.15, the following comments could be stated:

- Percentage of hysteretic to input energy ratio varies from 48% to 70%.
- The mean value of the E_h/E_i ratio for 20 ground motion records for the 3-story frame is 0.61, for the 5-story frame is 0.60, for the 7-story is 0.58 and for the 9-story frame is 0.57. The percentage of coefficient of variation is about 8% which means that the level of dispersion around the mean is low. According to the results of this study it could be concluded that for an RC moment-resisting frame that exhibits inelastic behavior, almost 60% of the input energy is dissipated through hysteretic action and 40% is dissipated through damping action.
- Comparing E_h/E_i ratio of all ground motions for each frame model in Figure 5.15 shows that E_h/E_i ratio line is nearly constant for 3 story frame and as the number of stories increases the ratio line become more sensitive to the ground motion. This means that as the fundamental period of structure increases, E_h/E_i ratio becomes more dependent on ground motion characteristics.
- The values on the vertical grid-lines in Figure 5.15 show the variation of the E_h/E_i ratios with respect to frame models for the same ground motion record. Looking from this perspective it can be stated that there is a slight dependence of E_h/E_i ratio to the selected frame model. However this slight dependence can be ignored for the sake of simplicity to develop simple and practical design procedures.
- To sum up, hysteretic demand and E_h/E_i ratio are dependent on both structural properties and ground motion characteristics. This dependence seems to be more pronounced for ground motion characteristics compared to the structural properties for the considered data set.

5.6. Distribution of Hysteretic Energy

This section focuses on the distribution of hysteretic energy, which is the spotlight of this study. After estimating cumulative irrecoverable hysteretic energy demand of the structure, it is necessary to know how the hysteretic energy is distributed within the stories and structural elements, in order to develop energy-based design and assessment methodologies. For this reason, the hysteretic energies of all plastic hinges of the selected 6 moment-resisting frames under 20 ground motion have been calculated as described in the next section. Then, in the following sections, the results of hysteretic energy distribution are illustrated. The results are presented in terms of the hysteretic energy demand of each story, total energy dissipated by column and beam members and finally, the dissipated hysteretic energy of each plastic hinge in the whole structure.

5.6.1. Calculation of hysteretic energy

Loading and unloading process of plastic hinge under earthquake action is calculated by the SAP2000 analysis platform using Takeda hysteresis rules. A backbone curve is defined for each hinge according to the moment-curvature relationship of the section and the hinge length as discussed in previous chapters. Figure 5.16 presents the hysteretic behavior of a typical beam hinge in 9 story frame model under G4 ground motion record given by the SAP2000 software. As it is shown, the hysteresis behavior is in the form of moment-rotation relationship. It is possible to achieve hysteretic energy of the hinge by calculating the cumulative enclosed area of the moment-curvature cycles. There is a considerable number of plastic hinges in the frame models and it would be time-consuming to calculate hysteretic energy of each hinge one by one. So, Matlab software is used to manage the data and calculate the hysteretic energy of the plastic hinges. After obtaining the hysteretic energy of the hinges, the results are presented in the following sections.

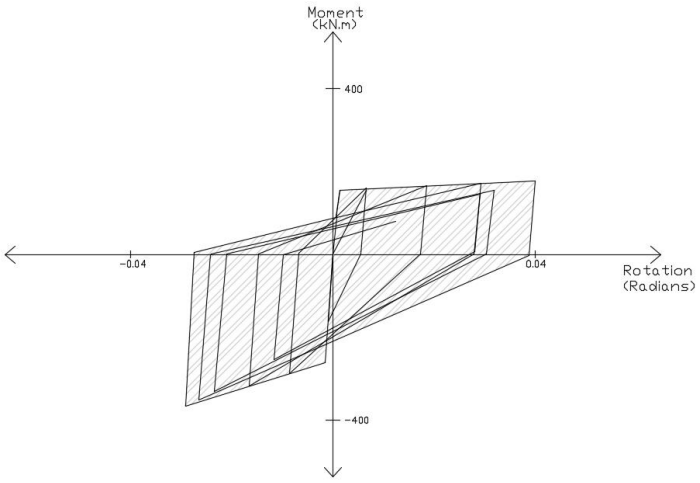

Figure 5.16. Hysteresis behavior of a typical hinge beam in 9 story frame model under G4 record.

5.6.2. Story-wise Distribution of the Hysteretic Energy

Hysteretic energy dissipated at the column and beam hinges are summed in each story and divided by the total hysteretic energy of the frame to find the cumulative hysteretic energy demand of each story. The distribution of story-wise hysteretic energy to total hysteretic energy ratio (E_{sh}/E_h) over the height of the structures for different ground motion record are shown in Figures 5.17-5.20 in which MG and ML represent mean value of the results for global and local records respectively. It is worth adding that the results obtained for 5 story frames with different bay numbers are the same. So a single plot is used to show results of 5 story frames with different bay numbers.

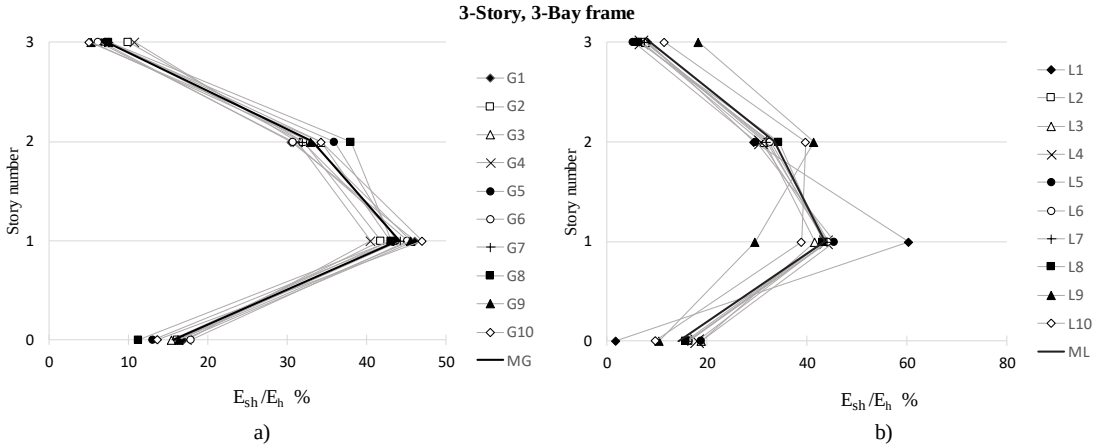

Figure 5.17. E_{sh}/E_h % for 3-story, 3-bay frame for a) global record set, b) local record set.

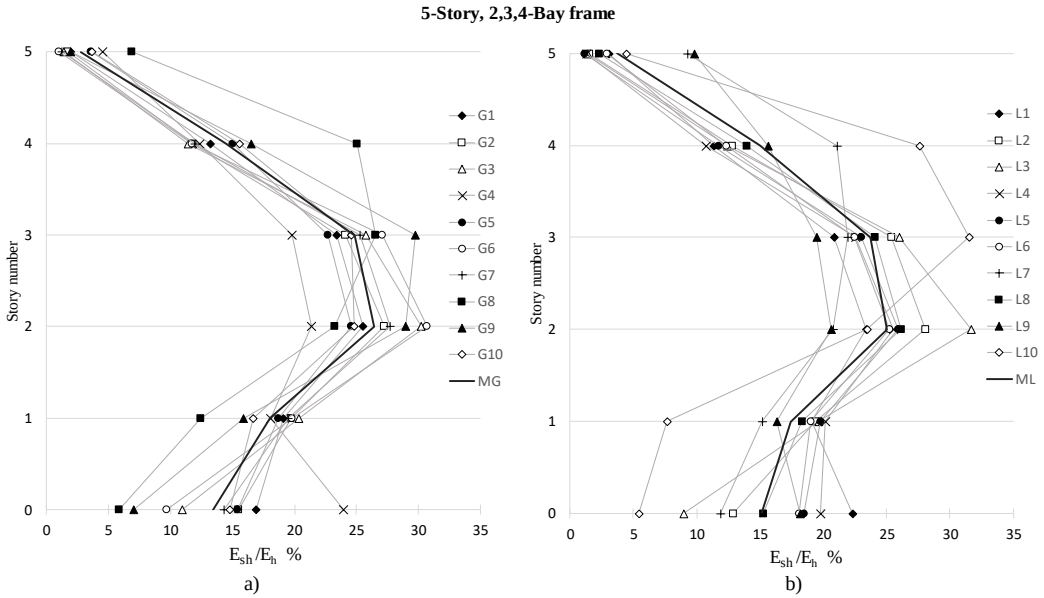

Figure 5.18. E_{sh}/E_h % for 5-story, 3-bay frame for a) global record set, b) local record set.

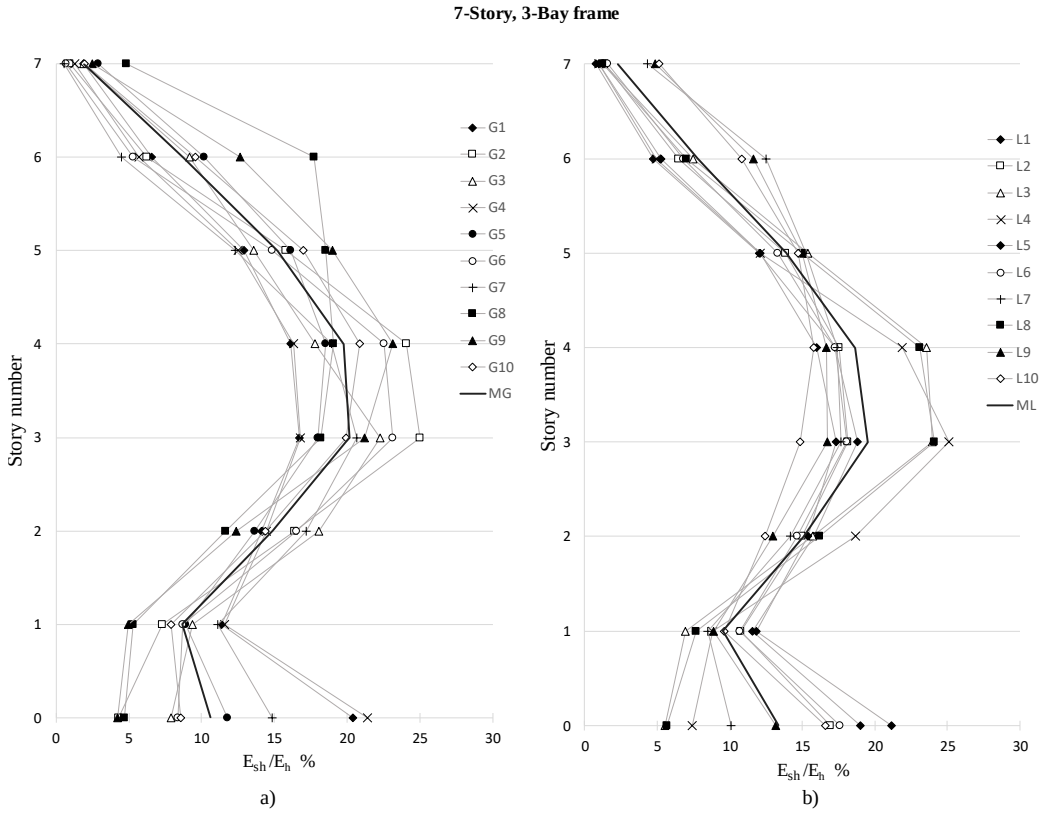

Figure 5.19. E_{sh}/E_h % for 7-story, 3-bay frame for a) global record set, b) local record set.

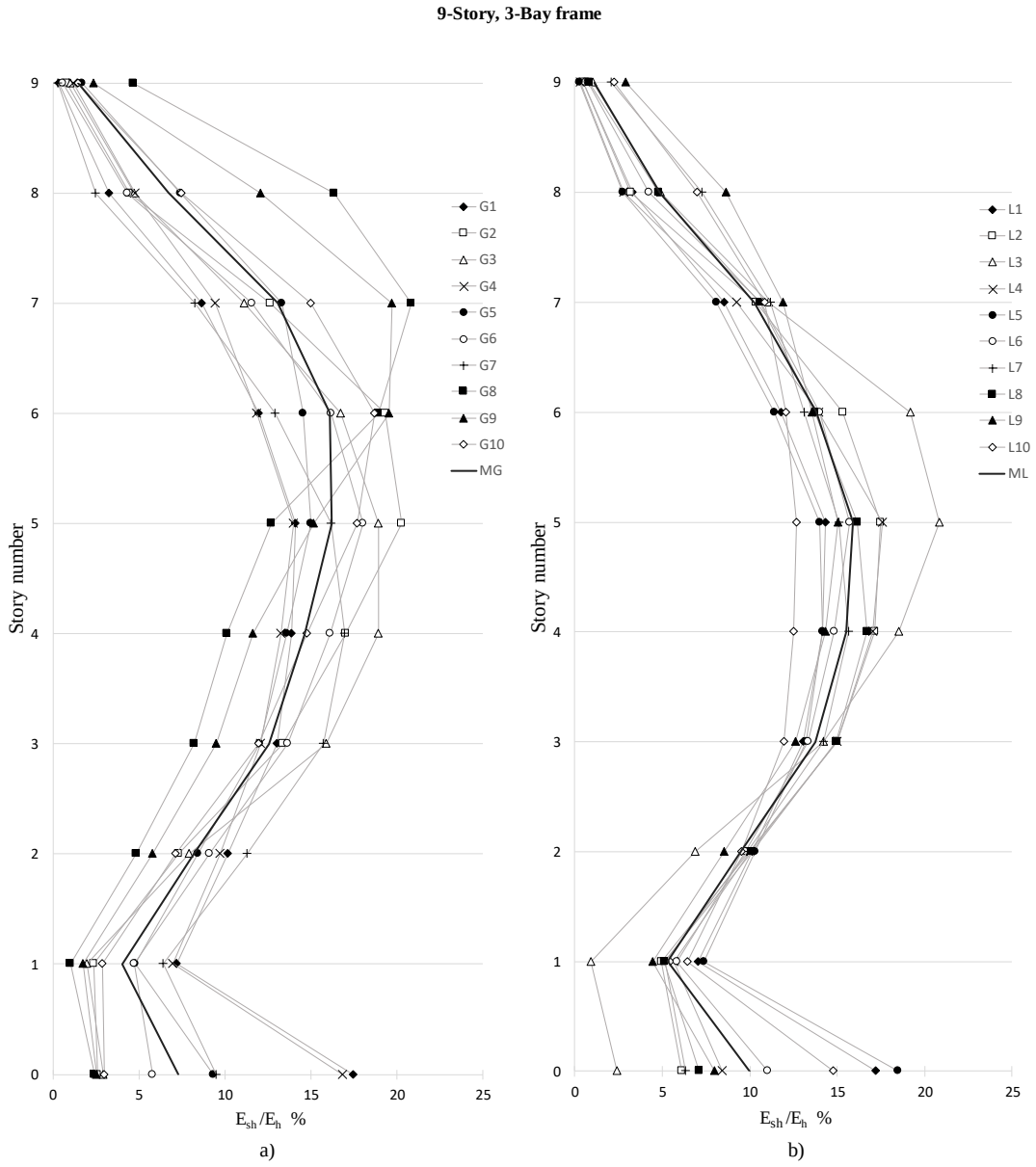

Figure 5.20. E_{sh}/E_h % for 9-story, 3-bay frame for a) global record set, b) local record set.

The mean values of E_{sh}/E_h ratio results for 10 global and 10 local records are calculated to obtain the normalized distribution pattern of story-wise hysteretic energy. The results are shown in Table 5.3.

Table 5.3. *Mean values of E_{sh}/E_h % for 10 global and local records*

Average Records	3-Story, 3-Bay frame		5-Story, 2,3,4-Bay frame		7-Story, 3-Bay frame		9-Story, 3-Bay frame	
	Local set	Global set	Local set	Global set	Local set	Global set	Local set	Global set
9th Story	-	-	-	-	-	-	1.4	1.1
8th Story	-	-	-	-	-	-	6.7	4.9
7thStory	-	-	-	-	1.9	2.3	13.0	10.2
6th Story	-	-	-	-	8.8	7.8	16.1	13.8
5th Story	-	-	2.8	3.7	15.2	13.9	16.2	15.9
4th Story	-	-	14.5	15.0	19.7	18.7	14.6	15.5
3rd Story	7.4	8.7	24.9	23.7	20.2	19.5	12.5	13.7
2nd Story	33.2	33.5	26.4	25.1	14.9	15.1	8.2	9.5
1st Story	44.0	43.5	18.0	17.4	8.6	9.5	4.0	5.3
Base	15.4	14.3	13.4	15.1	10.6	13.3	7.2	10.0

From evaluation of results obtained for the story-wise distribution of hysteretic energy the following comments can be concluded:

- General trend of the results show that distribution of hysteretic energy over the height of structure depends on both ground motion characteristics and structural properties.
- For 3 story frame, E_{sh}/E_h ratios for all ground motions (expect L1, L9 and L10), are close to each other whereas, the ratio values have more scatter for other frame models. This shows that story-wise distribution of hysteretic energy is less sensitive to ground motion characteristics for low-rise buildings.
- Table 5.3 reveals that about 75% of the hysteretic energy is dissipated in the second and third story for 3 story frame. This percentage decreases to 45% for the 5 story frame model, 25% for the 7 story frame model and 15% for the 9 story frame model. In addition, the dissipated hysteretic energy by the base columns decreases from 15% for the 3 story frame to 9% for the 9 story frame. It means that as the fundamental period of the structure increases hysteretic energy moves from the lower stories to the mid and upper stories.

5.6.3. Member-wise Distribution of Hysteretic Energy

This section focuses on the distribution of hysteretic energy that is dissipated by structural members. The dissipated hysteretic energy at each beam and column hinge is divided by the total hysteretic energy to obtain the ratio of member-wise (beam or column) hysteretic energy to total hysteretic energy (E_{mh}/E_h) for all ground motions as a measure. Total hysteretic energy percentage dissipated by the base columns (sum of E_{mh}/E_h% at base columns), story columns (sum of E_{mh}/E_h% at story columns) and story beams (sum of E_{mh}/E_h% at story beams) for all records and presented in Figures 5.21-5.24. Also, the mean values of hysteretic energy percentage dissipated by the beam and column members are obtained for 10 global and 10 local records. The results are presented in Table 5.4. As it has been described, member sections were designed considering strong column-weak beam criterion. So, it is expected that most of the hysteretic energy is dissipated by beam members

In order to have a deeper perception about the member-wise distribution of hysteretic energy, mean values of E_{mh}/E_h % at each plastic hinge for two record sets are illustrated in Figures 5.25-5.30. This contributes to compare the hysteretic energy demand of all beam or column hinges in the same story. It would take pages to show the E_{mh}/E_h % for all records so mean values of two record sets are decided to be presented. Appendix A is provided to show the hysteretic energy percentage dissipated by each joint of the frame models (sum of E_{mh}/E_h % of at a joint) for all ground motion records.

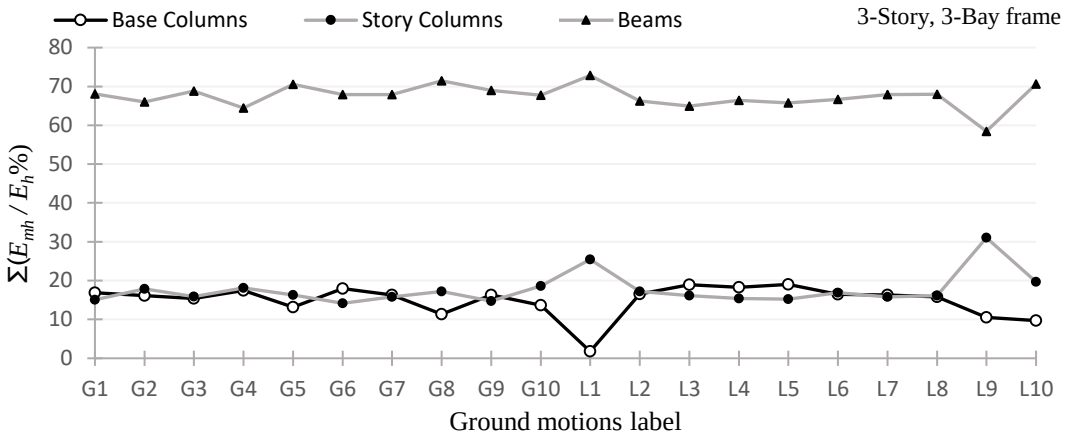

Figure 5.21. Member-wise hysteretic energy distribution for 3-story, 3-bay frame model

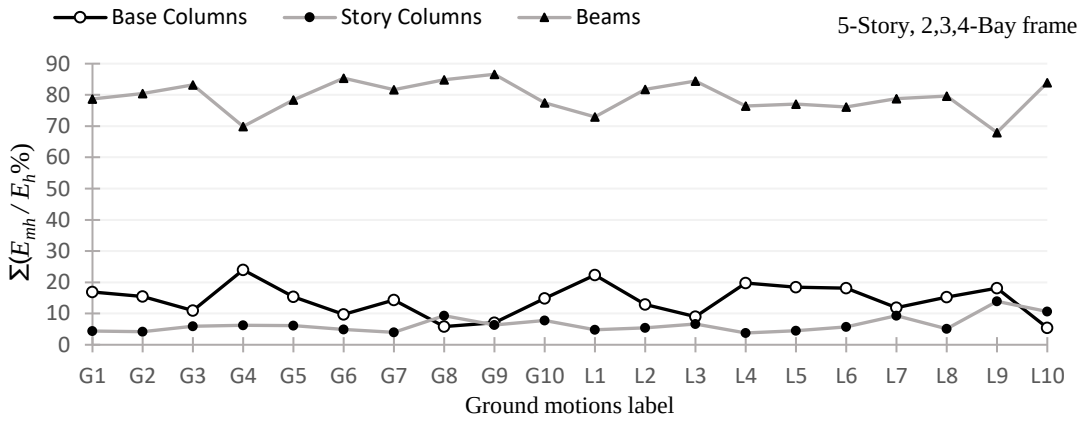

Figure 5.22. Member-wise hysteretic energy distribution for 5-story, 2,3,4-bay frame model

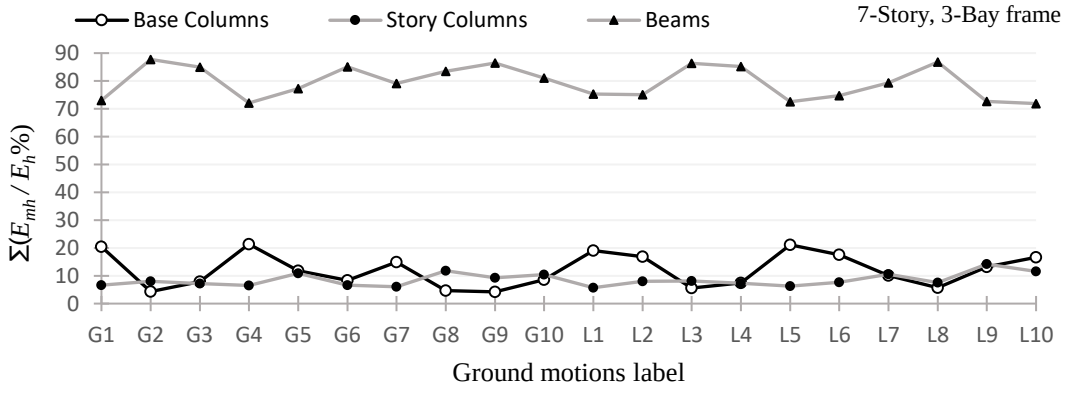

Figure 5.23. Member-wise hysteretic energy distribution for 7-story, 3-bay frame model

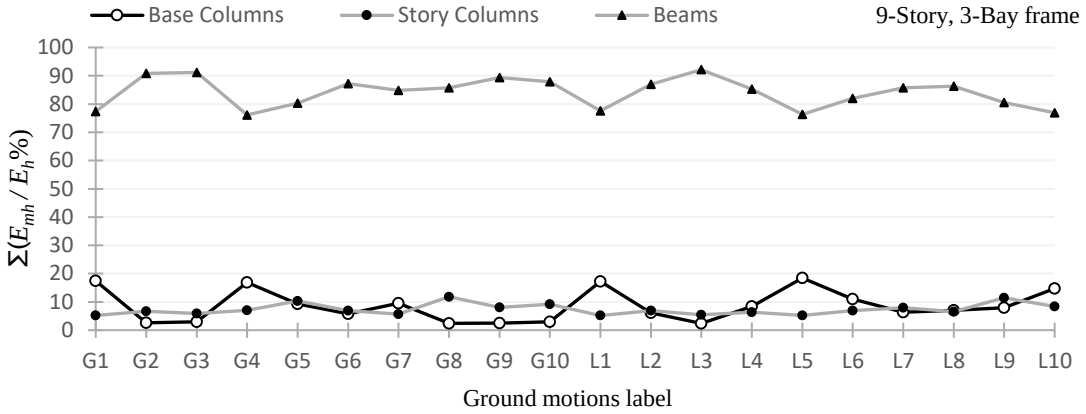

Figure 5.24. Member-wise hysteretic energy distribution for 9-story, 3-bay frame model

Table 5.4. *Mean values of hysteretic energy dissipated percentage by beam and column members for 10 global and local records.*

Frame case	Ground motion set	Structural Element		
		Base Columns	Story Columns	Beams
3-Story, 3-Bay frame	Global set	15.4	16.4	68.2
	Local set	14.3	18.9	66.8
5-Story, 2-Bay frame	Global set	12.8	5.7	81.6
	Local set	14.2	6.5	79.3
5-Story, 3-Bay frame	Global set	13.4	5.9	80.7
	Local set	15.1	7.0	77.9
5-Story, 4-Bay frame	Global set	13.9	6.1	80.1
	Local set	15.5	7.2	77.3
7-Story, 3-Bay frame	Global set	10.6	8.3	81.0
	Local set	13.3	8.7	78.0
9-Story, 3-Bay frame	Global set	7.2	7.7	85.1
	Local set	10.0	7.0	83.0

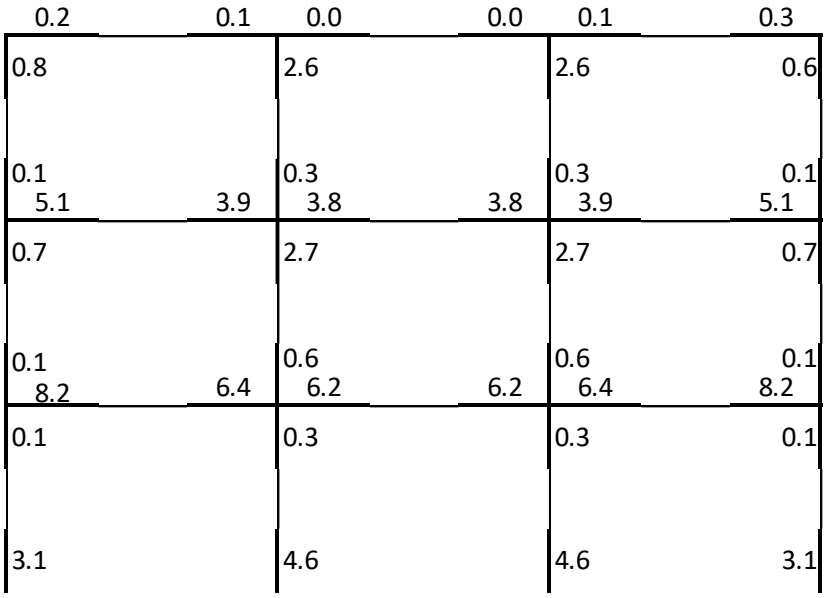

a)

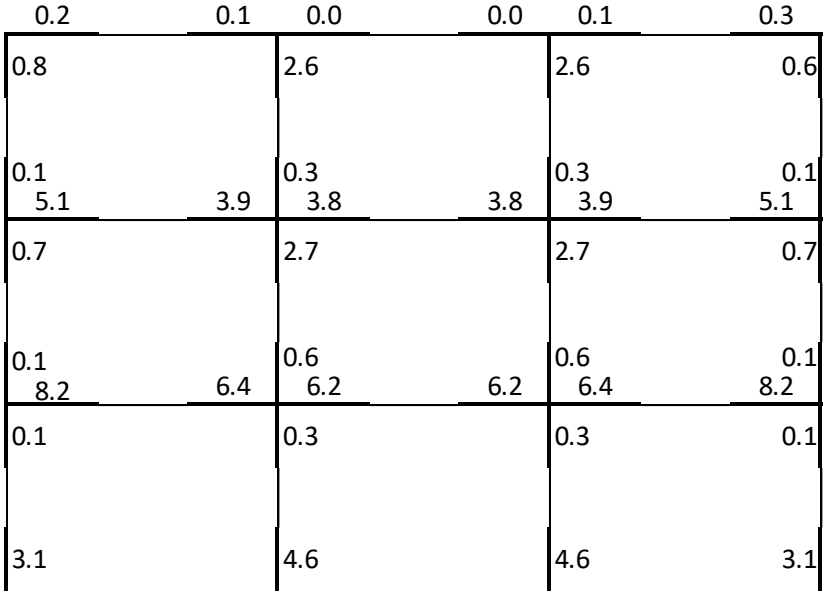

b)

Figure 5.25. Mean values of E_{mh}/E_h % of 3-story, 3-bay frame model. a) for global record set, b) for local record set

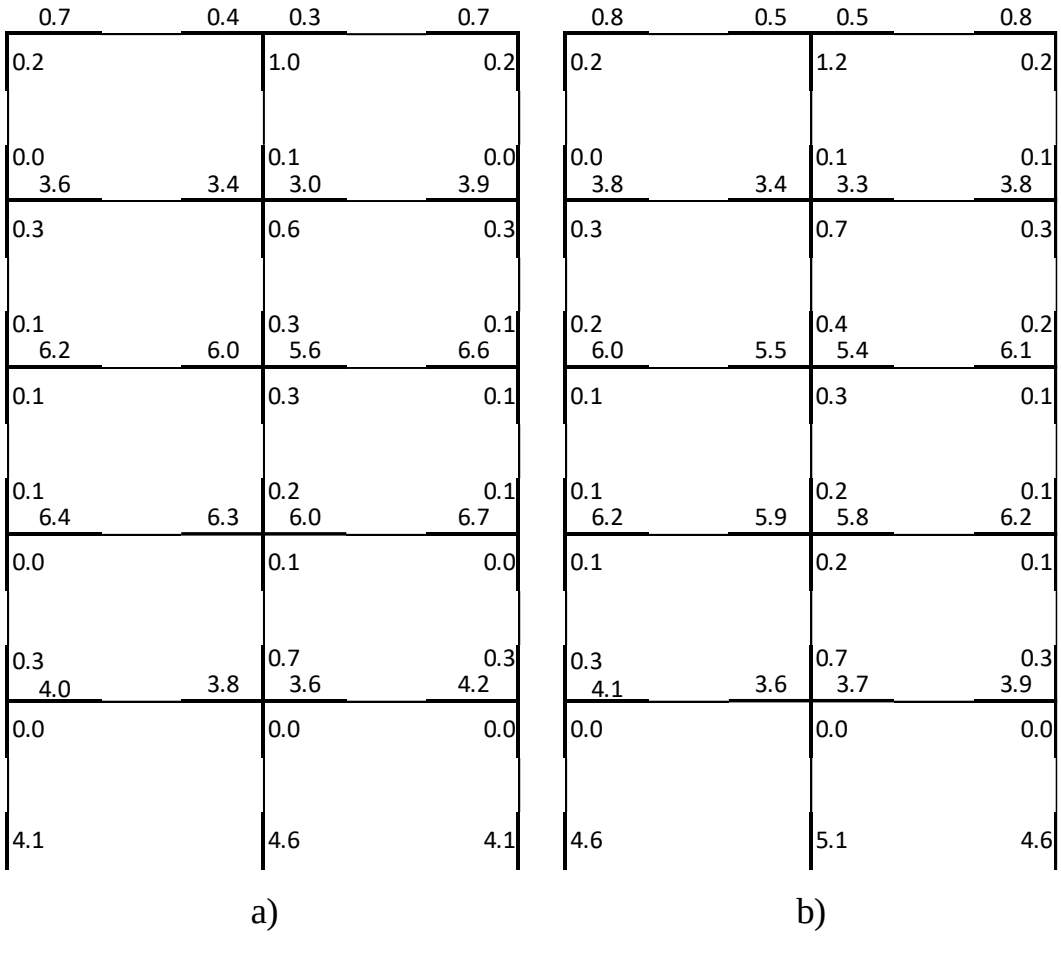

Figure 5.26. Mean values of Emh/Eh % of 5-story, 2-bay frame model. a) for global record set, b) for local record set

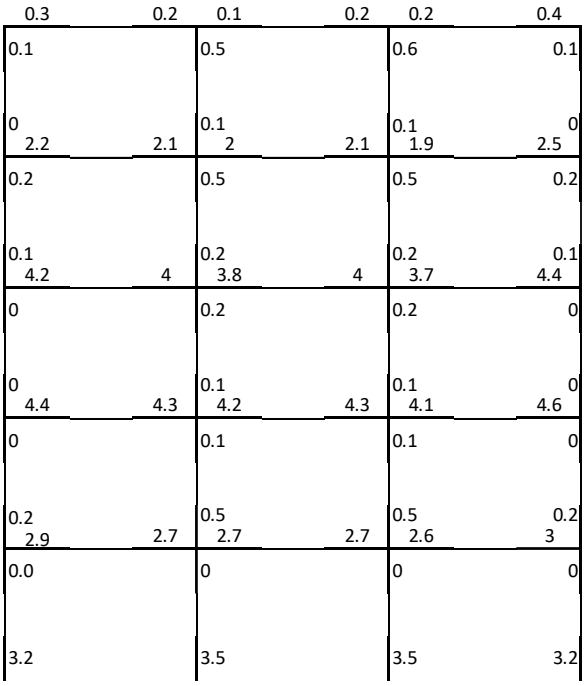

a)

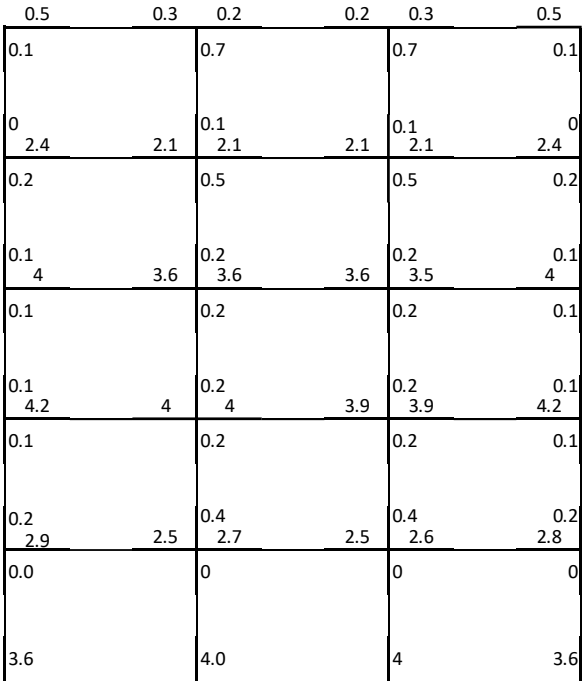

b)

Figure 5.27. Mean values of E_{mh}/E_h % of 5-story, 3-bay frame model. a) for global record set, b) for local record set

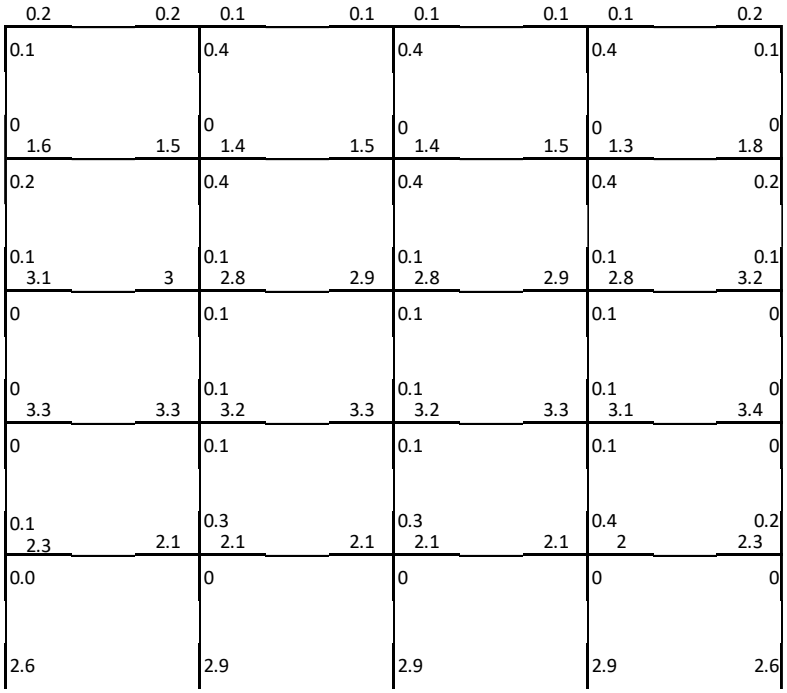

a)

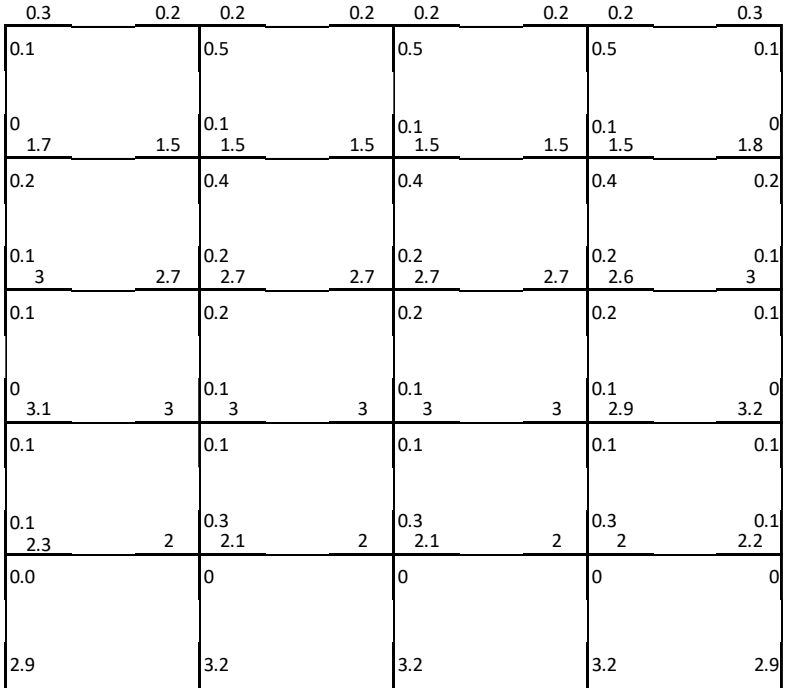

b)

Figure 5.28. Mean values of Emh/Eh % at 5-story, 4-bay frame model. a) for global record set, b) for local record set

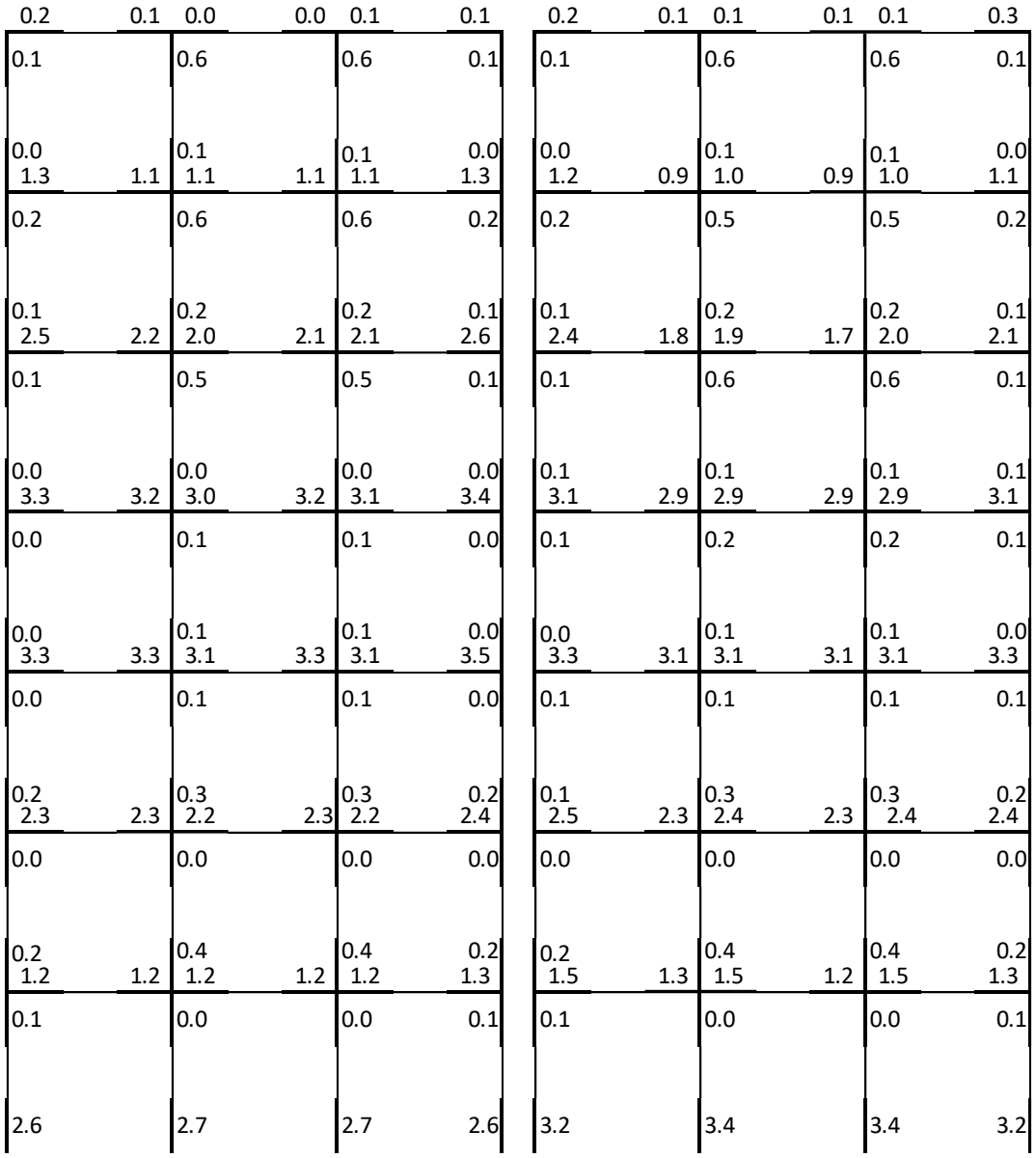

Figure 5.29. Mean values of E_{mh}/E_h at of 7-story, 3-bay frame model. a) for global record set, b) for local record set

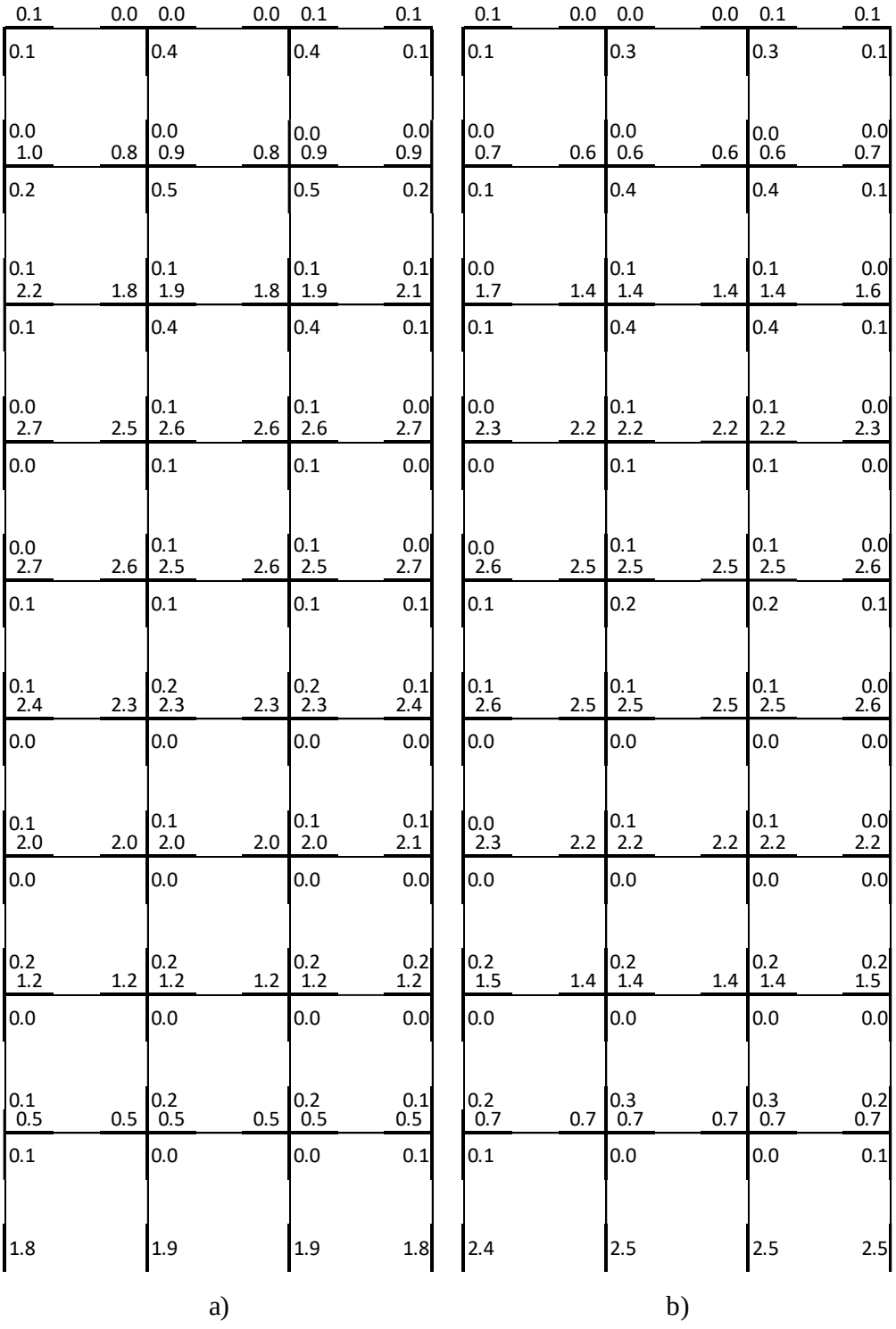

Figure 5.30. Mean values of E_{mh}/E_h at of 9-story, 3-bay frame model. a) for global record set, b) for local record set

Evaluating the member-wise distribution of hysteretic energy results from Figure 5.21-5.30 and Table 5.4, the following comments can be concluded:

- Calculated mean values of hysteretic energy dissipated by column and beam hinges for all analysis cases shows that 78% of total hysteretic energy is dissipated by beam hinges whereas 9% is dissipated by column hinges in the stories and 13% is dissipated by the hinges at the base columns. It can also be stated that in a beam-column joint, 10% of the hysteretic energy is dissipated by columns whereas 90% is dissipated by the beams.
- Approximately 7% of total hysteretic energy is dissipated by column hinges (except base column hinges) for the 5,7 and 9 story frame models. This percentage becomes 18% for 3 story frame model which is quite high when compared to the other frame models. While the column moment capacity to beam moment capacity ratio for 3 story frame is 1.7, it is about 2.0 for the other frame models. So, it seems that the ratio of dissipated hysteretic energy by columns to dissipated hysteretic energy by beams is sensitive to the ultimate moment capacities of column and beam sections.
- Although the column moment capacity to beam moment capacity ratio is more than 1.2 for all frame models, columns did not stay in the elastic zone, and they showed hysteretic behavior. It could be concluded that the 1.2 ratio that mentioned in many codes, does not guarantee the elastic behavior of columns and it causes a ductile beam-column failure mechanism.
- From Table 5.4 it is observed that as fundamental period of the structure increases, dissipated hysteretic energy from base columns is transferred to the beams.
- Comparing E_{mh}/E_h ratios from Figures 5.25-5.30, shows that the hysteretic energy is distributed equally between interior members and also it is distributed equally between exterior members (here beams are compared together and columns are compared together). However the percentage of

hysteretic energy dissipated by exterior and interior members are not always the same.

- E_{mh}/E_h ratios for exterior beam hinges are greater than the E_{mh}/E_h ratios for interior beam hinges. The inverse of this occurs for columns and the E_{mh}/E_h ratios for exterior column hinges are less than the E_{mh}/E_h ratios for interior columns hinges. This means that the hysteretic energy demand of exterior beams and interior columns are more than the hysteretic energy demand of the interior beams and exterior columns of the same story in RC moment-resisting frames.
- Finding the difference of E_{mh}/E_h ratios between exterior and interior beam hinges for all stories and taking their average, show that hysteretic energy dissipated by exterior beam hinges is 30% more than the hysteretic energy dissipated by the interior beam hinges for 3 story frame, 15 % for 5 story frame, 8% for 7 story frame and 4% for 9 story frame. This means that as fundamental period of the structure increases the difference of of E_{mh}/E_h ratios between exterior and interior beam hinges decreases.
- Since, the hysteretic energy dissipated by columns are slight and majority of the energy is dissipated by beams, it is possible to ignore the difference of E_{mh}/E_h ratios between exterior and interior column hinges.
- To sum up, member-wise distribution of hysteretic energy is directly influenced by the moment capacities of beam and column sections whereas the dependence is slight for ground motion characteristics. This shows that it is possible to propose practical energy-based design rules to control the distribution of inelastic action within a frame structure.

CHAPTER 6

SUMMARY AND CONCLUSIONS

6.1. Summary and Conclusions

Energy-based approach is an alternative tool for performance-based earthquake engineering to design or evaluate the performance of a structure under seismic action. It is the best way to consider cumulative inelastic deformation of structures and duration of the ground motion. The input energy in structures is dissipated through damping energy and hysteretic energy. The previous studies as well as this study show that it is possible to estimate the input energy of the earthquake and its hysteretic energy demand on the structure. Although many studies have been conducted to develop energy-based design and assessment methodologies, a practical and widely accepted approach has not been proposed yet. This study aims to evaluate the energy-based response of RC moment-resisting frames designed according to TBSC 2018. Since most of the previous studies have concentrated on the input energy, the main focus of this study is on the estimation of hysteretic energy and its story-wise and member-wise distribution. For this reason, 6 RC moment-resisting frames with different number of stories and bays are selected and designed according to TBSC 2018. Then, NLTH analyses are carried out under 20 selected strong ground motion records. Energy parameters of the frame models are calculated in terms of Ei and Eh/Ei . The obtained results are examined to understand the effect of ground motion characteristics and structural properties on Ei and propose a practical value for Eh/Ei ratio to estimate hysteretic energy demand. In last part of the study, hysteretic energy dissipated by each plastic hinge in the frame models is calculated to obtain the story-wise and member-wise distribution of hysteretic energy. The final results show that it is possible to propose a methodology to determine hysteretic demand of each story and member of a well-designed RC frame under seismic action.

This study has been conducted a specific type of structure under predefined seismic actions. It contains some assumptions and simplifications. Before presenting the

conclusions drawn in this study, it is appropriate to mention the scope and limitations as follows:

- This study is limited to well-designed RC moment-resisting structures with 5% damping ratio and R=8.
- All NLTH analyses are conducted by using 2-D numerical models.
- Lumped plasticity model is used to simulate inelastic action at the nodes. This means it has been assumed that inelastic behavior is concentrated at the beam-column connections of the frame models.
- The selected Takeda hysteresis model for the NLTH analyses has a constant moment-curvature relationship and it cannot be updated according to axial load variation during the analysis.

Based on the aforementioned limitations and the dataset used in this study, the following conclusions are drawn:

- Scaled ground motion records with the same spectral accelerations apply different input energies to the same frame model. This shows that PGA and PGV are not adequate intensity parameters to fully represent the damaging potential of earthquakes. It seems that ground motions with long effective duration and large number of high amplitude acceleration cycles exert considerable amounts of input energy to the structure. Also the results show that a ground motion record does not exert the same level of input energy to different frame models. Hence it can be concluded that input energy is dependent on both ground motion characteristics and structural properties and empirical equations proposed to estimate input energy should be dependent on both of them.
- A ground motion record exerts nearly the same input energy to different structures with similar fundamental periods and damping ratios although geometrical properties (like number of bays) may differ. Hence, the fundamental period is an important parameter for estimation of input energy.

- Eh/Ei ratio results for 20 ground motion records and 6 RC frame models show that the dependence of Eh/Ei ratio to structural properties is negligible. It seems that Eh/Ei ratio is more dependent on the ground motion characteristics. As fundamental period of the structure increases, the sensitivity of Eh/Ei ratio to ground motion characteristics increases.
- The mean value of the Eh/Ei ratios of 20 ground motion records for each frame model is approximately about 0.6. It could be concluded that for a well-designed RC moment-resisting frame that exhibits inelastic behavior in a controlled manner, almost 60% of the input energy is dissipated through hysteretic action and 40% is dissipated through damping action. The assessment of the results show that it is possible to suggest 0.7 value for Eh/Ei ratio in an energy-based design methodology after considering the variation in results.
- General trend of the story-wise distribution of hysteretic energy results reveals that distribution of hysteretic energy over the height of structure depends on both ground motion characteristics and structural properties. The dependency of the Esh/Eh ratio to ground motion characteristics become more obvious as fundamental period of structure increases.
- The Esh/Eh ratio of ground story and lower stories decrease as the number of stories increases. This means that the hysteretic energy demand shifts from lower stories to upper ones as fundamental period of structure increases. This shows that the second mode of the structures should be considered in an energy-based design or assessment methodology (during estimation of the story-wise distribution of hysteretic energy) for mid-rise and high-rise structures.
- The results of this study show that in a well-designed RC moment-resisting frame, approximately, (70%-85%) of the hysteretic energy is dissipated by beams, (8%-18%) is dissipate by columns in the stories and (7%-15%) is dissipated by the base column joints. Consequently, it seems that in a ductile

RC moment-resisting frame, majority of hysteretic energy is dissipated by beams, which is a verification of the intended behavior in force-based capacity design of RC frame structures. It also seems that the percentage of hysteretic energy dissipated by columns or beams strongly depends on the ultimate moment capacities of columns and beams sections at the joints of the frame.

- Although strong column-weak beam criteria is considered in design of frame models, the columns exhibited inelastic behavior. This observation indicates that assigned safety factor of 1.2 for the ratio of column moment capacity to beam moment capacity does not guarantee elastic behavior for columns and it causes a ductile beam-column failure mechanism. This is not surprising since the frame models are designed for Life Safety performance level, for which controlled damage is allowed. The important point is that the percentage of inelastic action is very limited in columns when compared to beams. This is an indication of success in the seismic design process for ductile behavior.
- Member-wise distribution of hysteretic energy in the same story shows that the hysteretic energy is distributed uniformly between interior members. This may also be verified for exterior members. However, comparing interior and exterior members together indicates that Emh/Eh of hinges are not equal. In addition to this, the hysteretic energy demand of exterior beam hinges are generally more than interior beam hinges whereas the hysteretic energy demand of interior column hinges are more than exterior column hinges. This difference in hysteretic energy demand between interior and exterior members becomes more pronounced in low rise RC frame building. Hence it can be stated that as number of stories and fundamental period of structure increase, hysteretic energy is distributed more uniformly in the same story.
- The aforementioned results regarding story-wise and member-wise distributions of hysteretic energy can assist to estimate the role of each member to dissipate a certain amount of energy in an energy-based design methodology and the capacities of members can be arranged in accordance with this demand. So, it can be finally stated that energy based parameters are promising in order

to estimate the distribution of energy demand in a RC frame structure. This leads to the motivation that simple yet robust energy-based approaches can be developed and implemented to the future releases of seismic codes if the energy dissipation capacities of the members can be determined in a satisfactory manner.

6.2. Future Recommendations

The following arguments are recommended for future studies:

- Distribution of hysteretic energy demand in RC frame buildings should be evaluated for a wider range of fundamental periods and structural properties before drawing solid conclusions. This statement is also valid for the selection of ground motion records. A larger set of ground motions should be used in order to generalize the results. However the problem is the scarcity of strong ground motion records all over the world, which will impose considerable amount of inelasticity to the structures to monitor their energy response. In this case, the solution is to use ground motion scaling techniques or make use of synthetic ground motion records.
- In order to obtain more realistic structural response during NLTH analyses, 3D generation and more sophisticated nonlinear models like Fiber-M2-M3 hinge models can be employed.
- In this study well-designed RC frame models are used to estimate the energy response. However existing structures have many structural deficiencies and they don't generally satisfy the requirements of modern seismic codes. Hence this study should be extended to examine the energy response of such deficient RC frame structures and monitor the change in both story-wise and member-wise distributions of energy. It is also possible to conduct a parametric study by changing structural parameters like damping ratio and reduction factor.

- The results reveal that although the first mode of vibration is dominant for energy response, there may be contributions from higher modes as the number of stories increase. Hence the study can be extended to examine also the mod-wise distribution of energy for different types of RC frames.

REFERENCES

Akbaş, B., Akşar, B., Doran, B., & Alacalı, S. (2016). Hysteretic energy to energy input ratio spectrum in nonlinear systems. Dokuz Eylul University Faculty of Engineering Journal of Science and Engineering, 18(2), 239-254.

Akbas, B., Shen, J., & Hao, H. (2001). Energy appproach in peformance-based seismic design of steel moment resisting frames for basic safety objective. The Structural Design of Tall Buildings, 10(3), 193-217.

Akiyama, H. (1985). Earthquake-resistant limit-state design for buildings. University of Tokyo Press.

Alıcı, F. S., & Sucuoğlu, H. (2018). Elastic and inelastic near-fault input energy spectra. Earthquake Spectra, 34(2), 611-637.

Amiri, J. V., Amiri, G., & Ganjavi, B. (2008). Seismic vulnerability assessment of multi-degree-of-freedom systems based on total input energy and momentary input energy responses. Canadian Journal of Civil Engineering, 35(1), 41-56.

ASCE/FEMA (2000), Prestandard and Commentary for the Seismic Rehabilitation of Buildings, FEMA. Publication No. 356, American Society of Civil Engineers for the Federal Emergency Management. Agency, Washington, DC.

ATC-13 (1985) Earthquake damage evaluation data for California. Applied Technology Council, ATC-13, Report, Redwood City, California.

Aviram, A., Mackie, K. R., & Stojadinović, B. (2008). Guidelines for nonlinear analysis of bridge structures in California. Pacific Earthquake Engineering Research Center.

Bruneau, M., & Wang, N. (1996). Some aspects of energy methods for the inelastic seismic response of ductile SDOF structures. Engineering Structures, 18(1), 1-12.

Caltrans (2000). Caltrans Bridge Design Specifications. California Department of Transportation, Sacramento, California.

Chopra, A. K. (1995). Dynamics of structures: theory and applications to earthquake engineering. Prentice Hall.

Chou, C. C., & Uang, C. M. (2003). A procedure for evaluating seismic energy demand of framed structures. Earthquake Engineering & Structural Dynamics, 32(2), 229-244.

Clough, R. W. (1966). Effect of stiffness degradation on earthquake ductility requirements. In Proceedings of Japan Earthquake Engineering Symposium.

CSI (2017). CSI Analysis Reference Manual for SAP200, ETABS, and SAFE. Computers and Structures, Inc. Berkeley, California.

CSI (2018). SAP2000 Version 20.1.0, Linear and Nonlinear Static and Dynamic Analysis and Design of Three Dimensional Structures: Basic Analysis Reference Manual. Computers and Structures, Inc. Berkeley, California.

Dowell, O. K., Seible, F., & Wilson, E. L. (1998). Pivot hysteresis model for reinforced concrete members. ACI Structural Journal, 95, 607-617.

Estes, K. R., & Anderson, J. C. (2004, August). Earthquake resistant design using hysteretic energy demands for low rise buildings. In Proceedings of the 13th World Conference on Earthquake Engineering, August (pp. 1-6).

Fajfar, P., Vidic, T., & Fischinger, M. (1990). A measure of earthquake motion capacity to damage medium-period structures. Soil Dynamics and Earthquake Engineering, 9(5), 236-242.

Fajfar, P., Vidic, T. O. M. A. Z., & Fischinger, M. (1992). On energy demand and supply in SDOF systems. In Nonlinear seismic analysis and design of reinforced concrete buildings (pp. 49-70). CRC Press.

Guan, M., & Du, H. (2013). Energy-based seismic performance of reinforced concrete frame structures. Magazine of Concrete Research, 65(8), 494-505

Gulkan, P., & Sozen, M. A. (1971). Response and energy-dissipation of reinforced concrete frames subjected to strong base motions. University of Illinois Engineering Experiment Station. College of Engineering. University of Illinois at Urbana-Champaign.

Housner, G. W. (1956). Limit design of structures to resist earthquakes. In Proc. of 1st WCEE (pp. 5-1).

Kalkan, E., & Kunnath, S. K. (2008). Relevance of absolute and relative energy content in seismic evaluation of structures. Advances in Structural Engineering, 11(1), 17-34.

Khashaee, P., Gross, J. L., Khashaee, P., Lew, H. S., Mohraz, B., & Sadek, F. (2003). Distribution of earthquake input energy in structures. US Department of Commerce, National Institute of Standards and Technology.

Kuwamura, H., & Galambos, T. V. (1989). Earthquake load for structural reliability. Journal of Structural Engineering, 115(6), 1446-1462.

Leelataviwat, S., Saewon, W., & Goel, S. C. (2009). Application of energy balance concept in seismic evaluation of structures. Journal of Structural Engineering, 135(2), 113-121.

Li, H. N., Wang, F., & Lu, Z. H. (2007). Estimation of Hysteretic Energy of MDOF structures based on equivalent SDOF Systems. In Key Engineering Materials (Vol. 340, pp. 435-440). Trans Tech Publications.

Manfredi, G. (2001). Evaluation of seismic energy demand. Earthquake Engineering & Structural Dynamics, 30(4), 485-499.

Massumi, A., & Monavari, B. (2013). Energy based procedure to obtain target displacement of reinforced concrete structures. Structural Engineering and Mechanics, 48(5), 681-695.

MathWorks, I. (2018). MATLAB and statistics toolbox release 2018b. Natick (Massachusetts, United States).

Mander, J. B., Priestley, M. J., & Park, R. (1988). Theoretical stress-strain model for confined concrete. Journal of Structural Engineering, 114(8), 1804-1826.

McKevitt, W. E., Anderson, D. L., & Cherry, S. (1980). Hysteretic energy spectra in seismic design. In Proceeding of the Seventh World Conference on Earthquake Engineering (pp. 487-494).

Merter, O., & Ucar, T. (2014). Design of RC frames for pre-selected collapse mechanism and target displacement using energy–balance. Sadhana, 39(3), 637-657.

Mollaioli, F., Bruno, S., Decanini, L., & Saragoni, R. (2004). On correlation between energy and displacement. In Proceedings of the 13th World Conference on Earthquake Engineering.

Newmark, N. M. (1960). Effect of Inelastic Behavior of the Response of Simple Systems to Earthquake Motions. IIWCEE, 1960.

Okur, A., & Erberik, M. A. (2014). Adaptation of Energy Principles in Seismic Design of Turkish RC Frame Structures. Part II: Distribution of Hysteretic Energy. In Proceedings of the 2nd European Conference on Earthquake Engineering and Seismology (pp. 25-29).

Otani, S., & Sozen, M. A. (1972). Behavior of multistory reinforced concrete frames during earthquakes. University of Illinois Engineering Experiment Station. College of Engineering. University of Illinois at Urbana-Champaign.

Otani, S., & Sake, A. (1974). A computer program for inelastic response of R/C frames to earthquakes. Civil Engineering Studies, Report UILU-Eng-74-2029.

Ozcebe, G., & Saatcioglu, M. (1989). Hysteretic shear model for reinforced concrete members. Journal of Structural Engineering, 115(1), 132-148.

Powell, G. H. (1975). Supplement to computer program DRAIN-2D. Supplement to Report, DRAIN-2D User's Guide, University of California, Berkeley, Berkeley, CA.

Sawada, K., Matsuo, A., & Ujiie, K. (2005). A study on hysteretic plastic energy input into single and multi-degree of freedom systems subjected to earthquakes. WIT Transactions on the Built Environment, 81.

Shen, J., & Akbaş, B. (1999). Seismic energy demand in steel moment frames. Journal of Earthquake Engineering, 3(04), 519-559.

Sucuoğlu, H., & Akkar, S. (2014). Basic Earthquake Engineering. Switzerland: Spring International Publishing.

Sucuoğlu, H., & Erberik, A. (2004). Energy-Based Performance Evaluation of Deteriorating Structures. In Proc. 13th World Conf. Earthquake Eng., Paper (No. 3205)

Sucuoğlu, H., & Erberik, A. (2004). Energy-based hysteresis and damage models for deteriorating systems. Earthquake Engineering & Structural Dynamics, 33(1), 69-88.

Surahman, A. (2007). Earthquake-resistant structural design through energy demand and capacity. Earthquake Engineering & Structural Dynamics, 36(14), 2099-2117.

Takeda, T., Sozen, M. A., & Nielsen, N. N. (1970). Reinforced concrete response to simulated earthquakes. Journal of the Structural Division, 96(12), 2557-2573.

Tu, B. B., & Zhao, D. (2018). Distribution of accumulated irrecoverable hysteretic energy in MDOF structures. Multidiscipline Modeling in Materials and Structures, 14(2), 202-215.

Turkish Earthquake Code, TEC (2007) Specifications for the buildings to be constructed in disaster areas. Ministry of Public Works and Settlement, Ankara, Turkey.

Turkish Building Earthquake Code, TBEC (2018) Republic of Turkey Prime Ministry Disaster and Emergency Management Authority, Ankara, Turkey.

Turkish Standard Institute (1997). Turkish Standard, TS498: The Calculation Values of Loads used in Designing Structural Elements. Ankara, Turkey.

Turkish Standards Institute (2000). Turkish Standard, TS500: Requirements for design and construction of reinforced concrete structures. Ankara, Turkey.

Uang, C. M., & Bertero, V. V. (1990). Evaluation of seismic energy in structures. Earthquake Engineering & Structural Dynamics, 19(1), 77-90.

Uçar, T., & Merter, O. (2018). Hysteretic Energy Demand in SDOF Structures Subjected to an Earthquake Excitation: Analytical and Empirical Results. Journal of Natural and Applied Sciences, 22(2), 364-374.

Veletsos, A. S., & Newmark, N. M. (1960). Effect of inelastic behavior on the response of simple systems to earthquake motions. Department of Civil Engineering, University of Illinois.

Zahrah, T. F., & Hall, W. J. (1984). Earthquake energy absorption in SDOF structures. Journal of structural Engineering, 110(8), 1757-1772.

Zhu TJ ,Tso WK, Heidebrecht HC.(1993). Seismic energy demands on reinforced concrete moment-resisting frames. Earthquake Engineering and Structural Dynamics 1993; 22(5):533–545.

Zhu, T. J. (1989). Inelastic response of reinforced concrete frames to seismic ground motions having different characteristics (Doctoral dissertation).

APPENDICES

A. Distribution Pattern of Hysteresis Energy Dissipated by the Frame Joints

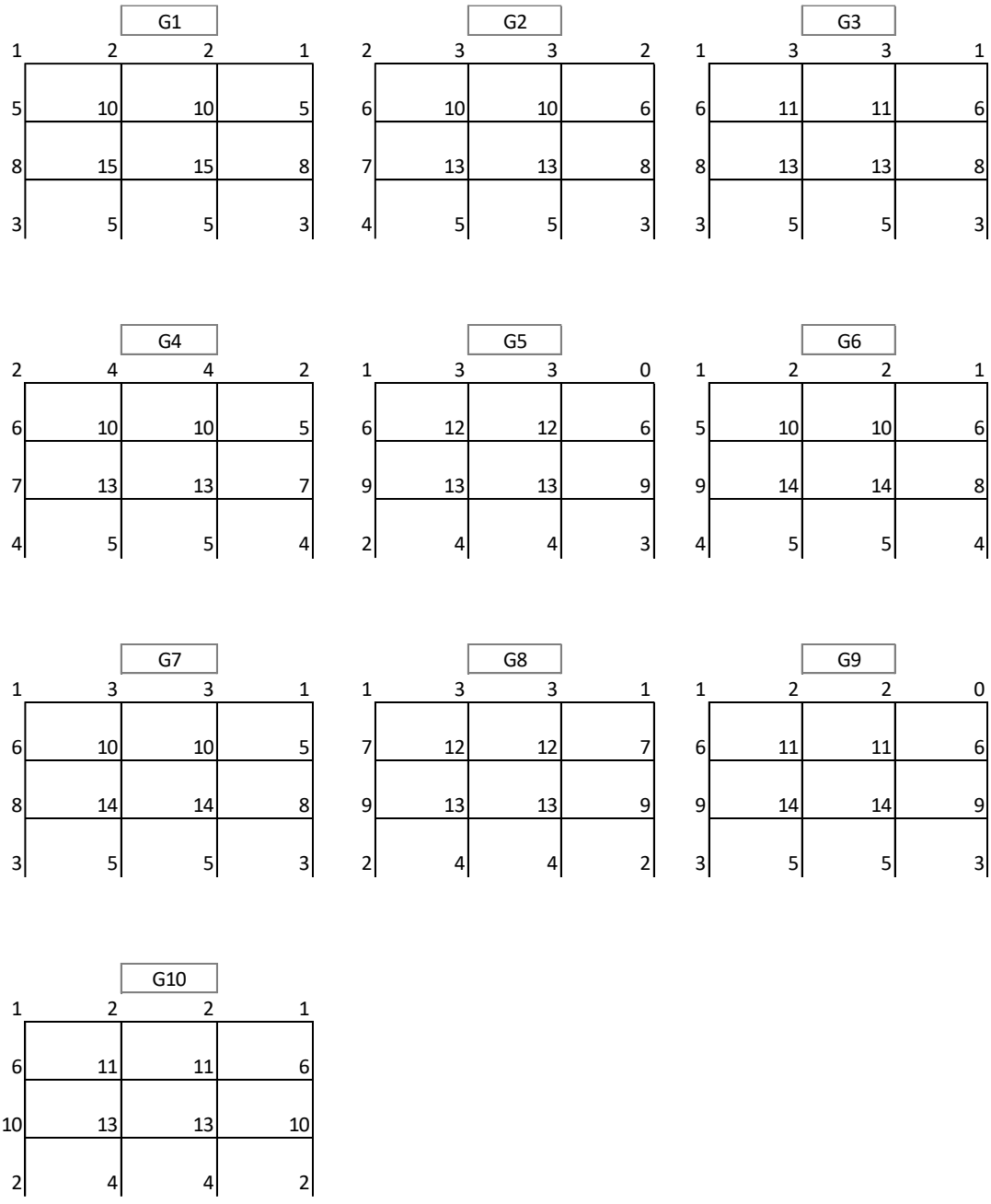

Figure A.1. Percentage of hysteretic energy dissipated by joints in 3-stoy, 3-bay frame for global records

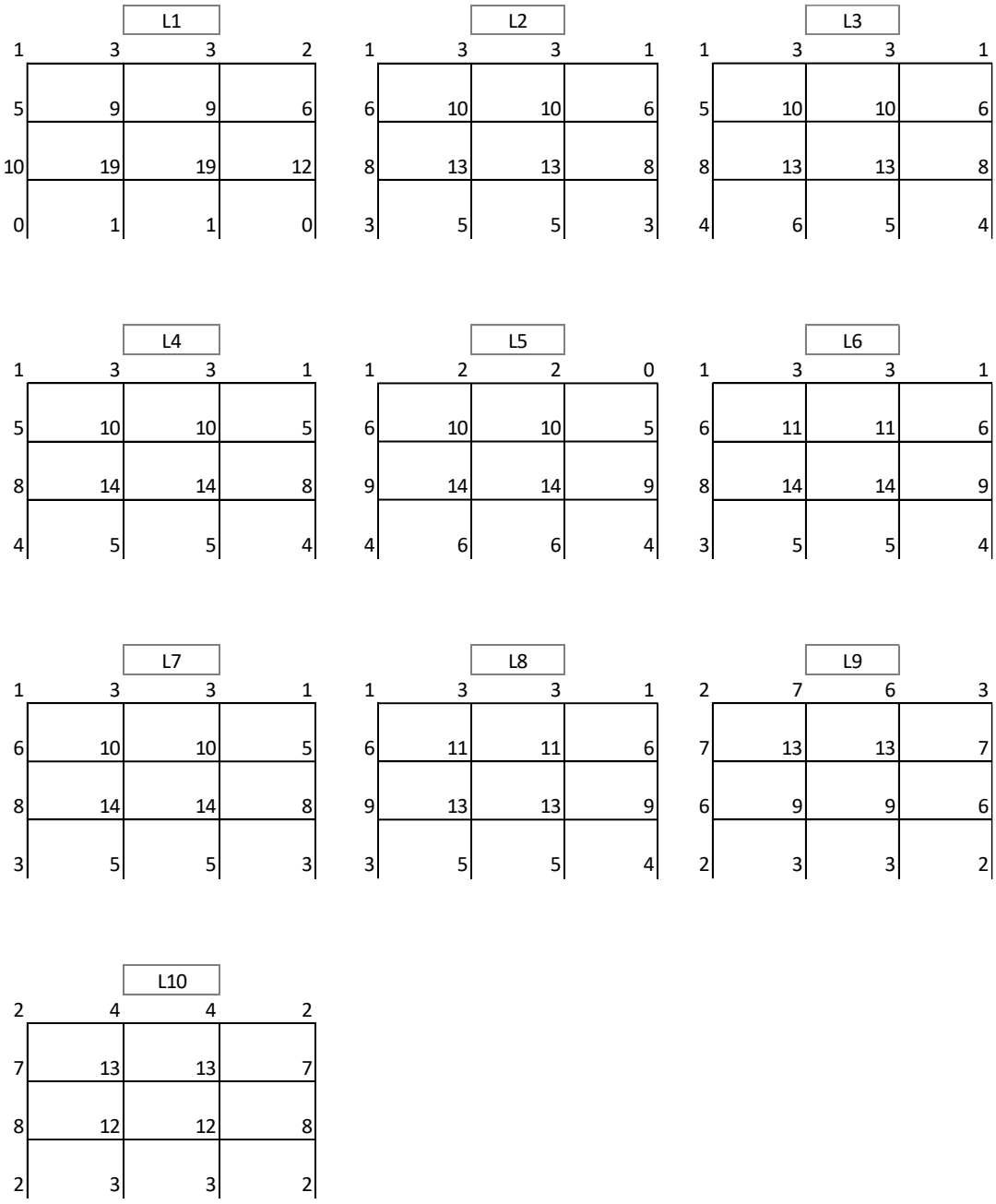

Figure A.2. Percentage of hysteretic energy dissipated by joints in 3-stoy, 3-bay frame for local records

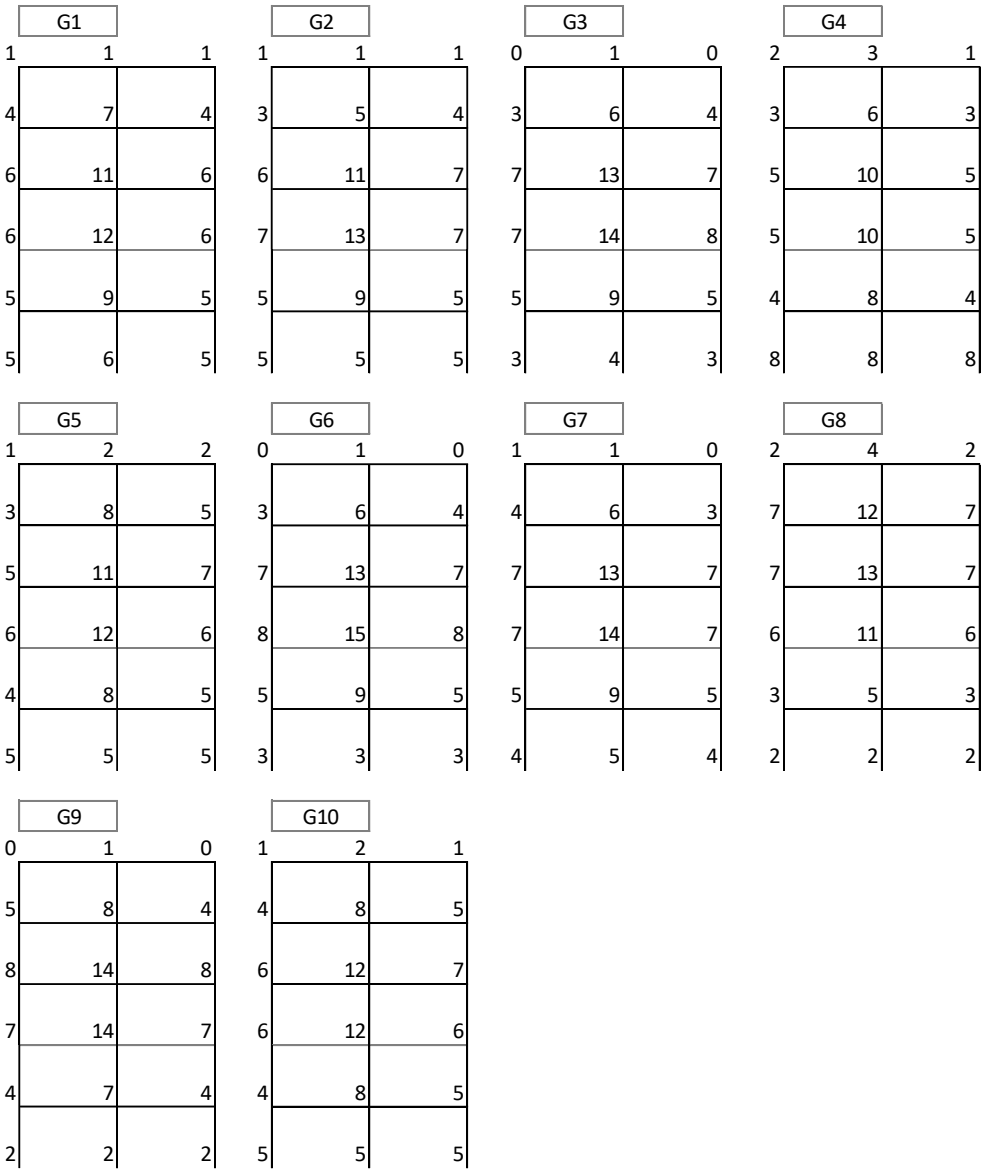

Figure A.1. Percentage of hysteretic energy dissipated by joints in 5-stoy, 2-bay frame for global records

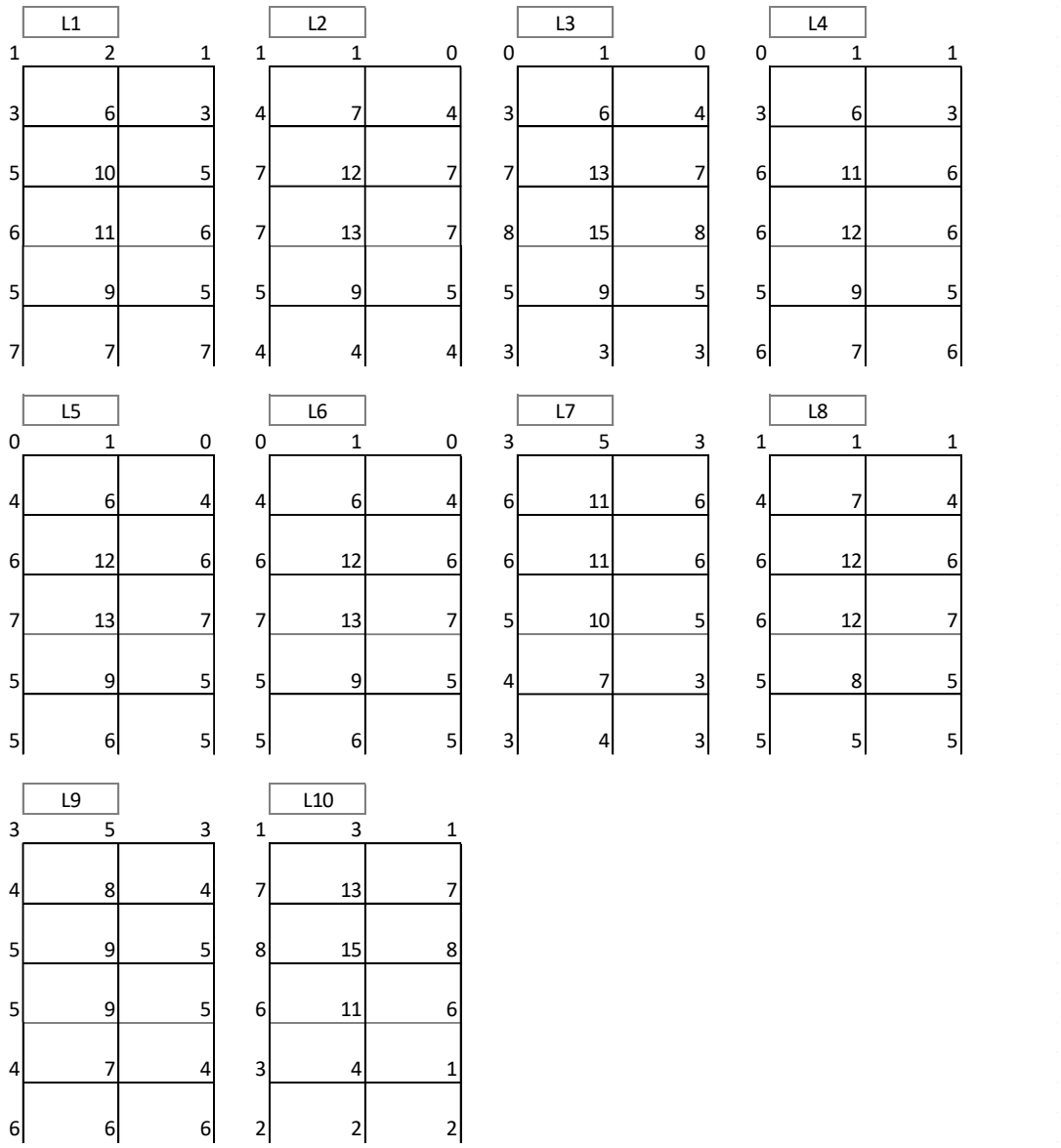

Figure A.2. Percentage of hysteretic energy dissipated by joints in 5-stoy, 2-bay frame for local records

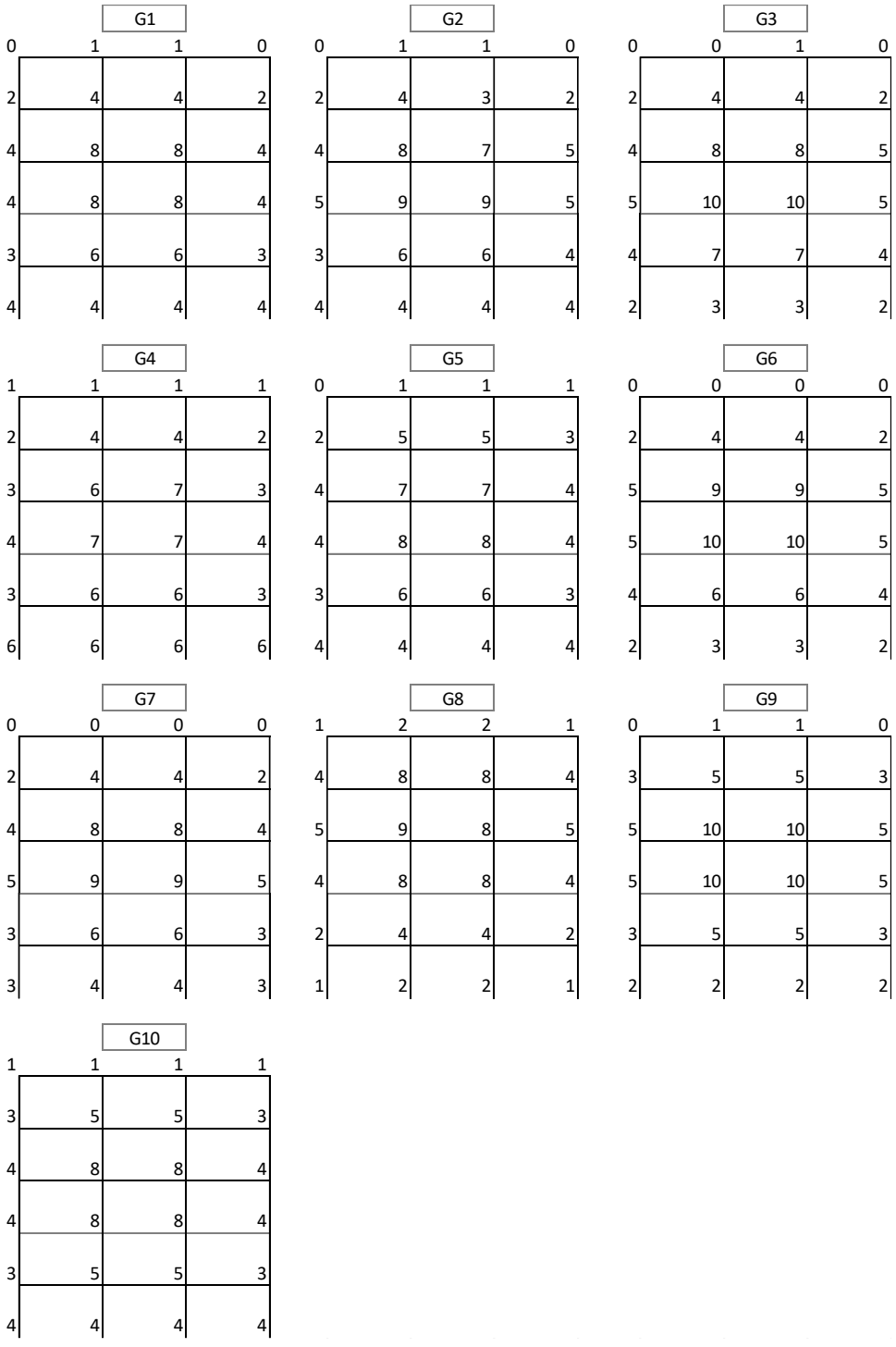

Figure A.3. Percentage of hysteretic energy dissipated by joints in 5-stoy, 3-bay frame for global records

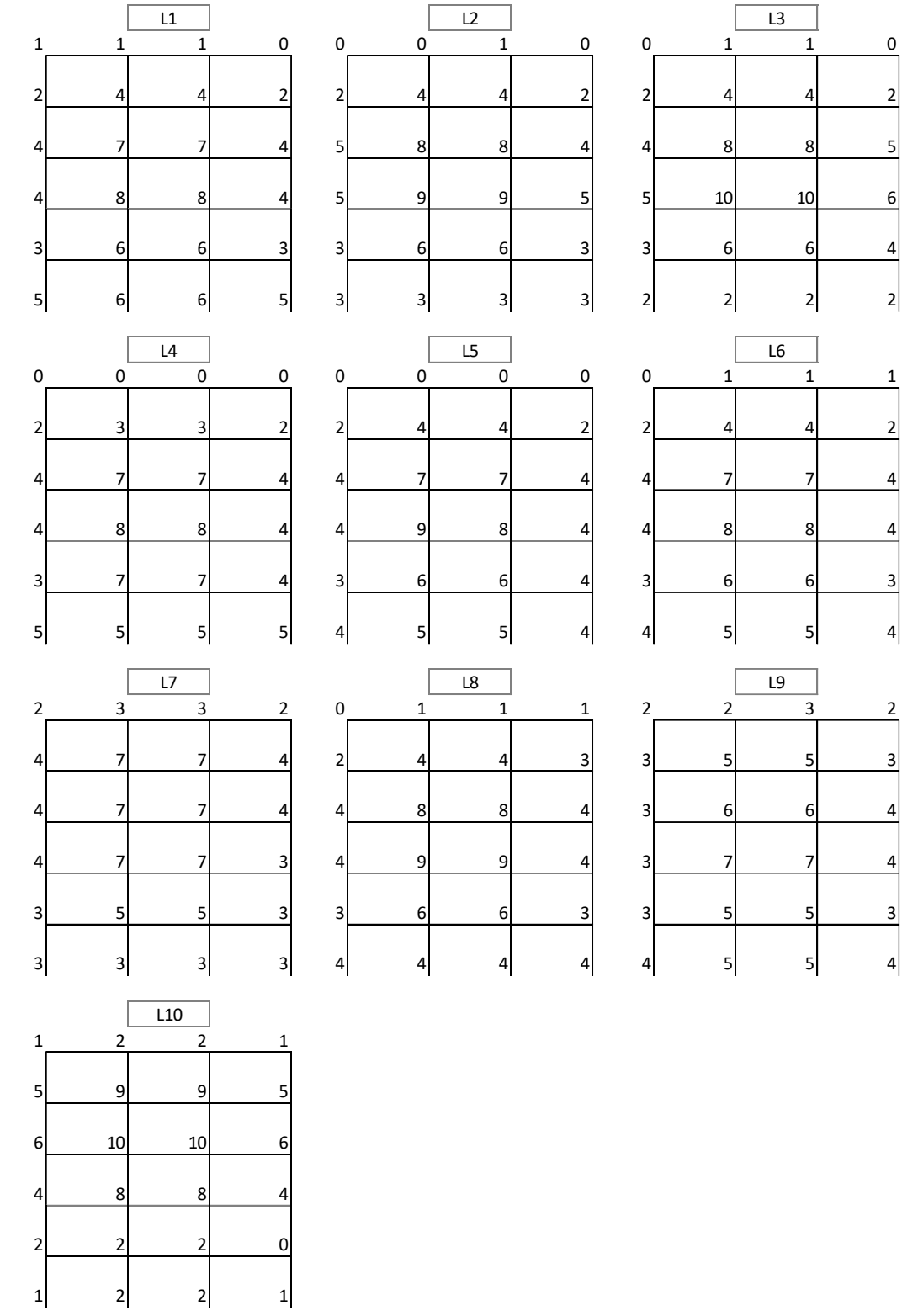

Figure A.4. Percentage of hysteretic energy dissipated by joints in 5-stoy, 3-bay frame for local records

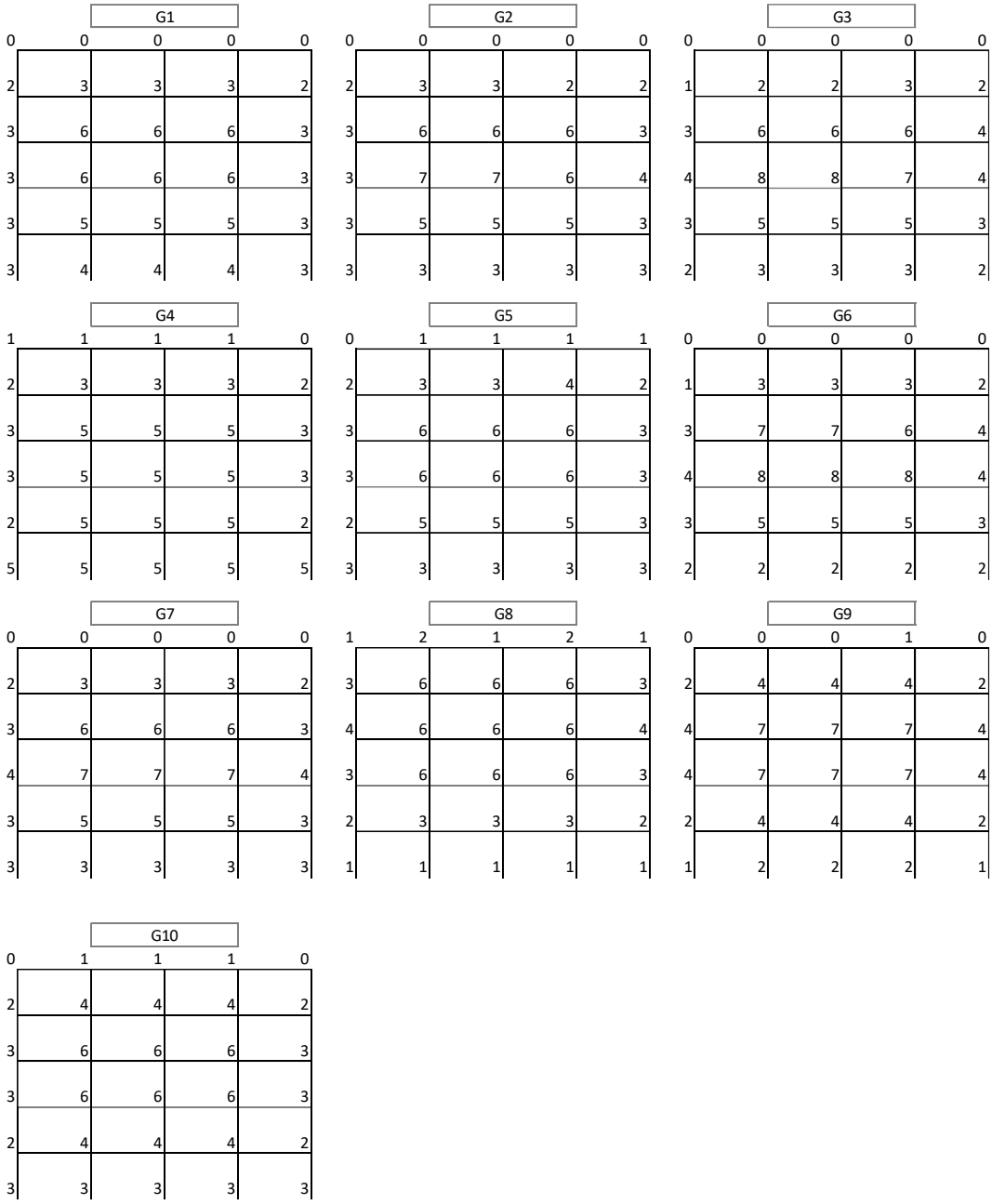

Figure A.5. Percentage of hysteretic energy dissipated by joints in 5-stoy, 4-bay frame for global records

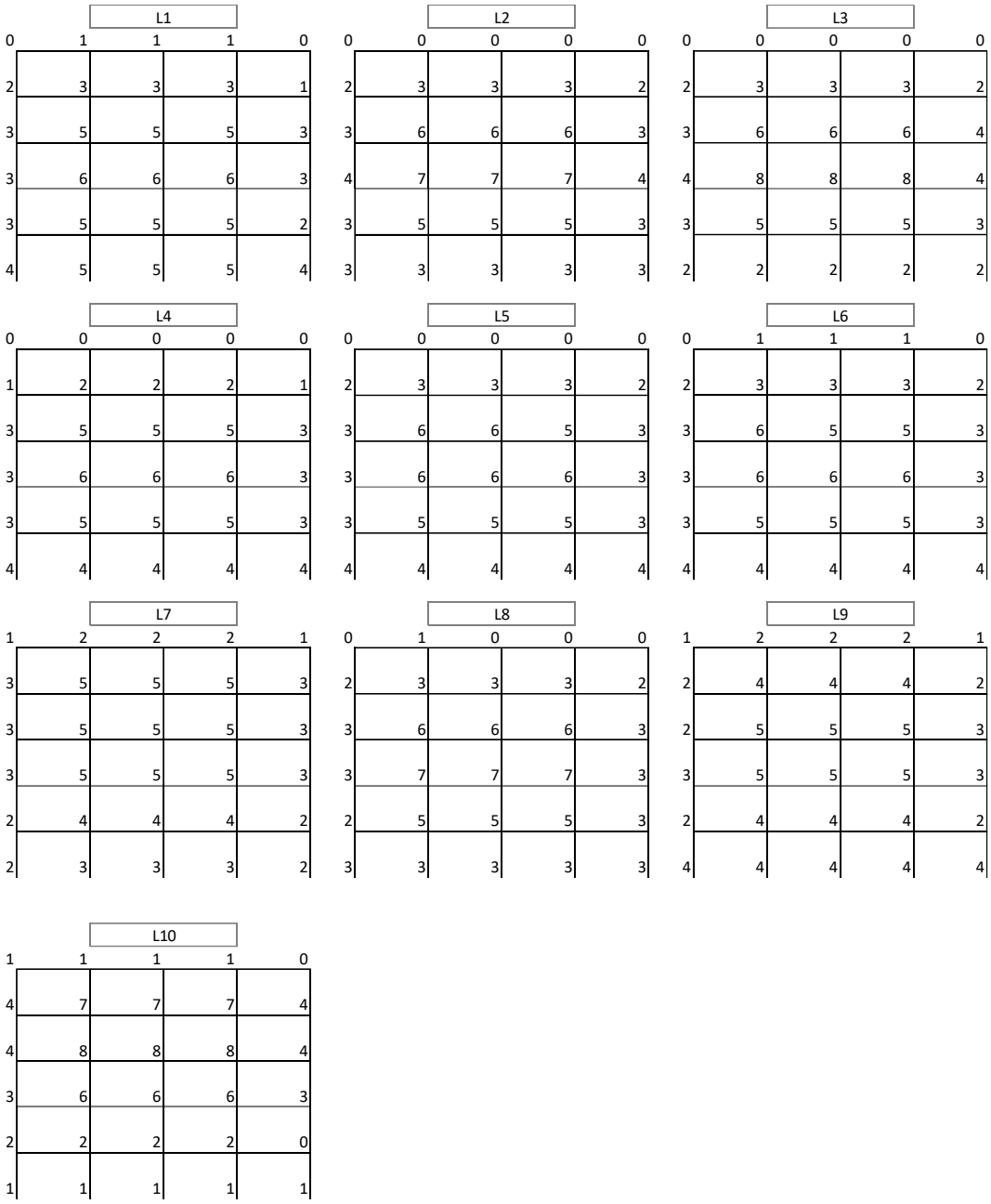

Figure A.6. Percentage of hysteretic energy dissipated by joints in 5-stoy, 4-bay frame for local records

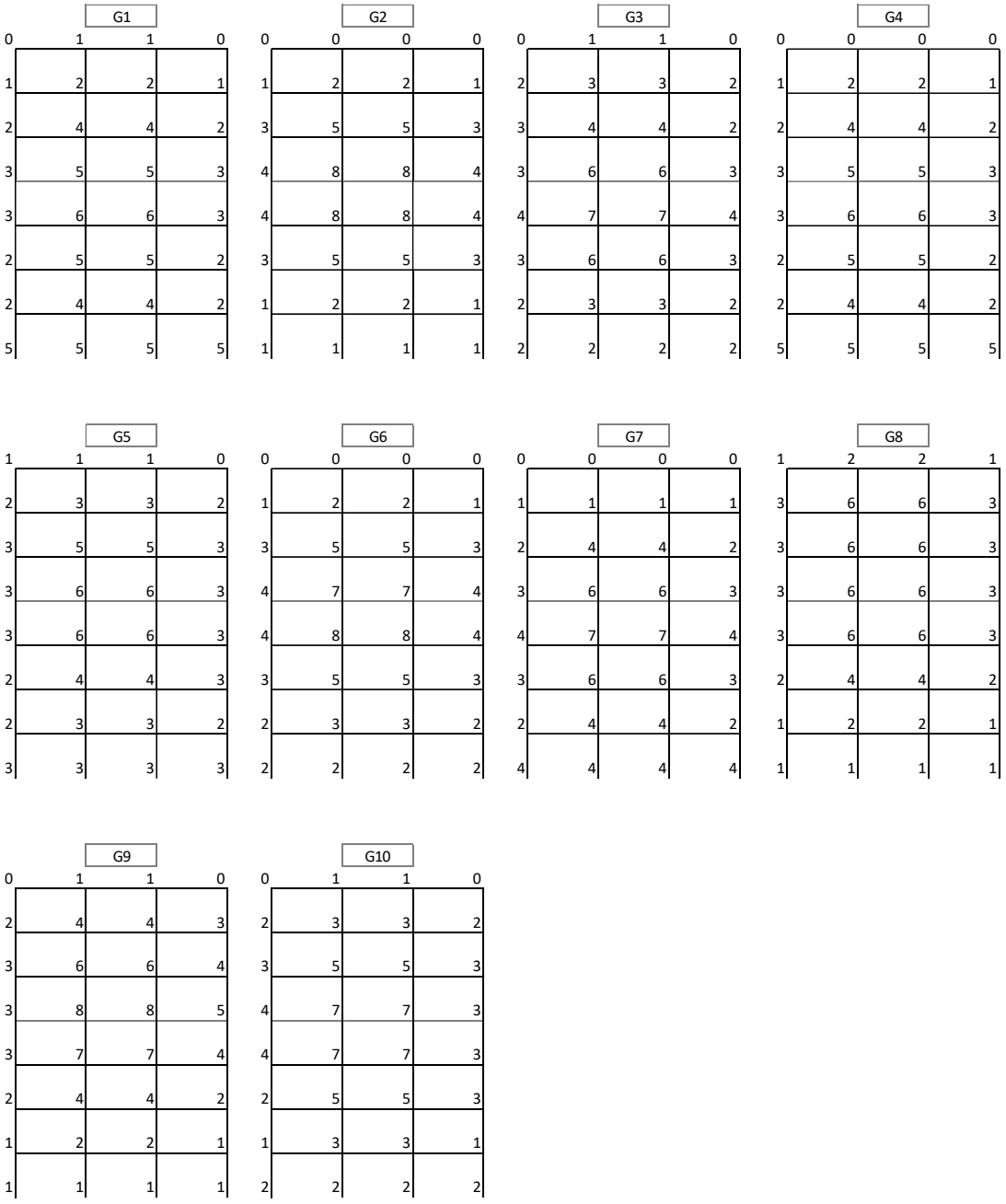

Figure A.7. Percentage of hysteretic energy dissipated by joints in 7-stoy, 3-bay frame for global records

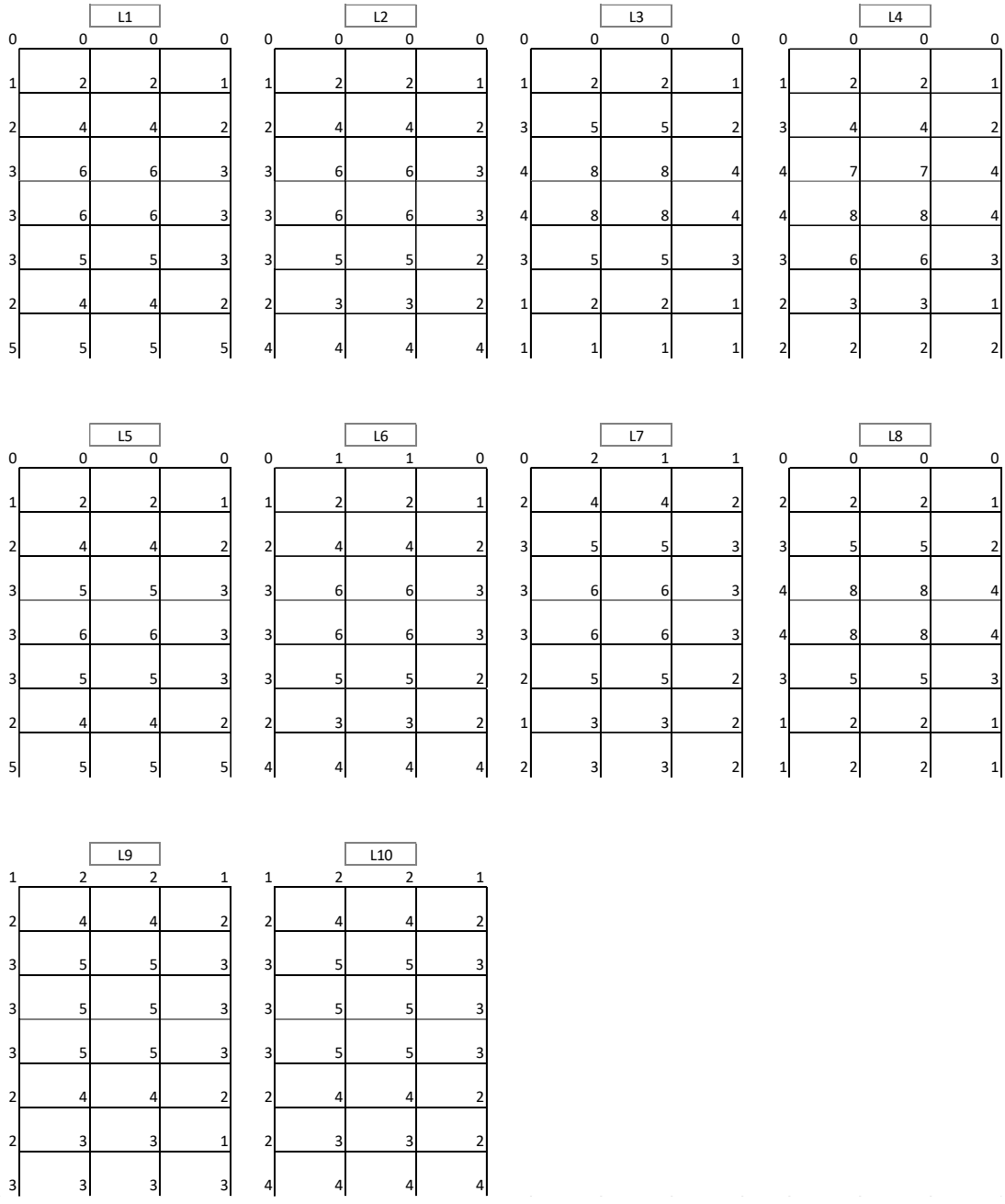

Figure A.8. Percentage of hysteretic energy dissipated by joints in 7-stoy, 3-bay frame for local records

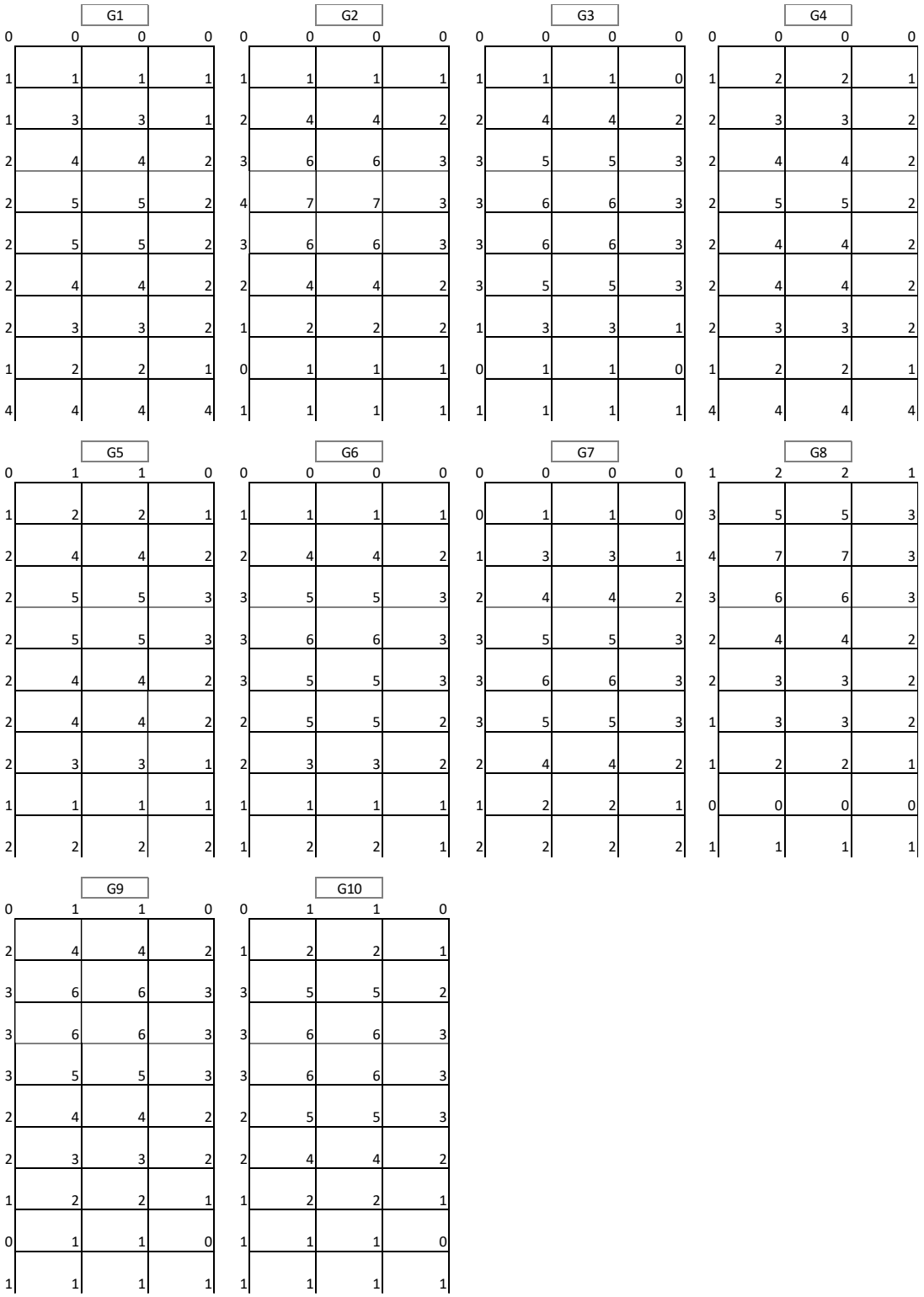

Figure A.9. Percentage of hysteretic energy dissipated by joints in 9-stoy, 3-bay frame for global records

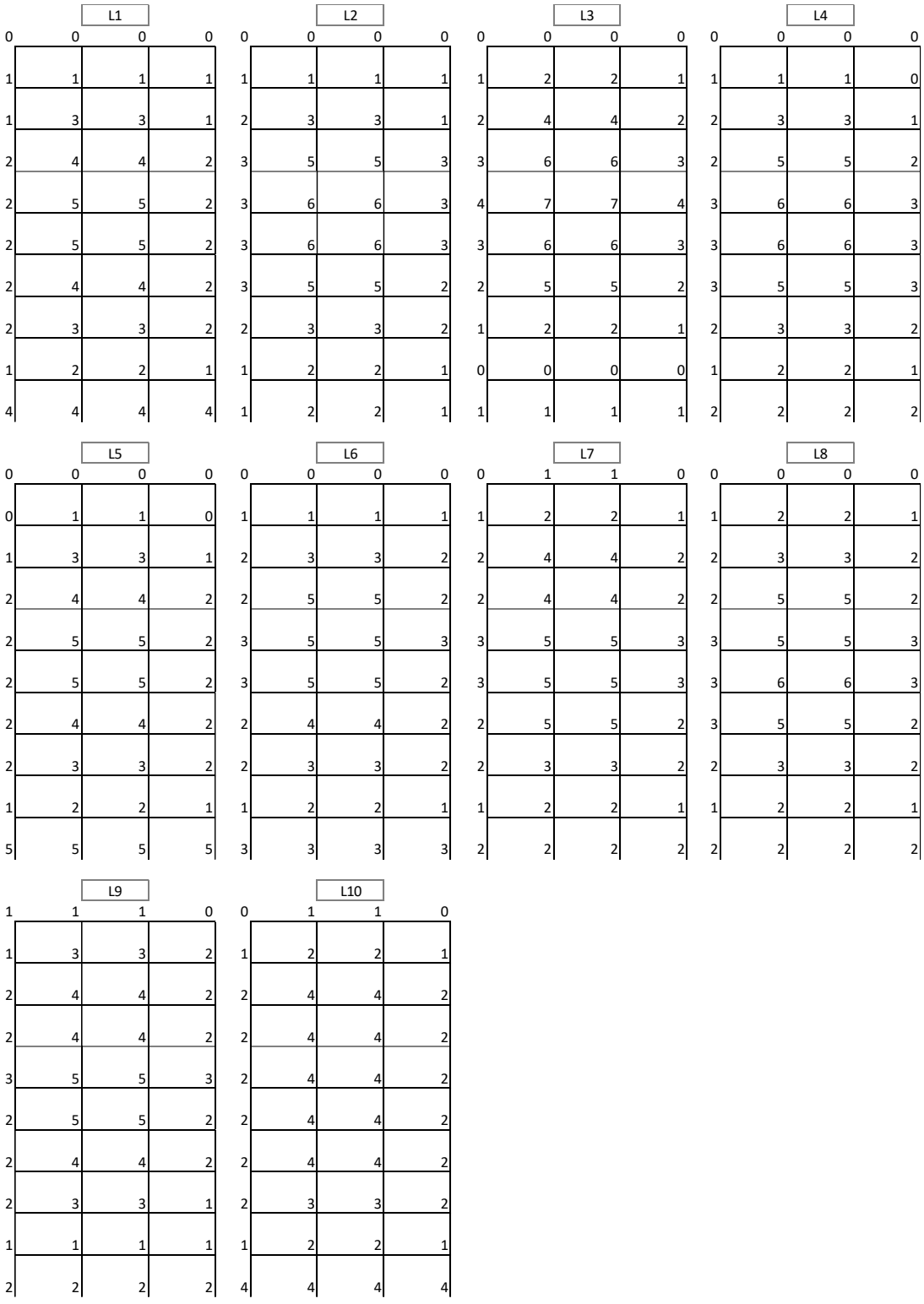

Figure A.10. Percentage of hysteretic energy dissipated by joints in 9-stoy, 3-bay frame for local record